รหัสโครงการ SUT7-706-44-36-18

รายงานการวิจัย

การจำลองทางคอมพิวเตอร์ของการไหลในเครื่องตกผลึกแบบสารแขวนลอยที่มีการแยกผลึกแบบผสม
(Computer Modeling of Fluid and Particle Flow in a Mixed Suspension, Mixed Product Removal Crystallizer)

ได้รับทุนอุดหนุนการวิจัยจาก

มหาวิทยาลัยเทคโนโลยีสุรนารี

ผลงานวิจัยเป็นความรับผิดชอบของหัวหน้าโครงการวิจัยแต่เพียงผู้เดียว

รหัสโครงการ SUT7-706-44-36-18

รายงานการวิจัย

การจำลองทางคอมพิวเตอร์ของการไหลในเครื่องตกผลึกแบบสารแขวนลอยที่มีการแยกผลึกแบบผสม (Computer Modeling of Fluid and Particle Flow in a Mixed Suspension, Mixed Product Removal Crystallizer)

คณะผู้วิจัย

หัวหน้าโครงการ

รองศาสตราจารย์ ดร.เอเดรียน ฟลัด
สาขาวิชาวิศวกรรมเคมี
สำนักวิชาวิศวกรรมศาสตร์
มหาวิทยาลัยเทคโนโลยีสุรนารี

รองศาสตราจารย์ ดร.ทวิช จิตรสมบูรณ์
สาขาวิชาวิศวกรรมเครื่องกล
สำนักวิชาวิศวกรรมศาสตร์
มหาวิทยาลัยเทคโนโลยีสุรนารี

ผู้ร่วมวิจัย
นางสาวจารุวรรณ ตั้งต้นสกุลวงศ์

ได้รับทุนอุดหนุนการวิจัยจากมหาวิทยาลัยเทคโนโลยีสุรนารี ปีงบประมาณ พ.ศ. 2544
ผลงานวิจัยเป็นความรับผิดชอบของหัวหน้าโครงการวิจัยแต่เพียงผู้เดียว
สิงหาคม 2552

Acknowledgements

The research presented in this report was funded by the Suranaree University of Technology Research Fund, and this support is gratefully acknowledged. Ms. Jaruwan Tangtonsakoolwong should also be acknowledged for much of the experimental work described here.

บทคัดย่อ

ในกระบวนการตกผลึกแบบต่อเนื่อง การดึงสารละลายตัวอย่างออกจากถังตกผลึกด้วยวิธี isokinetic เพื่อมาวิเคราะห์หาความสม่ำเสมอของขนาดผลึกเป็นปัจจัยที่สำคัญมาก เพราะการวิเคราะห์ขนาดของผลึกที่ถูกต้องจะมีผลต่อตัวแปรอื่น ๆ เช่น การโตของผลึก อัตราการเกิดผลึก อัตราการแตกของผลึก และอัตราการเกาะตัวของผลึก

การดึงสารละลายตัวอย่างด้วยวิธี isokinetic ขึ้นอยู่กับลักษณะการไหลของสารละลายในถังตกผลึก งานวิจัยนี้จึงมีจุดประสงค์เพื่อจำลองตัวเลขและวิเคราะห์การไหลในถังตกผลึกจำลองของน้ำตาล ลักษณะการไหลภายในถังเป็นแบบต่อเนื่องที่มีระบบทำความเย็น โดยออกแบบถังเป็นทรงกระบอกก้นมน

งานวิจัยนี้ได้ใช้โปรแกรมสำเร็จรูปเชิงพาณิชย์ "CFX5.5.1" เป็นโปรแกรมหลักในการจำลองการไหลแบบสามมิติ โดยใช้วิธีปริมาตรจำกัดและกริดไร้โครงสร้าง (unstructural grid) เป็นพื้นฐานในการทำงาน ขั้นตอนแรกของงานวิจัยได้ทำการศึกษาความสามารถของโปรแกรม โดยให้โปรแกรมแก้ปัญหาแบบจำลองหลายประเภท แล้วเปรียบเทียบผลที่ได้กับผลการทดลองที่มีอยู่แล้ว

ในขั้นตอนต่อมาได้ทำการจำลองถังตกผลึกอย่างรอบคอบ โดยจำลองทุกอย่างจากถังตกผลึกจริง ในโปรแกรมใบกวนที่ใช้เพิ่มความเร็วของสารละลายในถังตกผลึกถูกแทนที่ด้วยแหล่งกำเนิดโมเมนตัม ในการจำลองได้เปลี่ยนขนาดของแหล่งกำเนิดโมเมนตัม 7 ค่า จากผลการคำนวณพบว่าความเร็วตามแนวแกนสูงขึ้นเมื่อขนาดของแหล่งกำเนิดโมเมนตัมสูงขึ้น แต่ไม่มีผลต่อความเร็วโดยรวม ยกเว้นบริเวณรอบๆ ท่อดูดสารตัวอย่าง

จากการจำลองพบว่าขนาดแหล่งกำเนิดโมเมนตัมที่ดีที่สุดของการดึงสารตัวอย่างด้วยวิธี isokinetic คือ 25,000 $kg/m^2/s^2$ เนื่องจากจะทำให้การวัดการกระจายตัวของผลึกในสารละลายตัวอย่างมีความถูกต้องกับการกระจายตัวของผลึกในถังตกผลึกมากที่สุด ซึ่งงานวิจัยนี้จะเป็นประโยชน์ต่องานวิจัย MSMPR (mixed suspension mixed product removal) ต่อไป

ผลการจำลองพบว่าพลังงานที่ใช้หมุนใบกวนมีค่าเท่ากับ 0.6 W สำหรับถังตกผลึกขนาด 2.5 ลิตร นอกจากนี้ยังพบว่าความเร็วของสารละลายที่จุดศูนย์กลางของก้นถังตกผลึกมีค่าต่ำกว่าบริเวณรอบถัง ซึ่งในถังตกผลึกจริงจะทำให้เกิดการตกตะกอนของผลึกที่ก้นถัง และจะเป็นปัญหาต่อการวิเคราะห์การกระจายตัวของผลึกในสารละลายตัวอย่าง

Abstract

Isokinetic withdrawal of solution from research crystallizers is a key factor in obtaining a representative crystal-size distribution and is critical for correct analysis of the crystallization process to accurately determine crystallization kinetic parameters such as crystal growth rates, nucleation rates, breakage rates, and agglomeration rates. Isokinetic withdrawal, in turn, depends upon the characteristics of the flow field in the crystallizer. The objective of this research numerically simulates the fluid flow field in a small-scale (experimental) cylindrical round bottomed, continuous-flow, cooling crystallizer set up for analysis of kinetic parameters in sugar production.

The commercial software "CFX 5.5.1" was employed to perform the 3 dimensional simulations with a finite volume method using an unstructured mesh. Initially the ability of the software to perform flow calculations on complex geometries was investigated by solving a series of model problems, and comparing these solutions to known solutions for the systems involved. A series of experiments was also performed to determine the ability of the momentum source feature of the program to model features such as impellers.

A model of the crystallizer being considered was carefully produced using a real crystallizer as a model. The impeller used for increasing the gross velocity of the solution inside the crystallizer is modeled using a momentum source, since this had been shown to be suitable for an impeller in a baffled crystallizer, particularly when the main feature of the flow to be considered is the flow at the product tube (to determine whether the product flow is isokinetic or not). Seven momentum source strength values were used to perform the simulation. The results show that the momentum source strongly increases the axial flow velocity but only slightly influences the overall flow pattern, except the flow near the outlet tube. The isokinetic withdrawal condition can be achieved at a momentum source strength of about 25,000 $kg/m^2/s^2$. The isokinetic condition for the nuclei crystals is best for the research MSMPR, as it will make the particle size distribution in the product stream most accurate for the analysis of the nucleation and growth rates in the crystallizer. For larger particles the settling velocity is required for determination of isokinetic withdrawal. The power transmitted by impeller shaft is 0.6 W for a 2.5 L crystallizer, which allows the impeller rotational speed to be estimated. Furthermore, the velocity at the center of the tank's bottom is lower than that of the surrounding region. This could cause a collection of settled crystals which is problematic for the operation and analysis of the crystallizer.

Contents

Figures

Chapter I

Introduction

1.1 The Mixed Suspension-Mixed Product Removal Crystallizer

The Mixed Suspension-Mixed Product Removal (MSMPR) crystallizer is the ideal continuous crystallizer from the viewpoint of theoretical calculations: it is the crystallization equivalent of an ideal steady-state Continuous Stirred Tank Reactor (CSTR). For this reason it is the most commonly used crystallizer (essentially the *only* crystallizer used) in the determination of simultaneously crystal growth rate and nucleation rates from solution.

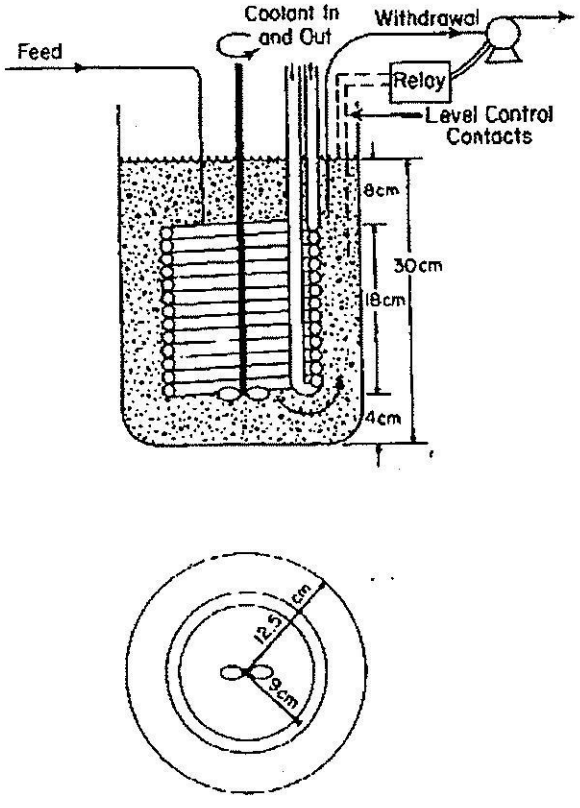

Fig. 1.1 A schematic diagram of a cooling MSMPR crystallizer[1] similar to the crystallizer used for growth and nucleation kinetics at S.U.T. that is simulated in the present study.

For a crystallizer to be a true MSMPR crystallizer (rather than just in name only) several preconditions must be met: if the conditions are not met the crystallizer does not

meet the specifications for a MSMPR, and crystal growth and nucleation kinetics predicted from such a crystallizer will not be correct. The conditions are as follows[2].

The ideal MSMPR crystallizer has the following assumptions:

(a) The vessel is perfectly mixed with respect to both the liquid phase (there are no spatial variations in concentration, temperature, or driving force) and the solid phase (no spatial variation in the population density function). [The mixed suspension (MS) assumption].

(b) The suspension in the product stream is identical to the suspension in the crystallizer vessel. [The mixed product removal (MPR) assumption].

(c) There are no crystals or particles in the feed stream. The population of crystals in the crystallizer is entirely due to the nucleation of particles within the crystallizer and their subsequent growth.

(d) The system operates at a steady-state

In addition, to obtain an ideal population density distribution from the MSMPR crystallizer the following set of conditions should be met

(a) There is no agglomeration or breakage of particles in the crystallizer.

(e) Nucleation within the crystallizer occurs at zero size. This allows the nucleation rate to be considered via a boundary condition (n^0) rather than as a birth term.

(f) The growth rate is size independent [$G \neq G(L)$].

If these seven conditions are all met, it is simple to analyze the system to obtain exact growth and nucleation rate kinetics from the particle population density result. The full form of the population balance, which models the evolution of particle size for a population via a continuity balance on the particles, is

$$\frac{\partial n}{\partial t} + \nabla \cdot (\mathbf{v}n) + \frac{\partial (Gn)}{\partial L} - B + D = 0 \qquad (1.1)$$

In this equation n is the particle population density function (#/m^3.m) which is dependent on the particle size, time, and the spatial position at which the function is determined; G is the crystal growth rate, which is also dependent on the particle size, time, and the spatial position at which the function is determined; $\mathbf{v}$ is the particle velocity vector; B and D () are the birth rate function of particles (and depend on the same variables as n); L represents the particle size, and t represents the time.

However since the system can be characterized as completely mixed, it is possible to use a simplified form of equation (1.1), the spatially averaged form of the population balance:

$$\frac{\partial n}{dt} + n\frac{\partial(\log V)}{\partial t} + \frac{\partial(Gn)}{\partial L} = \sum \frac{Q_{in,i} n_{in,i}}{V} - \sum \frac{Q_{out,i} n_{out,i}}{V} + B - D \qquad (1.2)$$

Here the variables are defined as in equation (1.1), and the additional variables represent: V (m^3) is the volume of the completely mixed region (and is equal to the crystallizer volume if the crystallizer is completely mixed); $Q_{in,i}$ and $Q_{out,i}$ (m^3/s) represent flowrates of inflows and outflows to the crystallizer respectively, with the subscript required if multiple inflows or outflows are present; the particle population densities in the streams represented by $Q_{in,i}$ and $Q_{out,i}$ are given by $n_{in,i}$ and $n_{out,i}$ respectively. Although the equation does not appear to be substantially simpler than equation (1.1) the equation removes partial derivatives with respect to the spatial variables (x, y, z), thus greatly reducing the order of the partial differential equation.

With the assumptions implicit in an MSMPR the equation can be simplified further. In a true MSMPR the system operates at a steady-state, and thus the time dependent partial derivatives (terms 1 and 2 of equation 1.2) are zero. Since the growth rate is independent of the particle size, the variable G may be removed outside the differential with respect to the particle size. Since there are no particles in inflow streams the first term on the right hand side is zero. Since the nucleation occurs at zero size, the birth rate due to nucleation can be included in a boundary condition, and B_{nucl} is equal to zero. The other terms in B and D are zero in the absence of agglomeration and breakage. Since the product stream has the same conditions as the suspension inside the crystallizer $n_{out} = n$ (no subscript on the population density is required since there is only one product stream). Thus, the population balance simplifies to

$$G\frac{dn}{dL} = -\frac{Q_{out}}{V} n \qquad (1.3)$$

Defining the drawdown time as $\tau = V/Q_{out}$ and rearrangement gives a first order homogeneous ordinary differential equation of standard form

$$\frac{dn}{dL} + \frac{1}{G\tau} n = 0 \qquad (1.4)$$

The boundary condition for this equation is $n(L = 0) = n^0$ (#/m^3.m). This represents the population density at zero particle size. This may be related to the nucleation rate, which is defined as:

$$B^0 \equiv \left.\frac{dN}{dt}\right|_{L=0} = \frac{dN^0}{dt} \qquad (1.5)$$

Where N is the cumulative number of particles, and therefore N^0 is the cumulative number of particles up to $L = 0^+$.

We can consider the rate of change of the cumulative number as

$$\frac{dN^0}{dt} = \left[\frac{dL}{dt}\frac{dN}{dL}\right]_{L=0} \tag{1.6}$$

From the definition of the growth rate (here assumed to not be a function of L)

$$G = \frac{dL}{dt} \tag{1.7}$$

and the definition of the population density (as the derivative of the cumulative population)

$$\left.\frac{dN^0}{dL}\right|_{L=0} = n^0 \tag{1.8}$$

then

$$B^0 \equiv \frac{dN^0}{dt} = Gn^0 \tag{1.9}$$

Knowing the boundary condition allows a solution for equation 1.4 to be found, and the solution is

$$n = n^0 \exp\left(-\frac{L}{G\tau}\right) \tag{1.10}$$

This solution is sketched in Figure 1.2. Plotting the data on a semilog plot will result in a straight line for an ideal steady-state MSMPR crystallizer *if there is no size dependence in the growth rate, nor any growth rate dispersion.* If there is size dependent crystal growth or growth rate dispersion then the plot will not result in a straight line; however if it is possible to be sure that the crystallizer is a true MSMPR crystallizer then it is possible to analyze the crystal population density distribution data to calculate the growth rate model. An example of this is shown in Figure 1.3, which is equivalent to the crystallization system in Figure 1.2, except now the crystal growth rate is size dependent, with a growth rate of the form $G = G_0(1 + \gamma L)^b$, with the growth dependent parameters being $\gamma = 0.005$, and $b = 0.4$ in this case. Note that the crystal population density distribution is now not straight on the semilog plot.

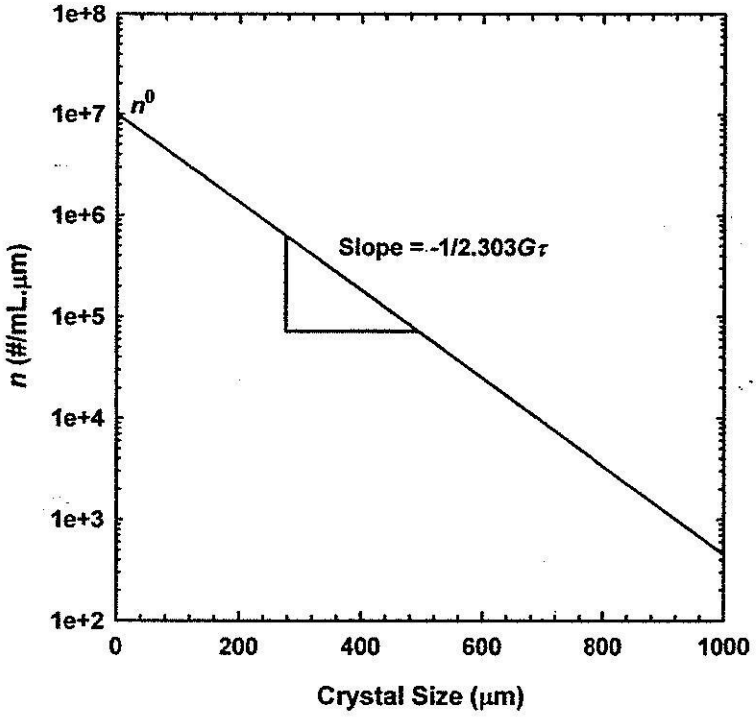

Fig. 1.2 Population density for a MSMPR crystallizer with no size dependent growth.

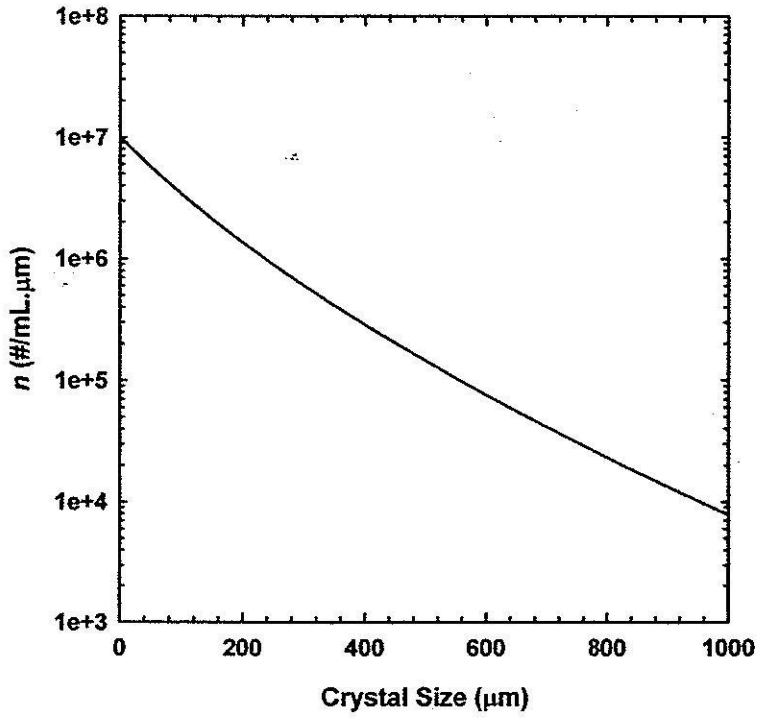

Fig 1.3 Population density for a MSMPR crystallizer with size dependent growth.

If nuclei form at discrete sizes, or if crystal growth rate dispersion occurs in the crystallizer, there will also be changes in the crystal population density distribution similar to those shown in Figure 1.3, although these mechanism can also be analyzed based on the measured crystal population density distribution.

The main difficulty to analysis of such data is that it is very difficult to determine whether any particular mixed continuous crystallizer really fits the assumptions required for the MSMPR crystallizer. Particularly, if the suspension is not well mixed, or if the product and sampling flows are not isokinetic (thus violating the mixed product removal condition) then the crystallizer will not operate as a true MSMPR crystallizer and the population density distribution will not be linear on the semilog plot even in the ideal case of size independent growth with no growth rate dispersion, and nucleation at zero size. This will result in an incorrect model of the crystal growth rates, and therefore incorrect designs of industrial crystallizers for the material.

Although it is commonly assumed that crystallizer in any tank stirred at a relatively high frequency will approximate a MSMPR crystallizer, this is not true: great care needs to be taken to ensure complete mixing of the suspension and the solution, uniformity of temperature in the crystallizer, and isokinetic sampling and product removal from the crystallizer. If these conditions are not met in the experimental crystallizer, then the data taken from the crystallizer will be spurious and incorrect models for the crystal growth rates and nucleation rates will be assumed. This will have serious consequences for the design of industrial crystallizers suing this data: incorrect data for crystal growth and nucleation rates leads to incorrect crystallizer volumes and residence times in the industrial crystallizer, leading to incorrect performance relative to the desired crystal size distribution and yield.

The most common failure in collection of growth rate data from continuous crystallizers is that the sampling and product removal from the tank is not performed isokinetically. It is easier to notice errors in mixing of the suspension because in incomplete suspensions there are crystals sitting on the bottom of the tank: in any case, agitation in the experimental crystallizers is typically high to ensure that mass transfer rates are not even partially crystallization rate determining. Usually the size of nuclei is very close to zero relative to average particle sizes in the vessel, and so the assumption of nucleation at zero size is typically very accurate.

Isokinetic sampling or product removal means that the outflow stream is removed at the same velocity as the stream flow at the point which it is sampled from, indicating that both the magnitude of the velocity and the direction of the flow must be the same at a point immediately outside the sampling tube and inside the sampling tube. The streamlines at the point of sampling the suspension should be straight, in order to avoid errors in sampling the crystal population. In the case of isokinetic sampling, the particles follow the streamlines, entering the sampling tube if, and only if, their path would have entered the area defined by the end of the sampling tube, thus resulting in a representative sample of the suspension at this point in the crystallizer. Since the crystallizer is fully mixed then this sample is also representative of any point within the crystallizer.

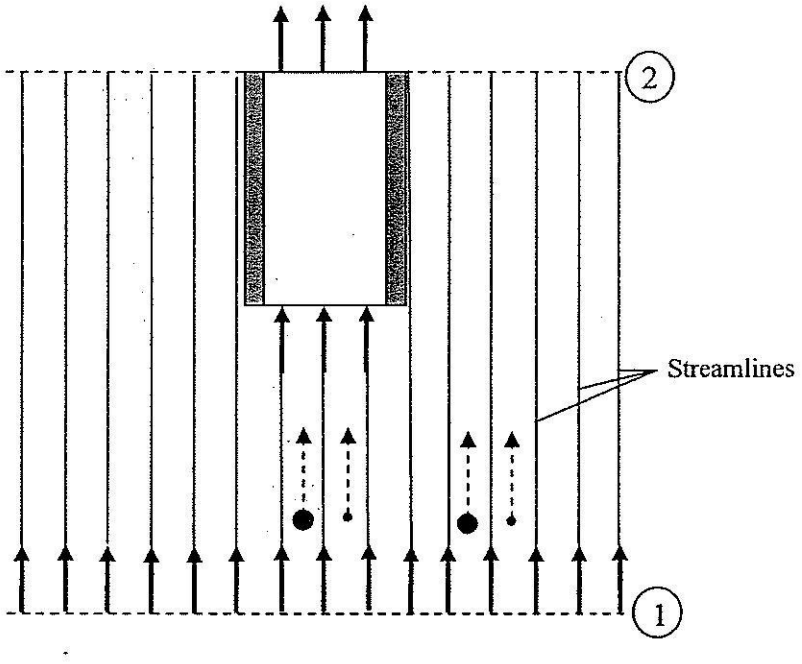

Fig. 1.4 Isokinetic sample from a point in a mixed crystallizer. Particles in an area normal to the end of the sampling tube will follow streamlines into the tube, while those particles outside this area will not be sampled.

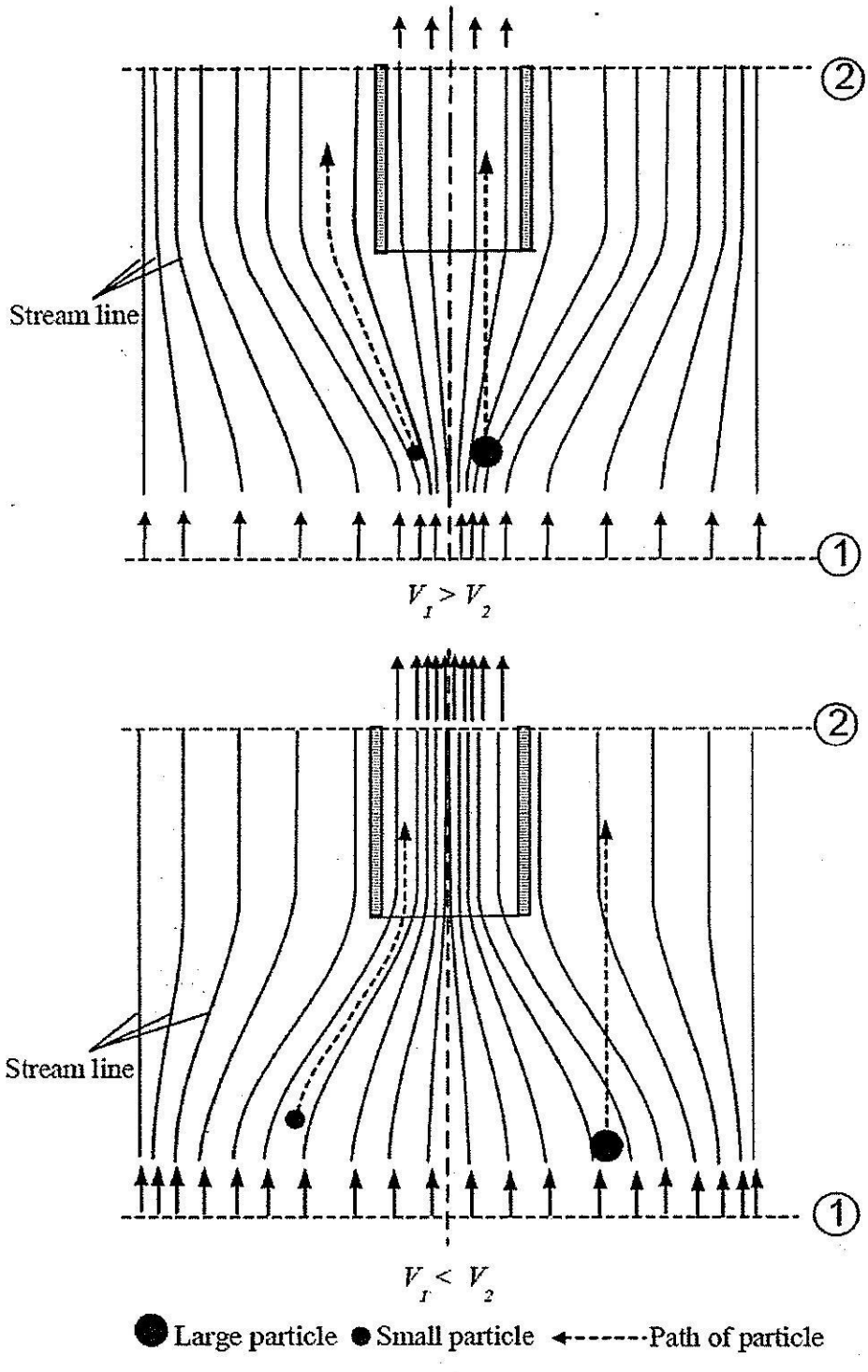

Fig 1.5 Schematic diagram of deviations from isokinetic sampling showing why non-isokinetic sampling results in incorrect measured particle size distributions. (Top) Insufficient sampling flow: (Bottom) Excessive sampling flow[2].

In order to achieve isokinetic sampling the streamlines at the point of sampling should be vertical. If this were not true then large and small particles would not follow streamlines due to the effect of gravity, with larger particles deviating from the streamline to a greater extent than small particles. Research crystallizers, and also most industrial crystallizers, are designed to force the streamlines to be vertical using a draft tube and baffles, creating a central zone where the streamlines flow downwards to a downflow impeller, and then pumped upwards in an area outside the drafttube where the sampling occurs.

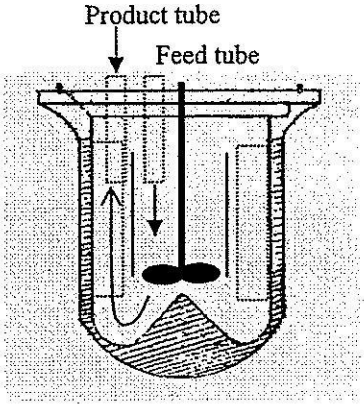

Fig 1.6 A mixed suspension crystallizer with a draft tube and vertical baffles to orient the streamlines so that the suspension can be sampled accurately.

1.2 Industrial Crystallizers

Industrial crystallizers come in a range of types, and although MSMPR crystallizers are used industrially they are not among the most common types: they are significant largely for their ability to accurately predict crystal growth and nucleation kinetics. These kinetics are essential for the design of the other types of crystallizers used in industry: without kinetic data it is impossible to design any crystallizer. The common types used for continuous crystallization from solution are shown in Figures 1.7 – 1.10.

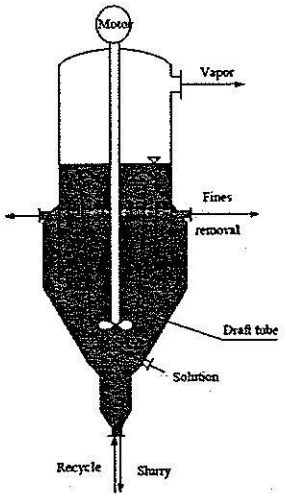

Fig. 1.10 Mixed suspension crystallizer with draft tube and fines removal.

1.3 Sugar Refining

Sucrose (table sugar) is one of the most important agricultural commodities in a number of countries, particularly those in the tropics. The total world production is currently in excess of 140 million tons per year, and the product is typically at 99% purity. Raw sugar is typically produced in regions that have significant areas of sugar cane (Brazil, Australia, South Africa, and Thailand, among others) or sugar beet (North America and Europe) production, and then exported to areas which have insufficient sugar supply in order to be processed into refined sugar, which is used as a domestic sweetener. It is possible to process directly to white sugar in beet producing regions.

Over the previous 5 years, Thailand has had an average yearly production of 6.17 million tons per year, consumption of 1.81 million tons per year, and has exported 4.38 million tons per year, making Thailand the second largest sugar exporting country in the world (behind Brazil). Unfortunately the price of bulk sugar on the world market dropped significantly over the previous decade (from US$0.17/lb in 1995 to US$0.082/lb in 2005) because of an increase in production by Brazil, and sugar export subsidies and agricultural support programs in the developed world, however this trend is reversing as Brazil uses more sugar production to create biofuels, particularly ethanol.

Crystallization is an essential step in the processing of sugar, and occurs several times in both the raw sugar and refined sugar manufacturing processes. The crystallization may be performed in either batch or continuous crystallizers, or a mixture of both types

(for instance batch vacuum pans followed by continuous plug flow crystallizers). In the design of any type of crystallizer, the crystal growth and nucleation kinetics must be known accurately in order to achieve a suitable crystallizer design. Before the crystallization occurs there are a number of steps to extract the juice from the cane, to purify the juice, and to concentrate the juice to a concentration suitable for aqueous crystallization. A typical flowchart for the raw sugar manufacturing process is given in Figure 1.11[3].

1.4 Sugar Crystallization

Crystallization of sucrose, as with other species, crystallizes from solution when its concentration is greater than the saturation point. The saturation point depends strongly on temperature, but only very weakly on pressure, and may be considered constant with respect to pressure unless the pressure is very high. The concentration of sucrose at the saturation point is very high, leading supersaturated aqueous solutions of sucrose to have very high viscosities. The solubility of sucrose in aqueous solutions as a function of temperature is shown in Figure 1.12.

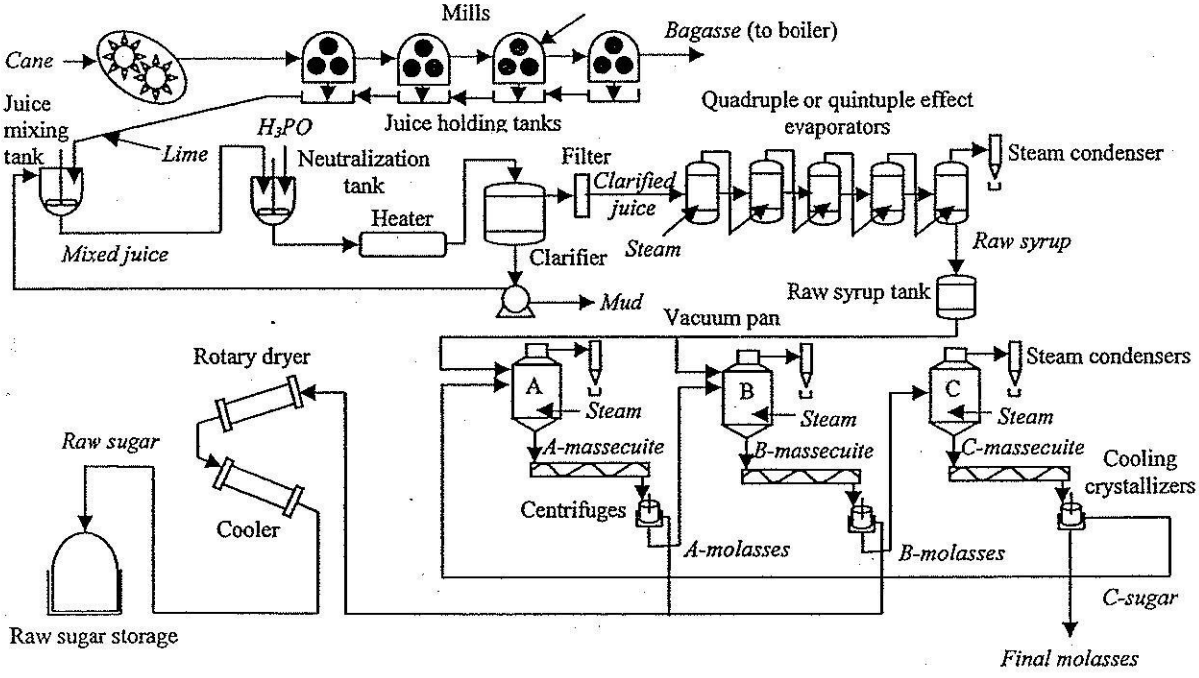

Fig. 1.11. Flowchart of a typical industrial process to crystallize raw sugar starting from sugar cane[3].

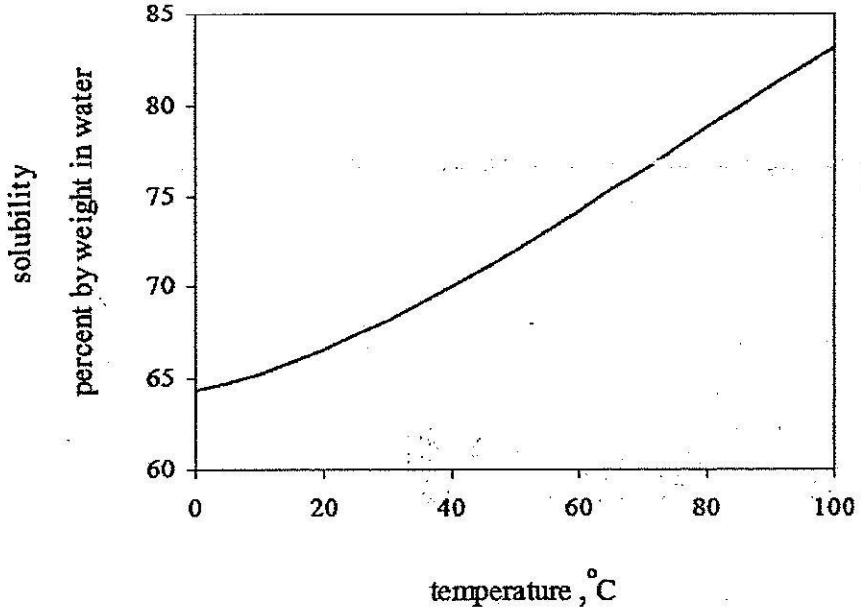

Fig. 1.12 Solubility of sucrose in aqueous solution as a function of temperature[4].

The sucrose molecule is a disaccharide sugar, composed of one moiety of glucose and one moiety of fructose connected together via a glycosidic bond. The chemical structure of sucrose is shown in Figure 1.13.

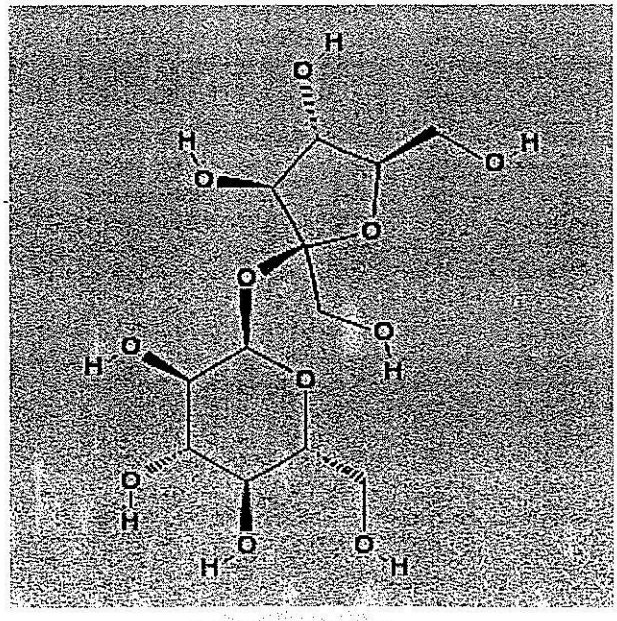

Fig. 1.13 The chemical structure of sucrose (from PubChem: US National Institute of Health).

The crystal form of sucrose is monoclinic, and there are two sucrose molecules in the unit cell. Many crystallographic faces are evident on the surface of the sucrose crystal, and the size of each face varies slightly with the temperature of the crystallizer, the concentration in the crystallizer, and any impurities present in the crystallizer. Figure 1.14 shows a schematic diagram of a typical sucrose crystal.

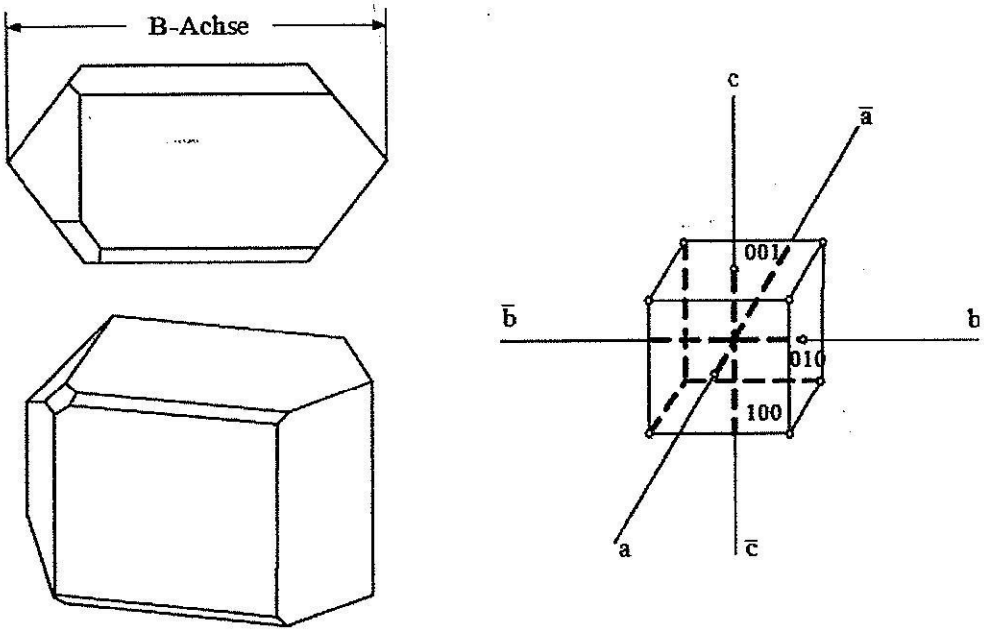

Fig. 1.14 Schematic diagram of a typical sucrose crystal showing the commonly seen faces.

The concentration of such crystals in an industrial crystallizer is very high (in the order of millions of crystals per cubic meter), however since the crystal are typically quite small, or the order of 0.1 mm, the suspension density is typically not high.

Chapter II

CFD Theory Used in the Current Study

2.1 Introduction

In industrial crystallizers there are often three phases; liquid (mother liquor), vapor (water vapor), and crystalline solids. However, the experimental MSMPR crystallizers for the determination of growth and nucleation kinetics are typically run as isothermal crystallizers, with supersaturation generated by cooling the solution from a saturation condition down to the temperature of the isothermal crystallization before initiating the crystallization, rather than boiling off the solvent during the crystallization. This means that the heat equations are not required, and that the crystallizer can be modeled as a two phase system. If the suspension density (defined as the mass of crystal per unit volume of crystallizer) is low, then it can be assumed that the solid phase has negligible effect on the liquid phase flow, and it can be neglected. If a more exact description of particle flowlines is required it is possible to do this using the two-phase simulation results and using a Lagrangian model for the particles. A model of the MSMPR crystallizer used in the Crystallization Technology research group at Suranaree University of Technology was studied using the CFD modeling software ANSYS CFX-4.5 and CFX-5.5.1. A three dimensional (3D) geometry was used in the simulations in order to account for the strong 3D element of the flow.

The aim of this chapter is to show the mathematical models in the CFD software used that describe the physical phenomena that are significant in industrial crystallizers. Not all equations presented here are written in the form used by the ANSYS CFX program: see ANSYS CFX-4.5 Manual, ANSYS Canada Ltd.[5]. It should be noted that as the experimental crystallizer being studied is an isothermal one, there is no necessity for solution of the heat equation in the system, and it will not be discussed further. In the study it was determined that it was not necessary to simulate both phases in the system since the suspension densities in the crystallization runs were quite low and the crystals relatively small, meaning that crystals followed the liquid streamlines in the crystallizer, and the crystals in the suspension had negligible effect of the fluid flow field. In addition it was determined through simulations that the fluid flow was laminar throughout the vessel, except possibly in a small region very close to the impeller, so turbulence theory was also not used in final simulations (to reduce the model complexity and run time without loss of

accuracy in this instance). However the two phase theory and turbulence theory applied in the program will be discussed, as runs were performed to show their change to the result was negligible.

2.2 Mathematical Models

In this section, the governing equations of fluid flow, and other phenomena required are described as they appear in the commercial CFD package used (CFX-5.5).

2.2.1 The Continuity equation

The full form of this equation is shown in concise form below for a single phase, single component system (or a system that can be modeled as a single component)

$$\frac{\partial \rho}{\partial t} + \nabla \bullet (\rho \mathbf{U}) = 0 \qquad (2.1)$$

where ρ and $\mathbf{U}$ respectively represent the density and cartesian velocity component of the fluid.

3.2.1.2 The momentum equation

The full form of this equation is shown in concise form below

$$\frac{\partial}{\partial t}(\rho \mathbf{U}) + \nabla \bullet (\rho \mathbf{U} \otimes \mathbf{U}) = -\nabla p + \rho \mathbf{g} + \nabla \bullet \mu \left(\nabla \mathbf{U} + (\nabla \mathbf{U})^T \right) + S_M \qquad (2.2)$$

where

S_M describes a user defined momentum source, p is the static pressure, and μ is the viscosity of the fluid.

Since the simulations are isothermal, and the system is at steady state with no phase change, the previous equation becomes

$$\nabla \bullet (\rho \mathbf{U} \otimes \mathbf{U}) = -\nabla p + \rho \mathbf{g} + \nabla \bullet \mu \left(\nabla \mathbf{U} + (\nabla \mathbf{U})^T \right) + S_M \qquad (2.3)$$

If there is more than one phase in the system (as in the case of systems having discrete (bubble) vapor phase or solid particles, then the continuity and momentum phases have to be written for each phase using a suitable volume fraction for each phase, as well as interphase transfer equations. Full details are given in the CFX 5.5 user manual.

3.2.1.5 Momentum sources

Sources are optional terms which may be attached to most equations, so as to model additional or specialized physical processes. In this work, the volume defined by a subdomain is represented as the impeller and this creates a momentum source that may have components in any direction. Based on an analysis of how the terms in the momentum source affected the flow near the outflow tube it was decided to

In the ANSYS CFX program, the user must specify directly in term of a momentum source value per unit volume of subdomain in a specified direction. A source can be specified for y-direction as follows:

$$\mathbf{S}_{M,y} = S_{spec,y}\mathbf{j} \tag{2.4}$$

where the $S_{spec,y}$ is the specified momentum component, as shown below:

$$S_{spec,y} = \frac{F_{net,y}}{V} = \frac{P_{net,y}}{U_{net,y}V} \tag{2.5}$$

where P is the power. This momentum source has dimensions of $ML^{-2}T^{-2}$ (e.g. $kg/m^2/s^2$). Considering Figure 3.1, the relationship between force and fluid velocity can be written as:

$$F_{net,y} = \rho A U^2 \tag{2.6}$$

where V and A respectively represent the volume of subdomain and cross-sectional area normal to the flow.

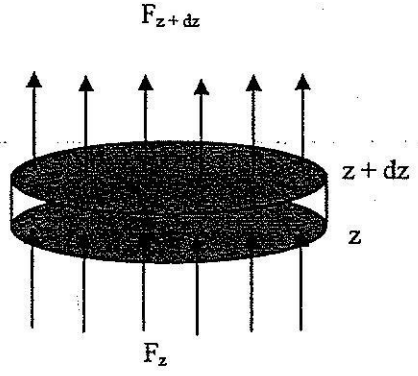

Fig. 3.1 A subdomain created to apply a momentum source.

3.2.1.7 Turbulence model

The turbulence models seek to solve a modified set of transport equations by the introduction of averaged and fluctuating components. A velocity $\mathbf{U}$ may be divided into an average component, $\overline{\mathbf{U}}$, and a time varying component, **u**.

$$\mathbf{U} = \overline{\mathbf{U}} + \mathbf{u} \tag{2.7}$$

The averaged component is given by:

$$\overline{\mathbf{U}} = \frac{1}{\Delta t}\int_{t}^{t+\Delta t} \mathbf{U} dt \tag{2.8}$$

where *dt* is a time scale that is large relative to the turbulent fluctuations, but small relative to the time scale to which the equations are solved. Substituting the time averaged quantities into the original transport equations (equations 2.1-2.3) results in the Reynolds-averaged equations given below. Note that the continuity equation (equation 2.3) has not been altered.

The momentum equation for the fluid is:

$$\nabla \bullet (\rho \mathbf{U} \otimes \mathbf{U}) = -\nabla p + \rho \mathbf{g} + \nabla \bullet \mu \left[\left(\nabla \mathbf{U} + (\nabla \mathbf{U})^T \right) - \rho \overline{\mathbf{uu}} \right] + S_M \tag{2.9}$$

Where $\rho \overline{\mathbf{uu}}$ represents the Reynolds stress.

In inhomogeneous multiphase flow, bulk turbulence equations are solved which are the same as the single phase equations; this means that a single turbulence field is solved using a single turbulence model. In this work, the turbulence was treated using the $k-\varepsilon$ model where both phases share the same values for k and ε (Micale and Montante, 1999). In this model, the Reynolds stresses is given (Chung, 2002)

$$-\rho \overline{\mathbf{uu}} = -\frac{2}{3} \rho k \delta + \mu_t \left(\nabla \mathbf{U} + (\nabla \mathbf{U})^T \right) \tag{2.10}$$

where μ_t is the eddy viscosity or turbulent viscosity. So that the equations (3.37) and (2.10) becomes

$$\nabla \bullet (\rho \mathbf{U} \otimes \mathbf{U}) = -\nabla p + \rho \mathbf{g} + \nabla \bullet \mu_{eff} \left[\left(\nabla \mathbf{U} + (\nabla \mathbf{U})^T \right) \right] + S_M \tag{2.11}$$

where μ_{eff} is the effective viscosity accounting for turbulence given by

$$\mu_{eff,c} = \mu_c + \mu_t = \mu_c + \mu_{tc} + \mu_{tb} \tag{2.12}$$

The turbulent viscosity of liquid phase is based on the $k-\varepsilon$ model and formulated as follows:

$$\mu_{tc} = C_\mu \rho_c \frac{k^2}{\varepsilon} \tag{2.13}$$

where $C_\mu = 0.09.$ The term μ_{tb} is particle induced eddy viscosity. There are several models available to take account of this viscosity. In this work the model proposed by Sato and Sekoguchi (1975) was used:

$$\mu_{tb} = C_{\mu b} \rho_c r_d d|U_d - U_c| \tag{2.14}$$

with $C_{\mu b}$ a model constant which equals 0.6 (Deen, Solberg, and Hjertager, 2002).

Special consideration is required for flow near a no-slip wall, where there are strong gradients in the dependent variables. The near-wall region can be subdivided into two layers .In the very near the wall, the layer is called the "laminar (viscous) sublayer", where the molecular viscosity plays a dominant role in momentum and heat transfer. Further away from the wall, in the "logarithmic layer", turbulence dominates the mixing process. Moreover, between the viscous sublayer and logarithmic layer, there is the "buffer layer", where the effect of molecular viscosity and turbulence are of equal importance. Figure 3.2 shows these subdivisions of near-wall region.

The logarithmic profile is reasonably assumed the velocity distribution near the wall; this provides a means to numerically compute the fluid shear stress as a function of the velocity at a given distance from the wall. This is known as a "wall function" and the logarithmic nature gives rise to the well known "log law of the wall'.

In this work the scalable wall function is conducted to model the flow near the wall, this function was developed by ANSYS CFX.

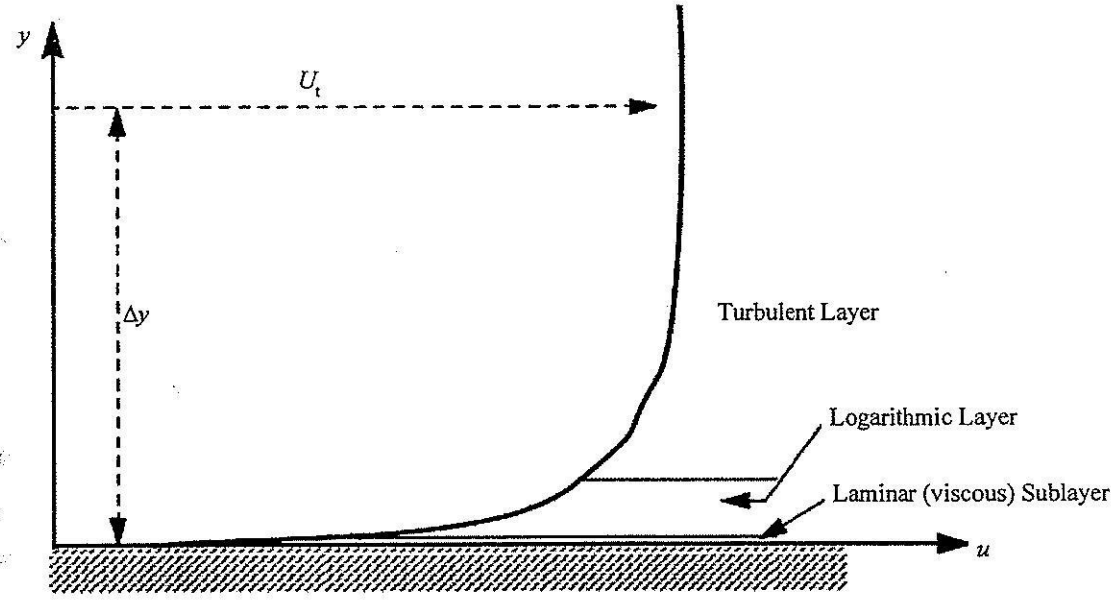

Fig. 3.2 Flow regions for describing turbulent flow near a wall. (ANSYS Canada Ltd., 2005).

The logarithmic relation for the near wall velocity is given by:

$$u^+ = C_\mu^{1/4} k^{1/2} \tag{2.15}$$

The friction velocity is given by:

$$u_\tau = \frac{U_t}{\frac{1}{\kappa}\ln(y^+) + C} \tag{2.16}$$

The absolute value of the wall shear stress is then obtained from:

$$\tau_\omega = \rho u^+ u_\tau \tag{2.17}$$

where U_t is the known velocity tangent to the wall at a distance of Δy, $\kappa = 0.41$ (von Karman constant or kappa coefficient), $C = 5.2$, and $y^+ = (\rho u^+ \Delta y)/\mu$ (dimensionless distance from the wall). Note that the minimum y^+ is 11.06.

Chapter III

Ensuring the Accuracy of the Computation Fluid Dynamics Program

A number of simulations were performed of isothermal systems with incompressible flow (as in the case of the MSMPR crystallizer) to test the accuracy of the CFD software used, and to check the performance and use of features such as the momentum source term, which are needed in the MSMPR simulation. This was done to ensure that the simulations performed to model the isothermal MSMPR crystallizer were accurate, and modeling the system as intended (for instance that the momentum source term feature was a suitable method of modeling an impeller). A number of test cases were performed, with each case being described as a sub-section of the current chapter.

Flow Over a Semi-Infinite Smooth Plate (The Blasius Problem)

The laminar flow of an isothermal incompressible (or equally valid, non-compressed) fluid over a flat plate is a problem of great significance in fluid dynamics, and one for which there can be found an exact solution. The exact solution to the problem (and its derivation) can be found in a number of texts in fluid dynamics, and in course notes on the subject on the internet. The system being modeled consists of an isothermal incompressible fluid flowing a constant velocity (such that its flow is in the laminar regime) meeting a flat plate at $x = 0$, and considers a 2-dimnensional (2-D) flow. At the surface of the plate a zero-slip boundary condition holds, creating a boundary layer (considered as the layer where the velocity is less than 99% of the velocity at infinite distance from the plate). A schematic diagram of the system simulated for a particular inlet velocity (70.36 m/s) is shown in Figure 3.1.

The Blasius solution is a 2-D problem, whereas the program CFX-5.5 performs 3-dimensional simulations. In order to achieve a simulation of the Blasius problem the width of the simulated area was made to be 1 mesh in width. The fluid density was considered to be 1.019 kg/m^3 and the viscosity to be 2.06×10^{-5} kg/m·s. The pressure in the simulation was 101.325 kPa (atmospheric pressure), and before the front of the plate, the uniform velocity was 70.63 m/s.

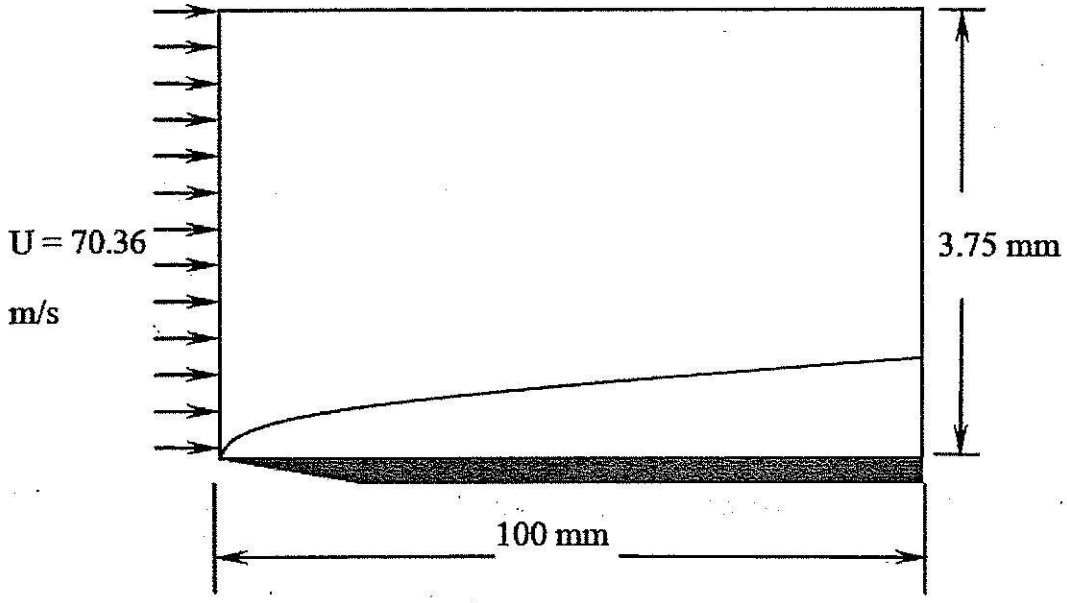

Fig. 3.1 Diagram of the first system for confirmation of the accuracy of the CFD program. The system consists of one dimensional flow of 3.75 mm thickness across a flat sheet of length 100 mm.

The solution to the problem was found through simulations be CFX-5.5 until a grid-size independent result was found. The velocity vectors derived from the solution are shown in Figure 3.2, which demonstrates the development of the boundary layer, which occurs after a short distance from the front of the plate.

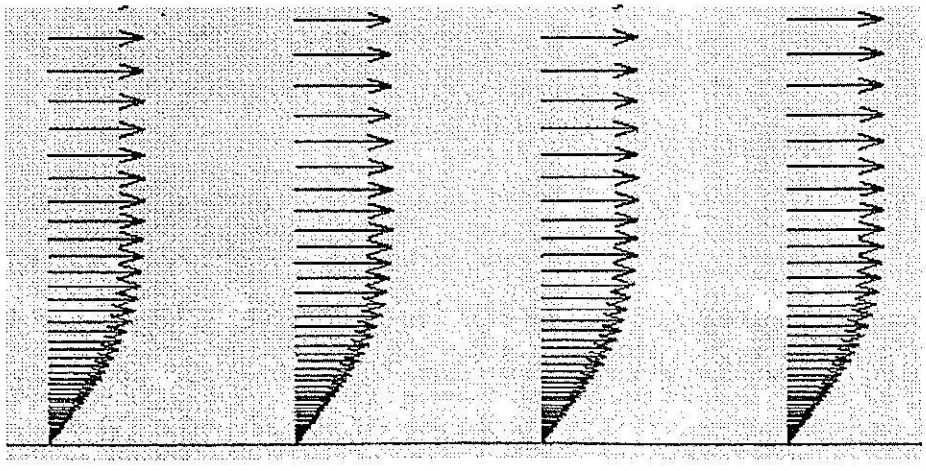

Fig. 3.2 Diagram displaying the velocity vectors for the flow in the system shown in Fig. 3.1.

A comparison between the theoretical solution of the equations describing the system and the prediction from the CFD solution is shown in Figure 3.3.

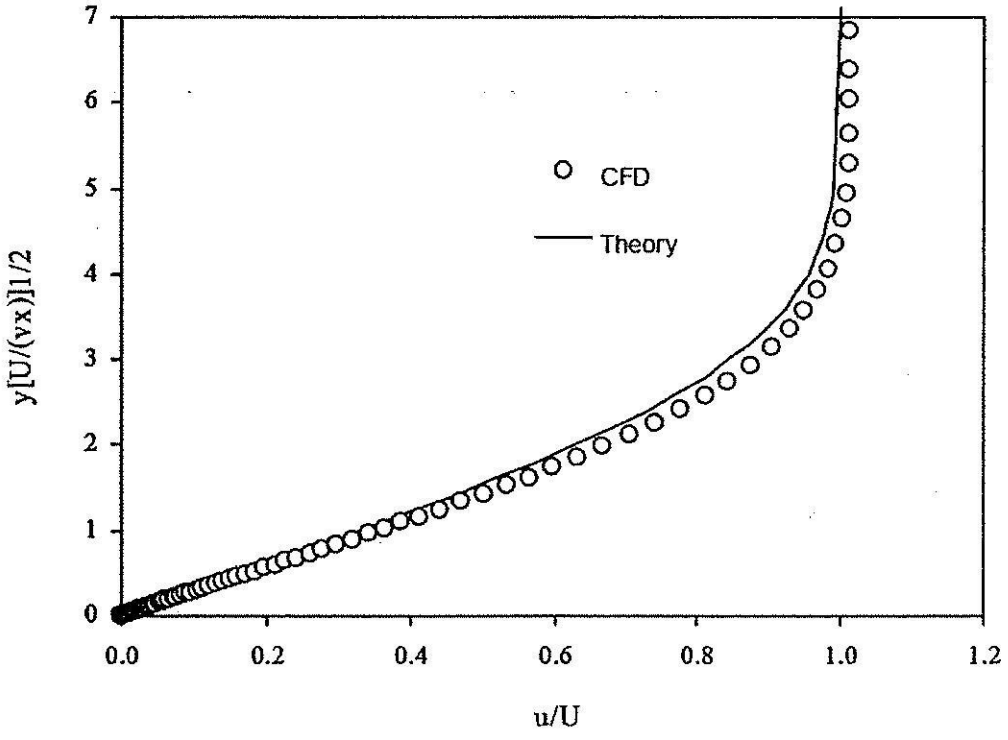

Fig. 3.3 A comparison between the solution of the Blasius system (in dimensionless form) and the CFX solution for the system.

Low-Velocity Flow Between Two Flat Plates Due to a Pressure Gradient

The low-velocity flow between two flat plates due to a pressure gradient can be solved analytically, giving the following solution

$$u = -\frac{dP}{dx}\frac{h}{2\mu}\left(1-\frac{y^2}{h^2}\right)$$

The fact that there is an analytical solution to the problem makes it suitable for checking the accuracy of the CFD code. The solution was studied for the flow of air at a pressure of 1 atmosphere and 20 °C between two plates which are 10 mm apart. The distance of flow studied by CFD was 500 mm, which was chosen so that the flow was free of end effects. The pressure differential along the length was 0.162 Pa. The basic

momentum transfer problem is two-dimensional, however only three-dimensional problems can be studied with CFX 5.5. In order to produce a three-dimensional problem the width of the simulation was set at 2 mm, which is equivalent to two mesh in this direction. Only half of the solution needs to be calculated due to the symmetry plane at the centerline between the two plates. A diagram of the system is shown in Fig. 3.4.

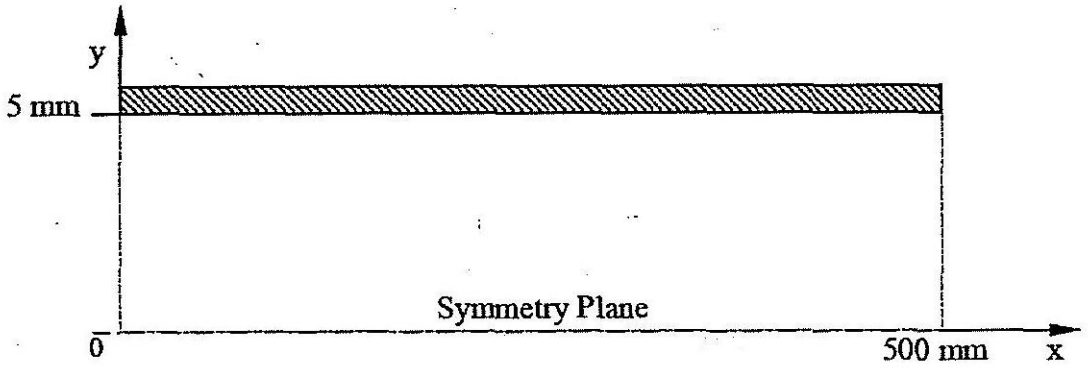

Fig. 3.4 Low velocity flow between two flat plates due to a pressure gradient. The system studied has a gap of 10 mm, and a length of 500 mm.

The solution to the problem as determined by CFX-5.5 is shown in Fig. 3.5. Here, the solution is shown near the downwind end of the system, in order to see the solution in the absence of the end effects. The velocity profile is clearly parabolic, as in the theoretical solution, however it is necessary to confirm that the maximum velocity corresponds to that predicted by the pressure gradient, fluid viscosity, and distance between the plates.

The change in the pressure along the system for the CFX-5.5 solution is shown in Fig. 3.6. It is clear that (as predicted from the analytical solution) the pressure gradient is essentially constant along the length of the system. The only exception to the constant pressure gradient occurs very close to the inlet of the system: the deviation here may be due to effects relating to the meshing at very small distances from the inlet, or to end effects related to boundary conditions assumed for the flow.

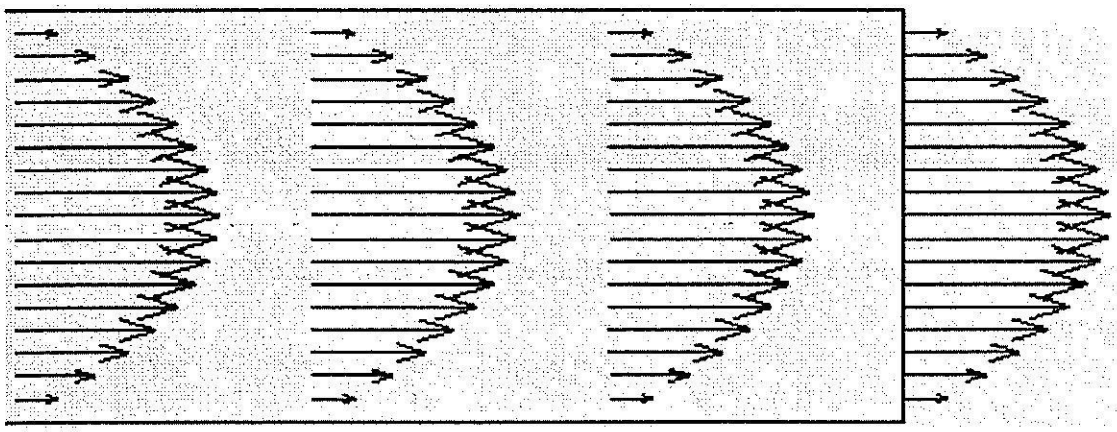

Fig. 3.5 The CFX-5.5 solution for low velocity flow between two flat plates due to a pressure gradient. The system studied has a gap of 10 mm, and a length of 500 mm.

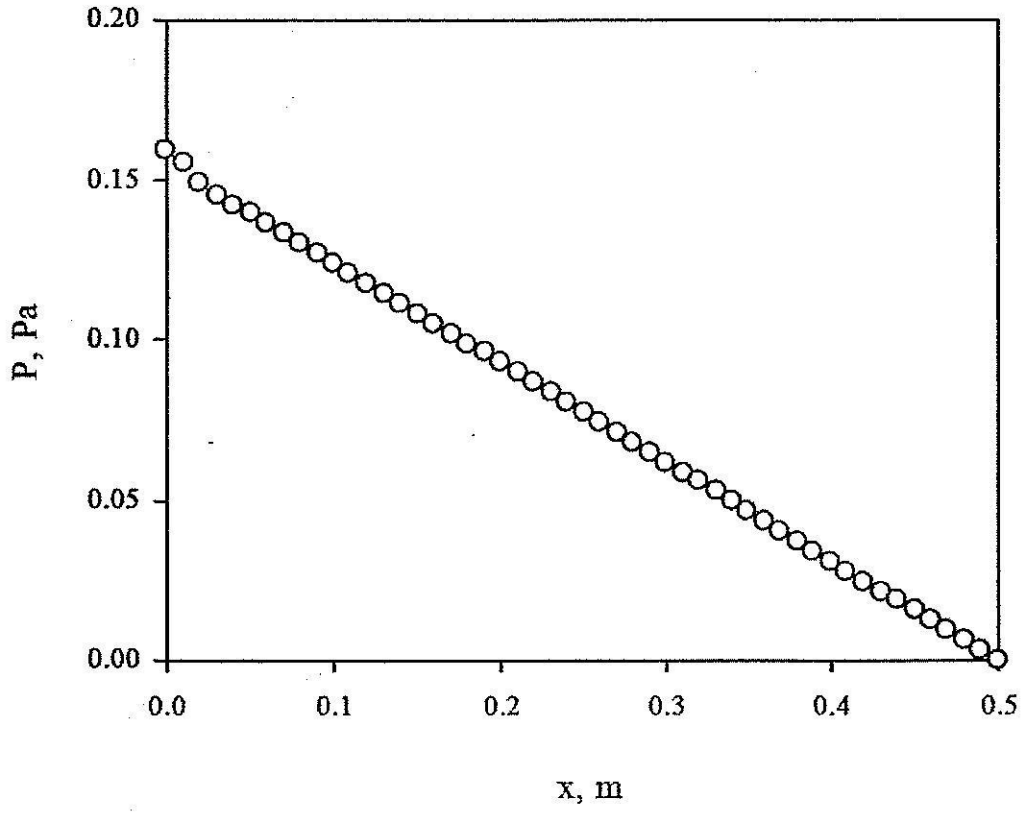

Fig. 3.6 The pressure gradient determined from CFX-5.5 solution for low velocity flow between two flat plates. The system studied has a gap of 10 mm, and a length of 500 mm.

The most important check of the solution relative to the applications we are using is the check of the velocity profile for the fluid in the gap between the two plates. The solution near the end of the flow determined from CFX-5.5 is compared to the analytical solution in Fig. 3.7. The comparison between the theoretical and the CFD solution shows that CFX-5.5 is able to describe the velocity in the system to a high degree of accuracy using the mesh size used in the solution: there is no discernable error in the velocity profile determined by CFX-5.5 in this problem.

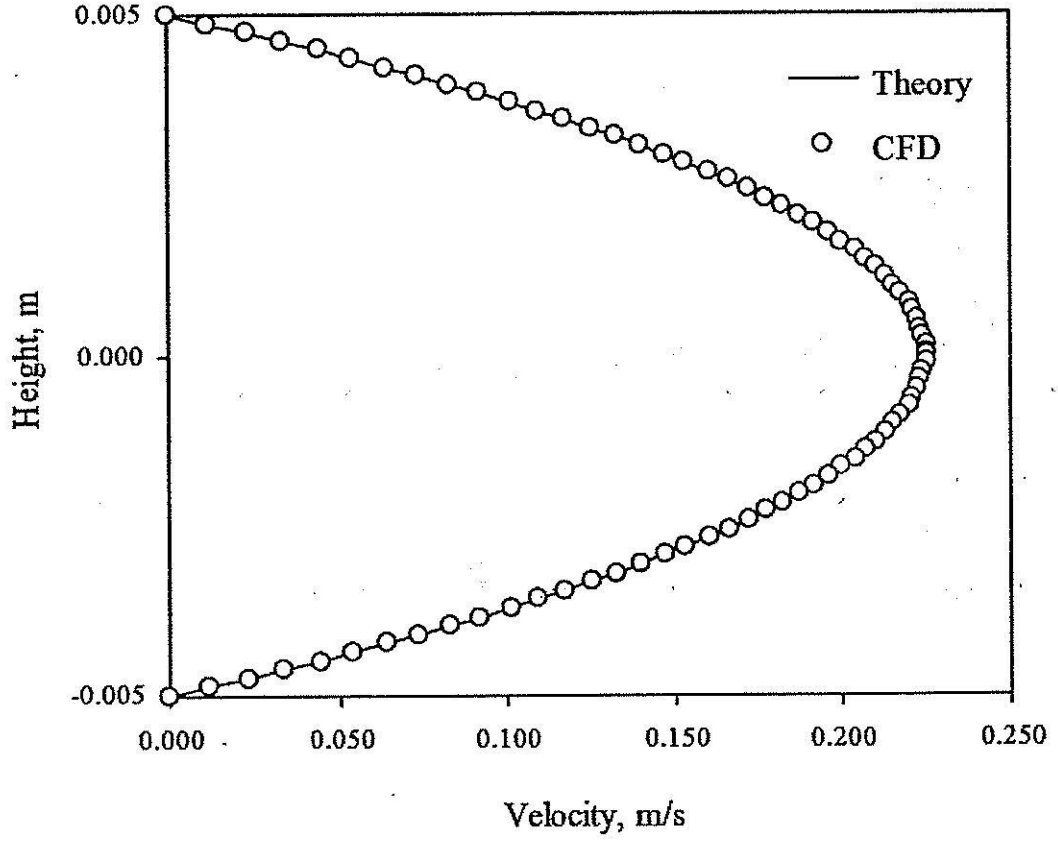

Fig. 3.7 The velocity gradients based on the theoretical solution and determined from the CFX-5.5 solution for low velocity flow between two flat plates. The system studied has a gap of 10 mm, and a length of 500 mm.

Pipeflow at Low Velocity Due to a Pressure Gradient

The next system studied to determine the accuracy of the CFD program was the flow of air through a pipe, for which there is also an analytical solution. The solution is given by the function

$$u = -\frac{dP}{dx}\frac{1}{4\mu}\left(R^2 - r^2\right)$$

Where the symbols are defined as before, and R and r represent the radius of the tube and the radial position of the location the velocity is being predicted for respectively. The conditions representing the fluid in the system are identical to that in the previous case study, i.e. air at 20°C and 1 atmosphere. A schematic diagram of the system is shown in Fig. 3.8, which shows a cross-section of one half of the tube. The second half of the tube can be modeled using a symmetry plane.

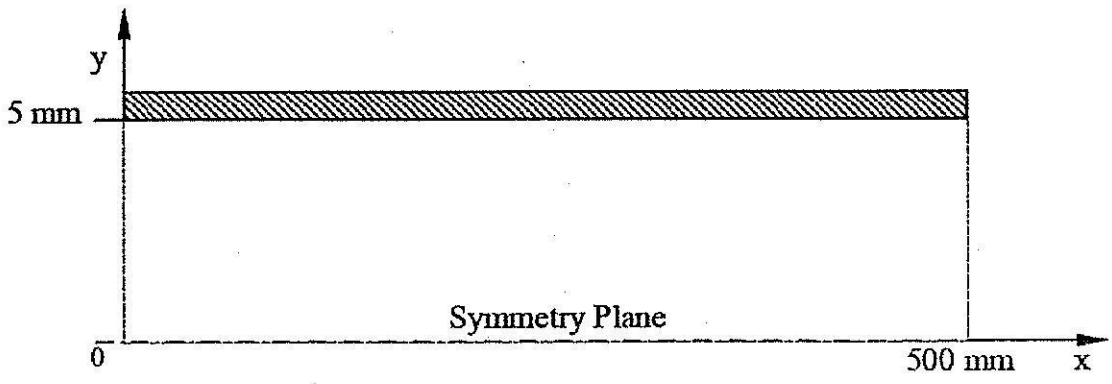

Fig. 3.8 Low velocity flow in a tube due to a pressure gradient. The system studied has a radius of 5 mm, and a length of 500 mm.

The velocity vector plot near the end of the tube for the CFX-5.5 solution is shown in Fig. 3.9. Again, it is clear that the velocity profile is parabolic as a function of the radial distance from the center of the tube, as in the theoretical solution for the problem. The predicted pressure gradient as a function of distance is shown in Fig. 3.10. Again, the pressure gradient is constant along the length of the tube, with the exception of a very small change very close to the start of the tube. The reasons for this are the same as given in the previous case study. These results show that the predicted solution for the flow is likely to be in very good agreement with the theoretical result.

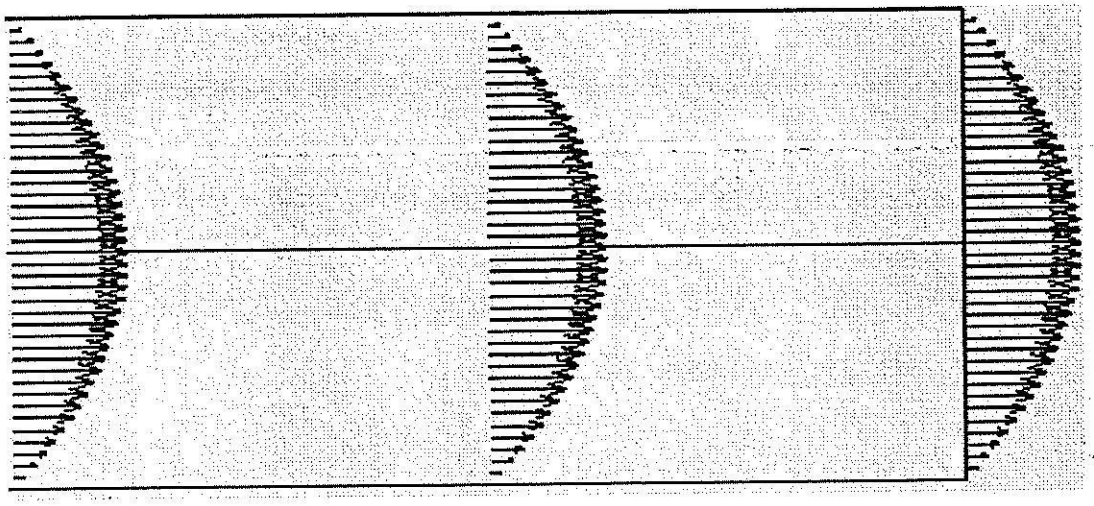

Fig. 3.9 The CFX-5.5 solution for low velocity flow in a tube due to a pressure gradient. The system studied has a radius of 5 mm, and a length of 500 mm.

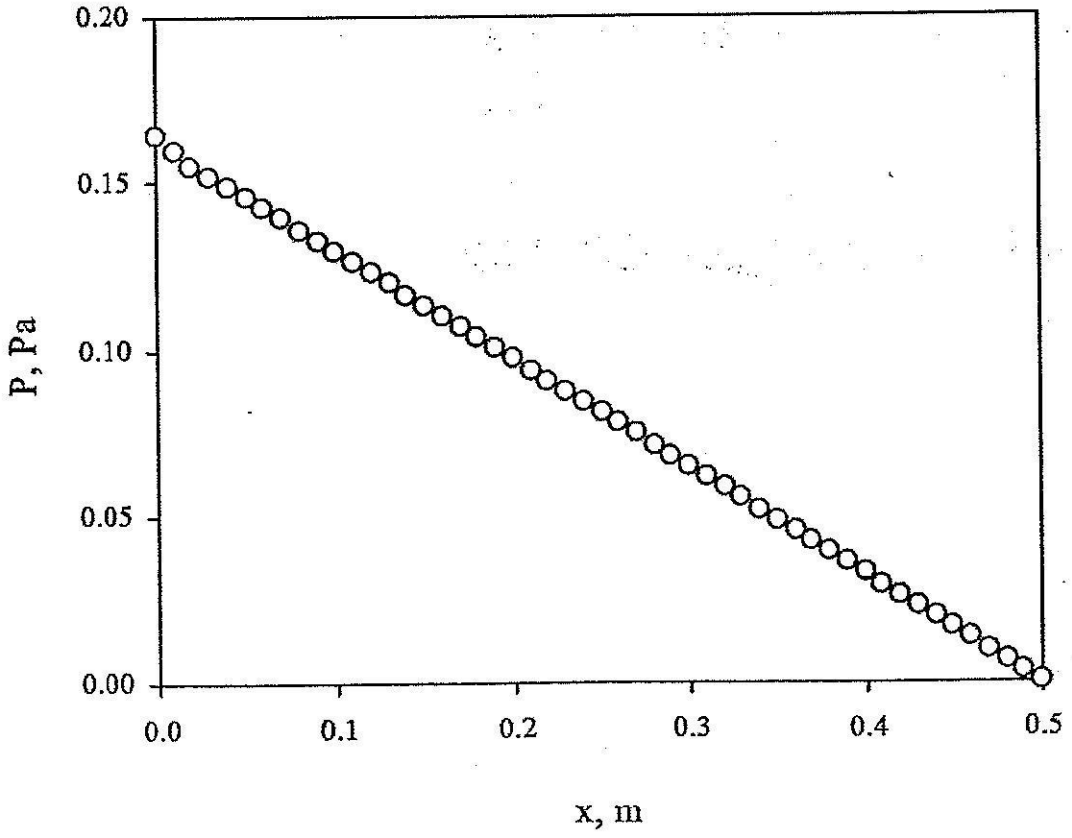

Fig. 3.10 The pressure gradient determined from CFX-5.5 solution for low velocity flow in a tube. The system studied has a radius of 5 mm, and a length of 500 mm.

Again, the most suitable comparison between the theoretical and CFD solutions is the velocity profile across the tube: this is shown in Fig. 3.11 for both the analytical solution and the CFD prediction via CFX-5.5. Again, the agreement between the analytical and predicted solutions is excellent.

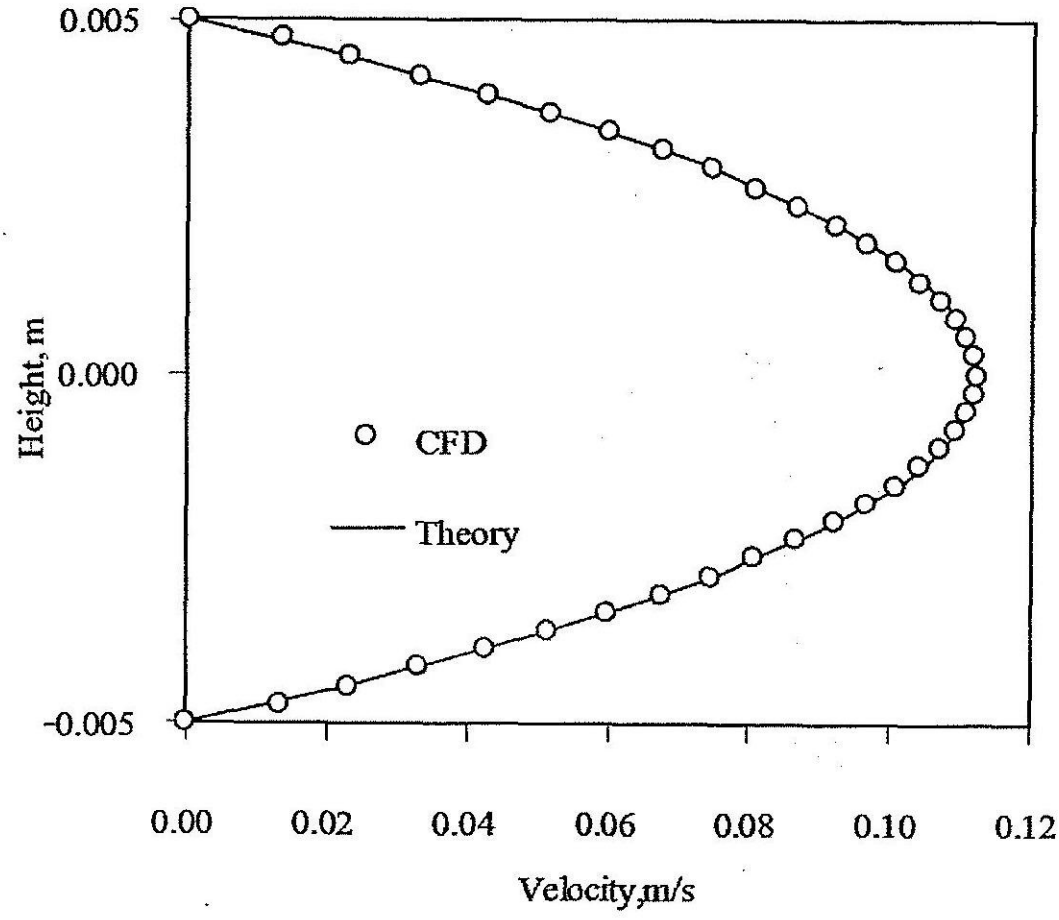

Fig. 3.11 The velocity gradients based on the theoretical solution and determined from the CFX-5.5 solution for low velocity flow in a tube. The system studied has a radius of 5 mm, and a length of 500 mm.

Flow in a Tube with a Contraction

It is also important to determine if the CFD program can deal with sudden changes in the geometry of the system, which often occur in industrial processing equipment. A tube of length 10.1 inches, and radius 1 inch was modeled with a contraction of width 0.1 inch occurring in one half of the tube, at a position halfway along the length of the tube.

The conditions were otherwise similar to the previous example, with a inlet pressure of 0.16 Pa in comparison with a reference pressure at the outlet of 0 Pa. A schematic diagram of the system is shown in Fig. 3.12.

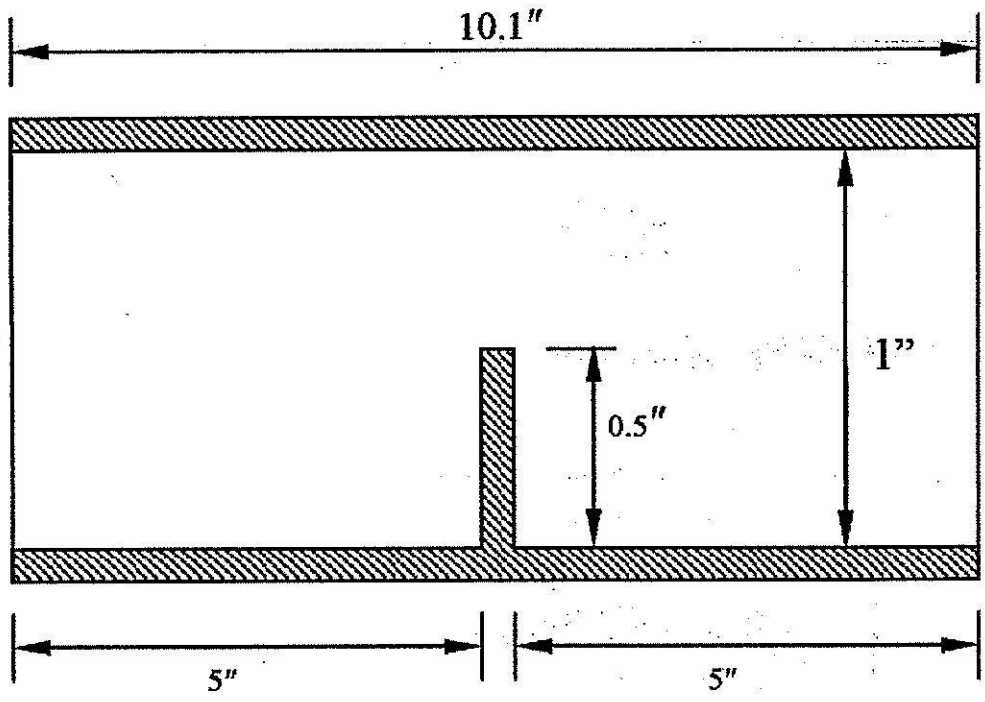

Fig. 3.12 Low velocity flow in a tube with a contraction, due to a pressure gradient. The system studied has a radius of 0.5 inch and a length of 10.1 inch.

In this instance there is no convenient theoretical model that can represent an analytical solution to the system, although it is useful to observe the CFD solution to the problem to check that it is consistent with known properties in such a system, particularly with respect to the flow characteristics in the system, and the pressure drop across the constriction.

The results of the CFD study of the system are shown in Fig. 3.13 to 3.16. Fig. 3.13 shows the pressure distribution along the centerline of the tube as a function of radial position in the tube and distance from the inlet. It is clear from the solution that the majority of the pressure drop in the system occurs at the position of the constriction as the fluid is forced into the top half of the tube. There is also a volume behind the constriction

that has a pressure lower than that of the outlet, creating a circulation loop behind the constriction.

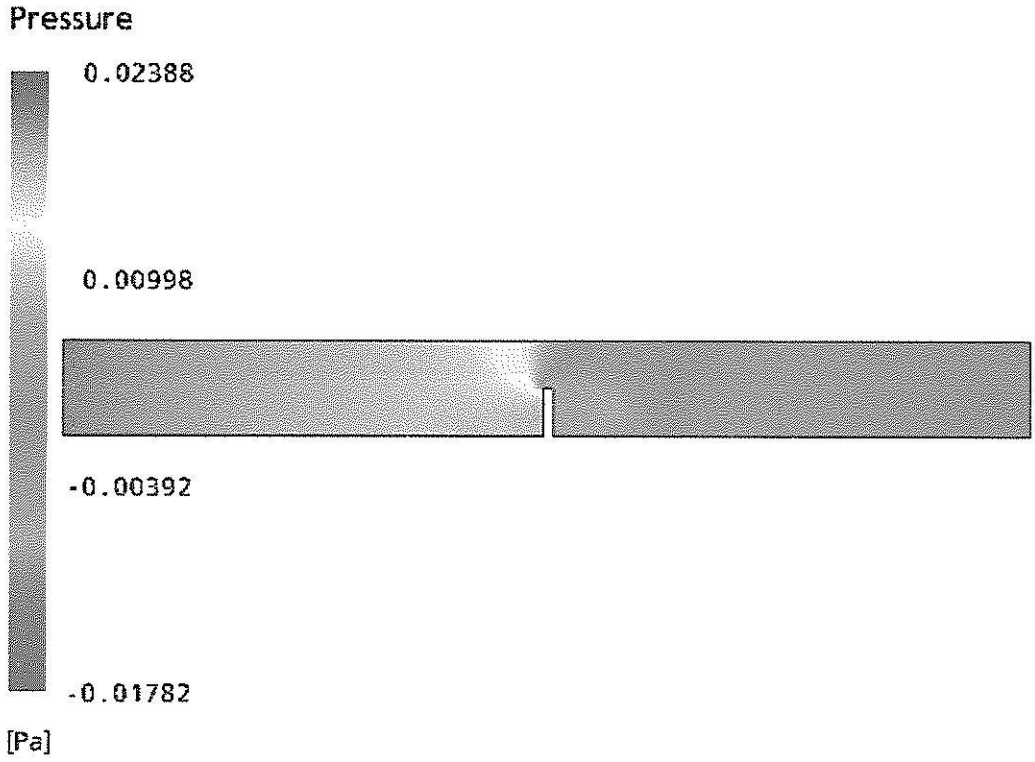

Fig. 3.13 Pressure distribution from the CFX-5.5 solution for low velocity flow in a tube past a constriction. The system studied has a radius of 1 inch and a length of 10.1 inch. The constriction has a thickness of 0.1 inch.

Fig 3.14 shows a magnified section of the tube around the position of the contraction to better visualize the effect of the constriction of the fluid. The pressure drop is quite substantial, starting well before the constriction in the top section of the tube. In the bottom section of the tube there is a slight increase in the pressure as the fluid interactions with the wall of the constriction. There is a low pressure zone in a small volume immediately above the constriction and also for a significant distance behind the constriction due to the circulation in that area.

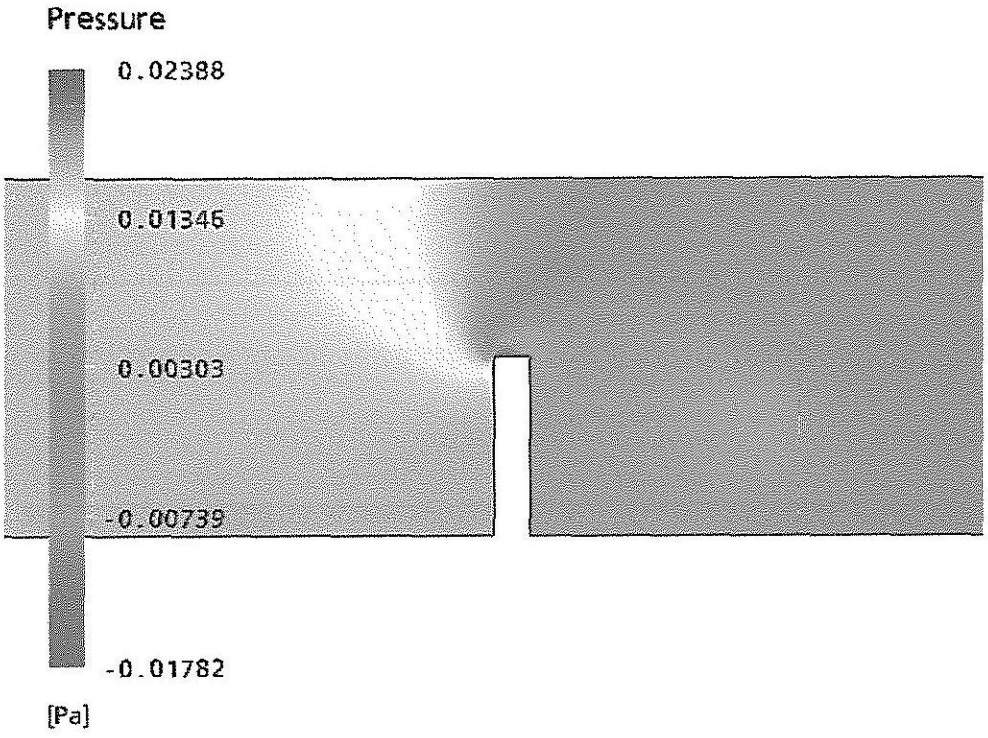

Fig. 3.14 Magnified plot of the pressure distribution near the constriction for low velocity flow in a tube past a constriction. The system studied has a radius of 1 inch and a length of 10.1 inch. The constriction has a thickness of 0.1 inch.

The plot of the velocity vectors for the flow is also interesting: this plot is shown in Fig. 3.15. The constriction forces the fluid upwards in the volume immediately before the constriction, which accelerates the fluid past the constriction causing a significant pressure drop. After the constriction the fluid expands again causing a reduction in the average flow velocity. In the section immediately downstream from the constriction there is a flow loop caused by the low pressure region behind the constriction. The flow behaves as is expected (and has been measured) in similar systems.

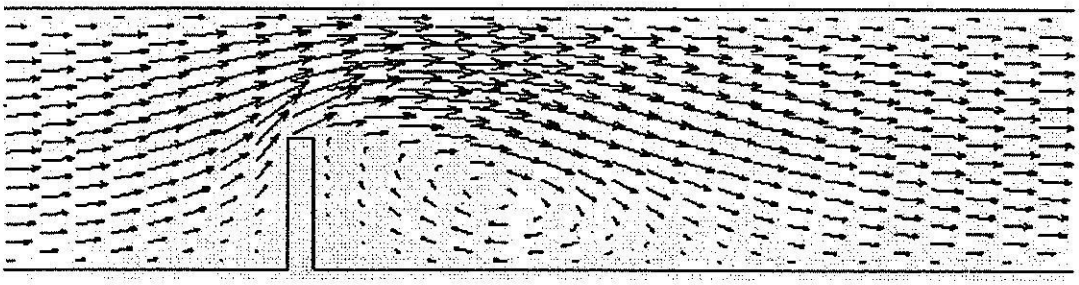

Fig. 3.15 Velocity vectors from the CFX-5.5 solution for low velocity flow in a tube past a constriction. The system studied has a radius of 1 inch and a length of 10.1 inch. The constriction has a thickness of 0.1 inch.

Fig 3.16 shows the fluid streamlines for the flow in this system. There is significant eddy formation in the volume immediately behind the constriction, with a significant portion of the fluid being recycled, as shown by the large number of streamlines in the eddy.

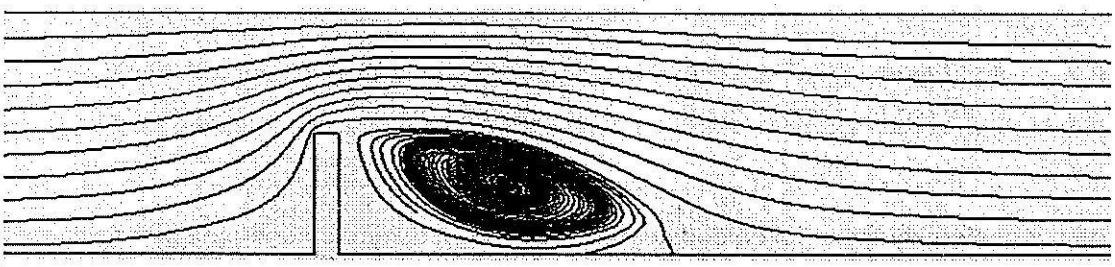

Fig. 3.16 Streamlines from the CFX-5.5 solution for low velocity flow in a tube past a constriction. The system studied has a radius of 1 inch and a length of 10.1 inch. The constriction has a thickness of 0.1 inch.

Flow in a Tube with a Non-Central Momentum Source

A tube with a non-centrally located momentum source containing a thin wall separating the top and bottom halves of the tube for a 15 mm section of tube preceding the source was modeled to investigate the ability of the commercial code to accurately realize flow fields in systems with power inputs to the process through impellers or similar features. A schematic diagram of the system being modeled is shown in Figure 3.17. The momentum source is contained in a 1 mm section of the pipe under, and at the end of the

thin wall. A schematic diagram showing the form in which a momentum source term may be added in CFX 5.5 is shown in Figure 3.18.

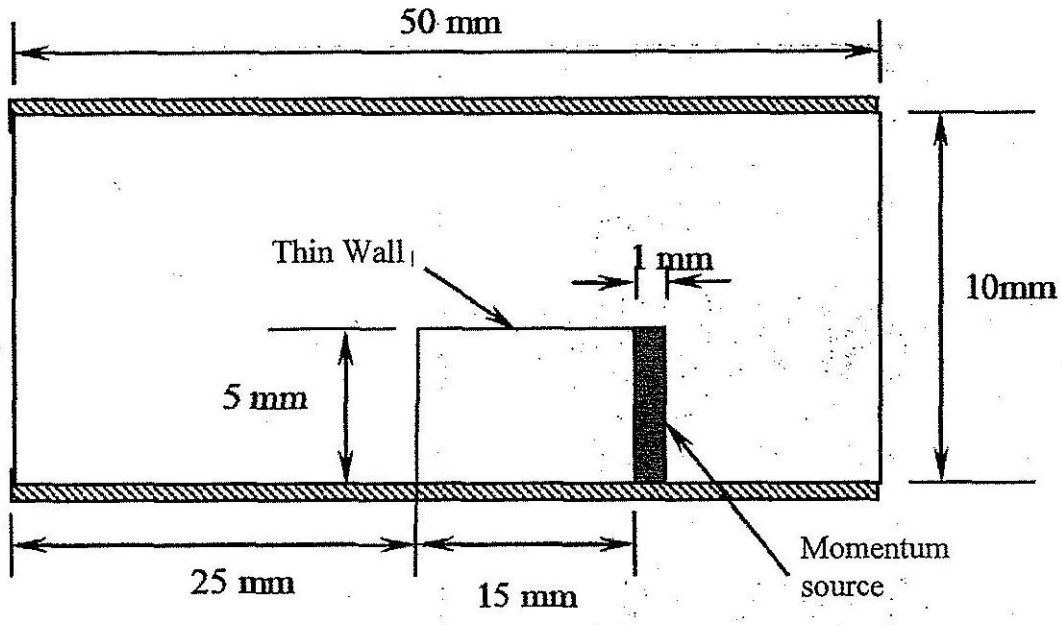

Fig. 3.17 Diagram of the system used to investigate momentum source additions in the commercial CFD software CFX-5.5. The system represents a tube with a thin wall separating the tube into two parts, and contains a momentum source term at the outflow end of the thin wall.

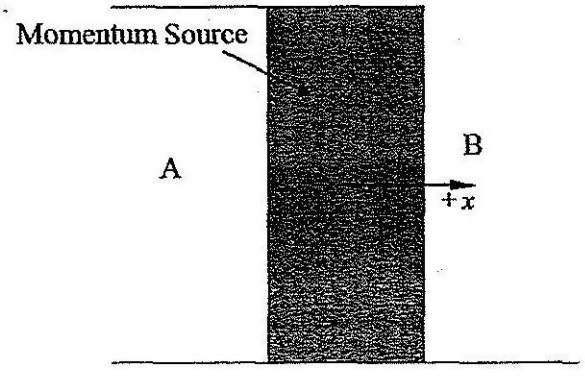

Fig. 3.18 Schematic diagram of a momentum source addition in a discrete volume, as applied in the commercial CFD software CFX-5.5.

The results of the simulations on the system are shown in Figures 3.19-3.21.

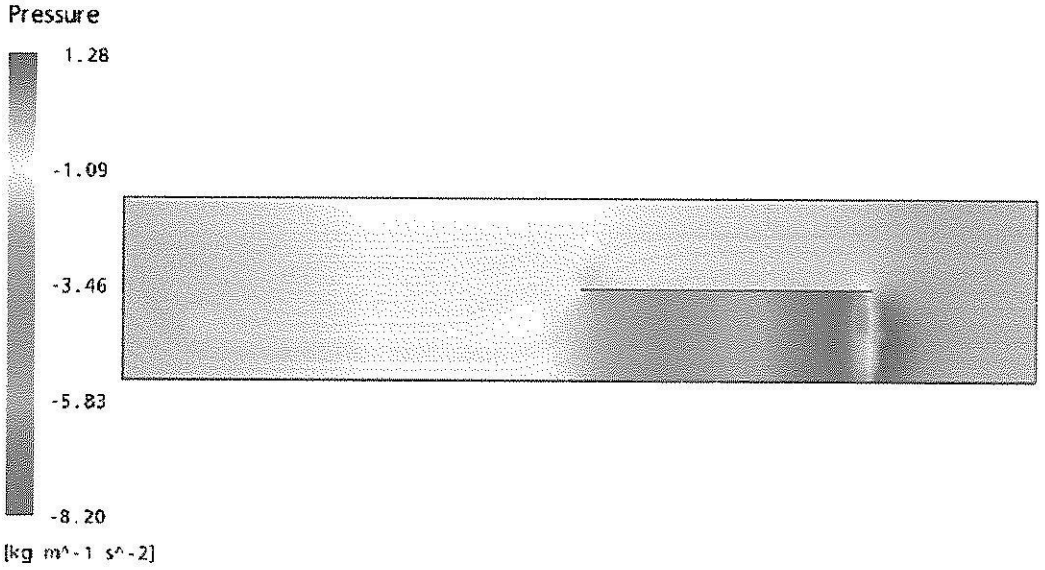

Fig. 3.19 Pressure distribution for flow in the system with the geometry sketched in Fig. 3.17 with a momentum source strength of 10000 kg/m^{2}s.

The Pressure distribution shows a system where there is a strong pumping effect created by the momentum source in the lower section of the tube. This effect can be seen in the very low pressure region in the region immediately before the momentum source (and preceding the entire length of the separated region of the tube), and the strong positive pressure in a small region immediately after the momentum source.

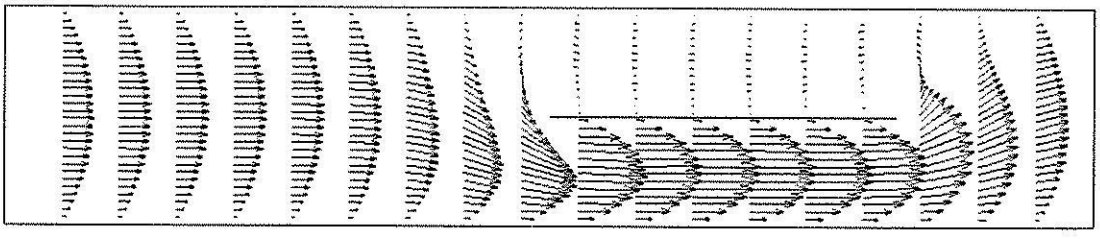

Fig. 3.20 Velocity vectors for flow in the system with the geometry sketched in Fig. 3.17 with a momentum source strength of 10000 kg/m^{2}s.

The pumping action is confirmed in the velocity vector plot which shows much higher velocities in the core of the separated region preceding the momentum source. This also results in significant draw of liquid from the top half of the tube into the separated region at the inlet of this region, and an expansion of the flow of the fluid at the exit of this region.

This also results in a small degree of backflow in the region of the tube that does not contain the momentum source as fluid from this higher pressure region is sucked into the lower pressure region at the entrance of the separated section.

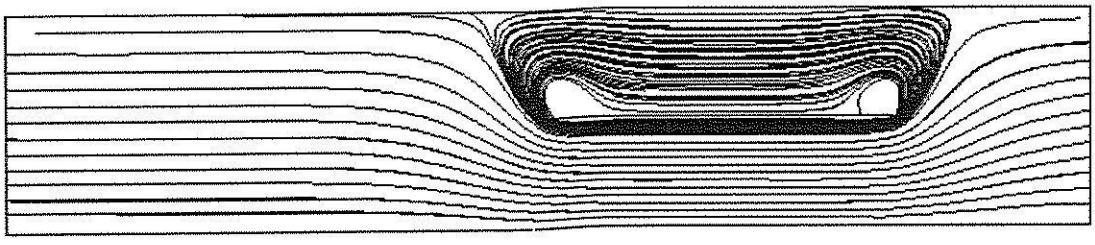

Fig. 3.21 Streamlines for flow in the system with the geometry sketched in Fig. 3.16 with a momentum source strength of 10000 kg/m^2s.

The streamline plot confirms the existence of the recirculation loop surrounding the wall between the two sections of the tube, the result of the momentum source in the bottom section of the tube. There are also two relatively stagnant zones created just above the partition between the two zones at either end of the partition, due to the characteristics of the flow loop between the two sections.

We can note that there is no recognized analytical solution for this system, and so it is not possible to make a comparison to a known solution; however the response of the simulation appears to give a realistic result, with no obvious deviations from what is expected in such a system.

Flow in a Tube with an Axial and a Spiraling Momentum Source

Based on the objectives of the current research, it is necessary to determine what level of complexity is necessary in order to model the agitator which is used in the MSMPR crystallizer to suspend the crystals and to mix the crystals and solution. In order to make this determination it is necessary to consider both the practical details of the MSMPR crystallizer modeled and also the objectives of the research. First, we must consider that the current study aims to determine the significance of the operating point of the system on whether the flow from the system is isokinetic or not, and therefore whether the crystallizer

really meets the MSMPR assumptions. This suggests that the most crucial region of the crystallizer to model with high accuracy is the region around the outlet tube, which will determine whether the isokinetic assumption exists. This region is in the annular space outside the draft tube, and contains four vertical baffles at 90° intervals that are used to remove radial flow in this space, and force the streamlines to be as vertical as possible. These baffles perform two purposes in straightening the flow: the first result is that the ability to suspend particles in the system (a necessary function in the crystallizer) will be much better if the streamlines are exactly counter to the gravitational force; the second function is that the straightened streamlines will then be exactly parallel to the direction of the outlet tube, which is an essential condition to be able to achieve isokinetic flow in this tube. Alternatively, it is clear that the flow conditions well away from this zone, particularly *inside* the draft tube only need to be known qualitatively. The impeller region could be analyzed to any level of accuracy (for instance using moving domains, and other modern techniques), however this will add enormous time and computational requirements for high accuracy, but will add little knowledge in relation to the objectives of the study. For this reason the common CFD technique of modeling impellers with momentum source terms was used, and it was wished to analyze what type of momentum source was suitable, with the knowledge that the flowlines are likely to have been made quite vertical by the baffles before the flow reaches the outlet tube.

In order to investigate the momentum source term in realistic applications, a system was studied where the momentum source is separated from the wall of the tube, as shown in Figure 3.22. The momentum source term was contained within a disk-shaped volume of diameter 7 mm, and thickness 1 mm contained centrally within a 10 mm tube. The source term was placed midway along the tube section investigated to determine its effect on both the upstream and the downstream flow. The momentum source was modeled as purely an axial source in some simulations, and as a source containing both axial and radial components in others, to view the ability of the momentum source to produce swirling (rotating) flows, which are common for impeller driven flows. The boundary conditions for the system are 0 relative pressures at both ends of the geometry: flow is produced by the pumping action of the impeller rather than due to a pressure gradient in the axial direction of the flow.

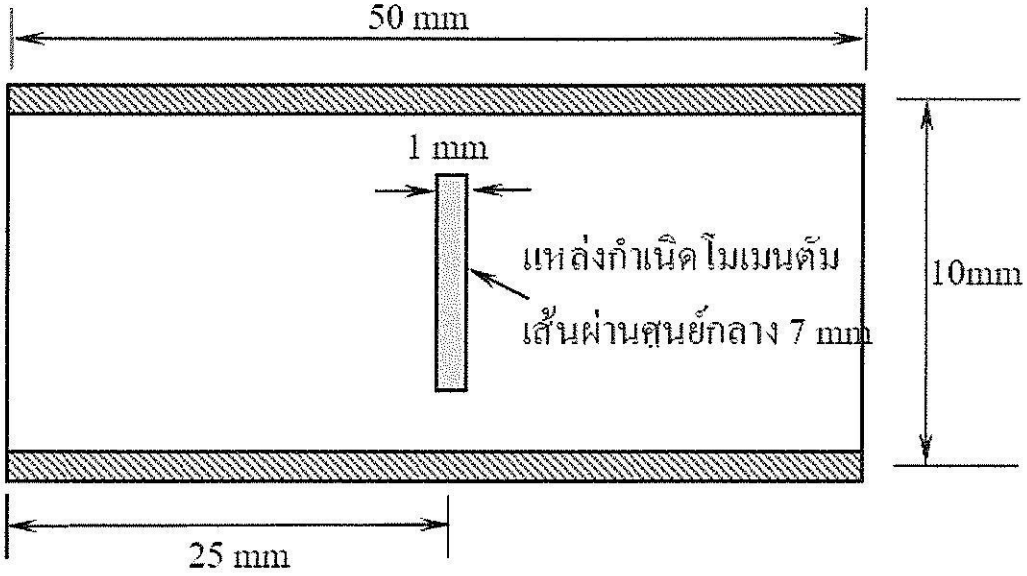

Fig. 3.22 Diagram of a system used to investigate momentum source additions in the commercial CFD software CFX-5.5. The system represents a tube with a centrally located momentum source term.

Figure 3.23 shows the pressure distribution within the geometry studied for the process.

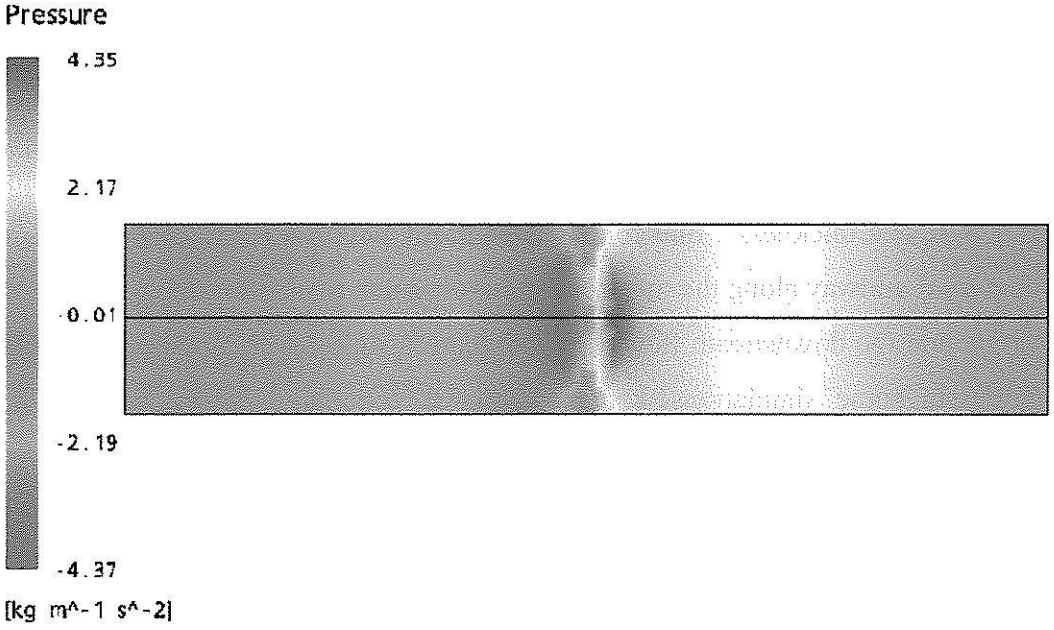

Fig. 3.23 Pressure distribution for flow in the system with the geometry sketched in Fig. 3.22 with a momentum source strength of 10000 kg/m^{2}s and momentum addition in the axial direction only.

The pressure distribution shows very clearly the pumping action of the impeller. In the section upstream of the impeller there is a low-pressure (suction) zone, particularly in the area immediately preceding the momentum source; the effect is less pronounced near the wall of the pipe, especially in the region adjacent to the source. In the section downstream from the source there is an equivalent volume of a high pressure region as the momentum source pushes fluid into this region. Again, this high pressure term is much stronger in the volume immediately downstream from the source than it is near the wall, particularly in the area adjacent to the source.

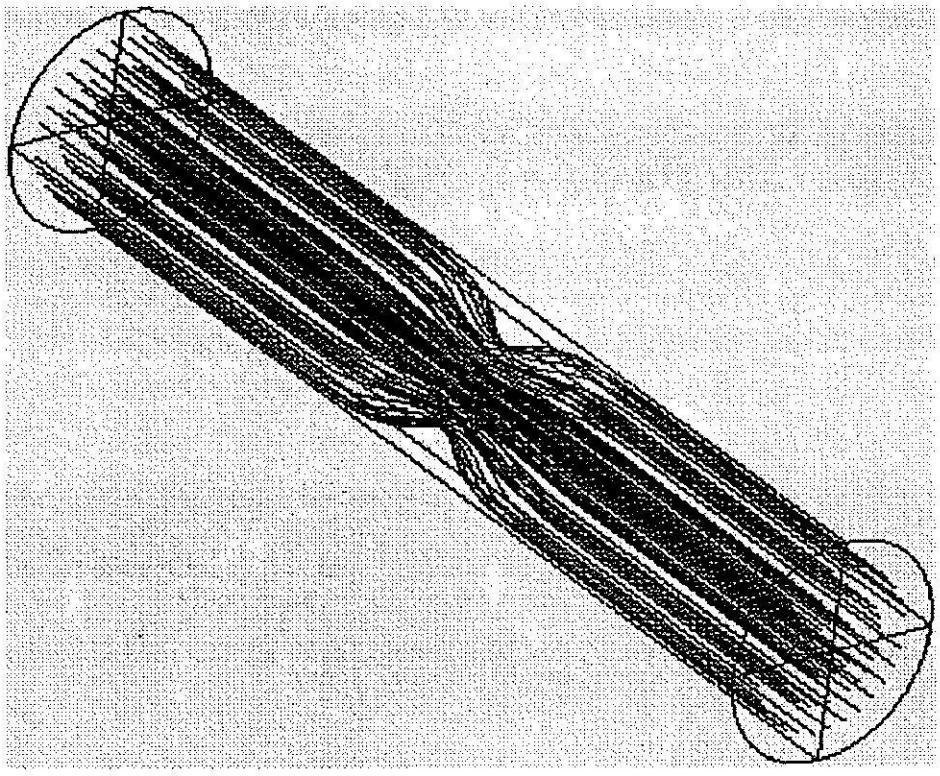

Fig. 3.24 Streamlines for flow in the system with the geometry sketched in Fig. 3.22 with a momentum source strength of 10000 kg/m^{2}s and momentum addition in the axial direction only.

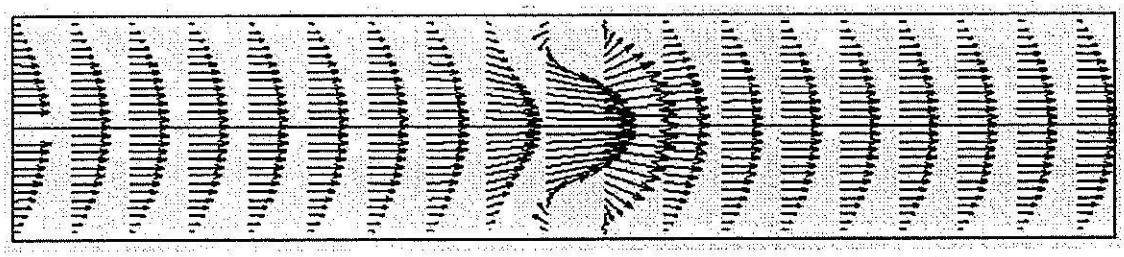

Fig. 3.25 Velocity vectors for flow in the system with the geometry sketched in Fig. 3.22 with a momentum source strength of 10000 kg/m^{2}s and momentum addition in the axial direction only.

In some systems, particularly in unbaffled systems containing an impeller, it may be necessary to model momentum addition in both the axial and radial directions to model 'swirl' created by an impeller. A momentum source with radial and axial components was used in the geometry defined in Figure 3.22, with results for streamlines shown in Figure 3.26, and the pressure profile is shown in Figure 3.27.

More details on the programming involved in these case studies, and more analysis of the results is given in the M.Sc. thesis of Jaruwan Tangtonsakoolwong[2].

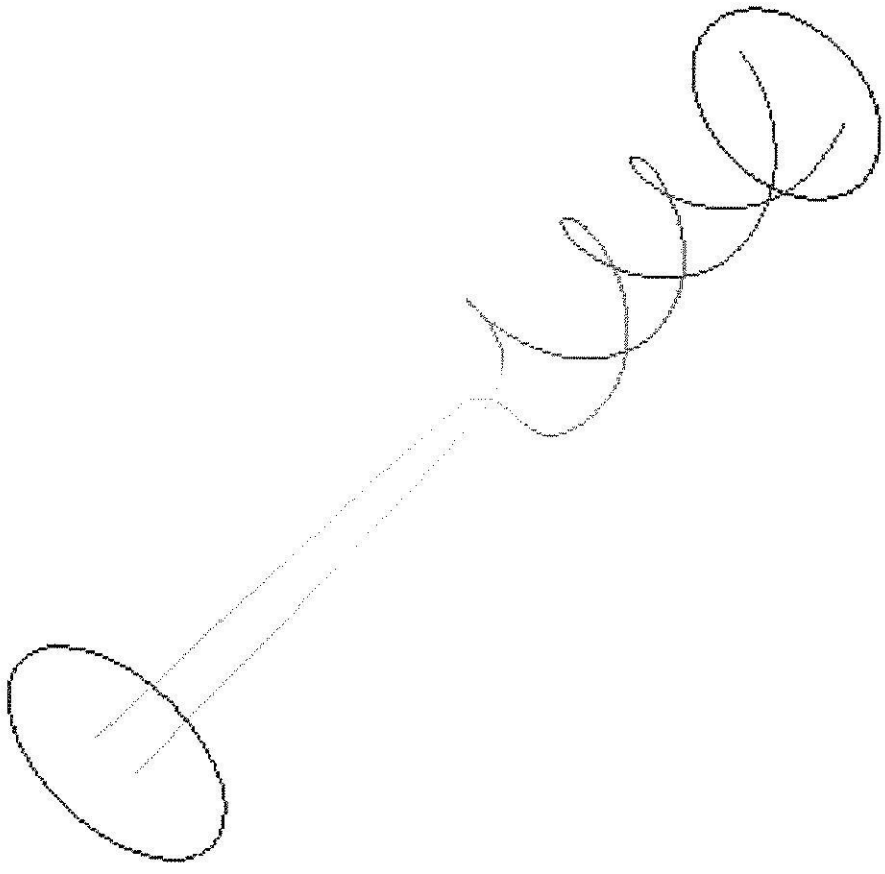

Fig. 3.26 Streamlines for flow in the system with the geometry sketched in Fig. 3.22 with a momentum source strength of 10000 kg/m^{2}s and momentum addition in a combination of the axial and radial directions.

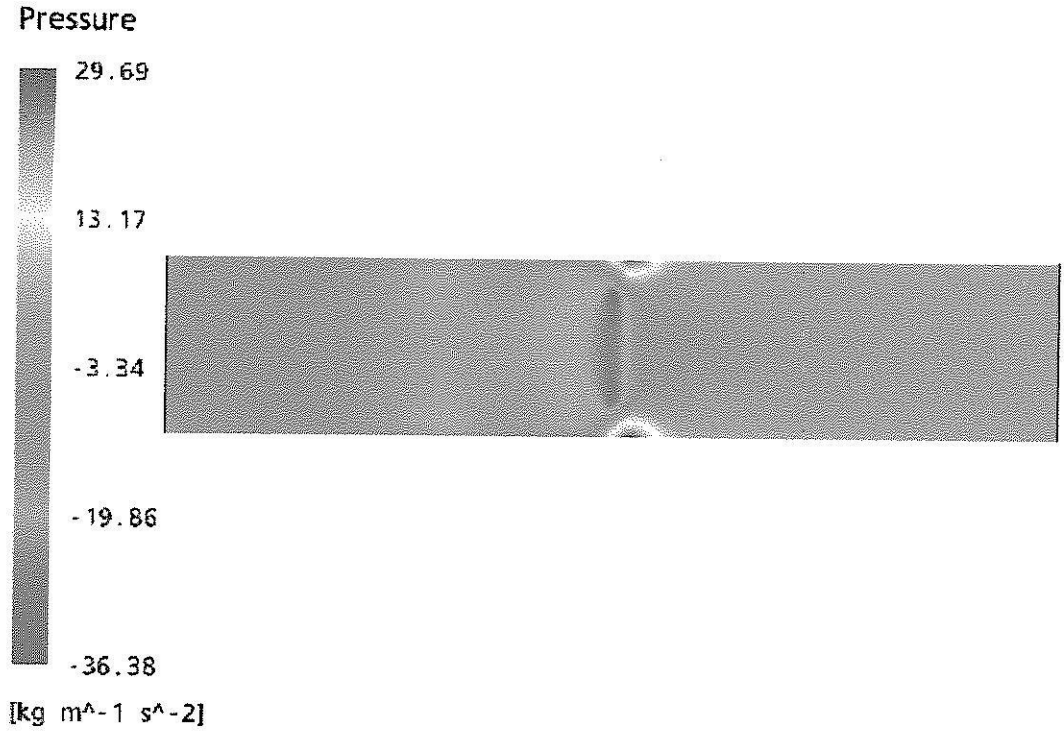

Fig. 3.27 Pressure distribution for flow in the system with the geometry sketched in Fig. 3.22 with a momentum source strength of 10000 kg/m^{2}s and momentum addition in both the axial and radial directions.

Chapter IV

Geometry and Physics of the Crystallizer

The crystallizer that is simulated in the current project is a bench scale MSMPR crystallizer at the School of Chemical Engineering, Suranaree University of Technology. The crystallizer is suitable for crystal growth and nucleation rate determinations in a wide range of materials, including organic and inorganic crystals. The working volume of the crystallizer is 2.5 L, and it is feed by a variable speed peristaltic pump (or two pumps if a reaction or non-solvent crystallization is used), and the product is taken using a high speed peristaltic pump, which can be switched on and off by a level controller to maintain a constant working volume. A schematic diagram of the system is given in Figure 4.1.

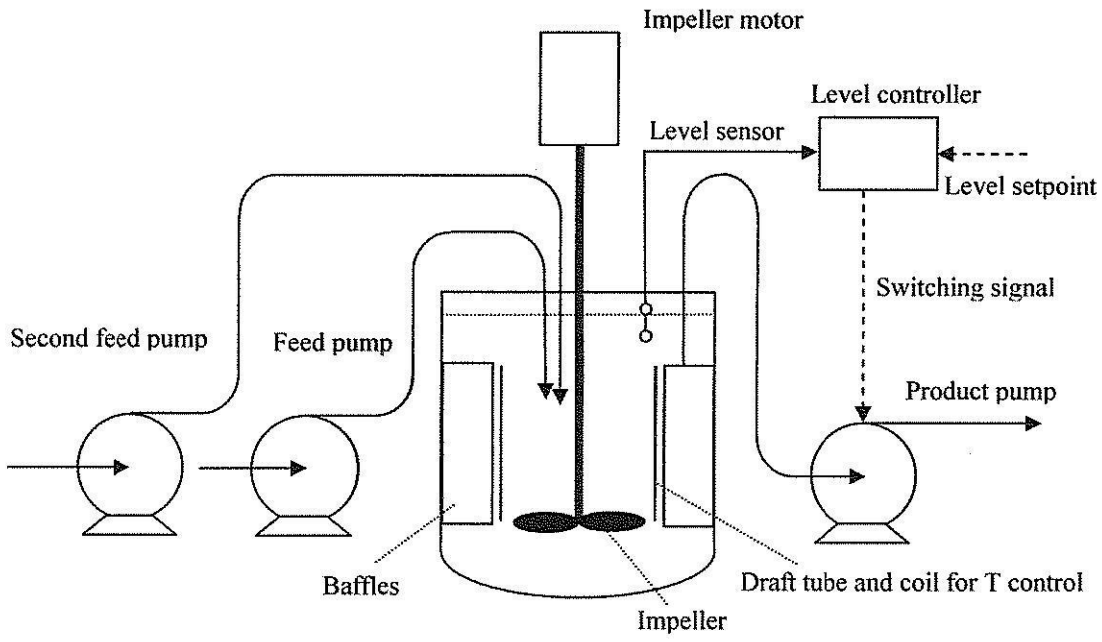

Fig. 4.1 Schematic diagram of the experimental MSMPR crystallizer at Suranaree University of Technology. The second feed pump is only required for a second reagent in reaction crystallizations or for a non-solvent in non-solvent crystallizations.

A photograph of the crystallizer and its internals is shown in Figure 4.2. The crystallizer has 4 equally spaced vertical baffles mounted around a copper coil which acts as a draft tube (to segregate the downflow in the impeller region from the upflow in the

outer body of the crystallizer) and also as a heat exchanger to maintain a constant (set) temperature in the crystallizer. Also shown in the figure is the impeller shaft. The blades are located near the base of the draft tube, and are hidden in this figure.

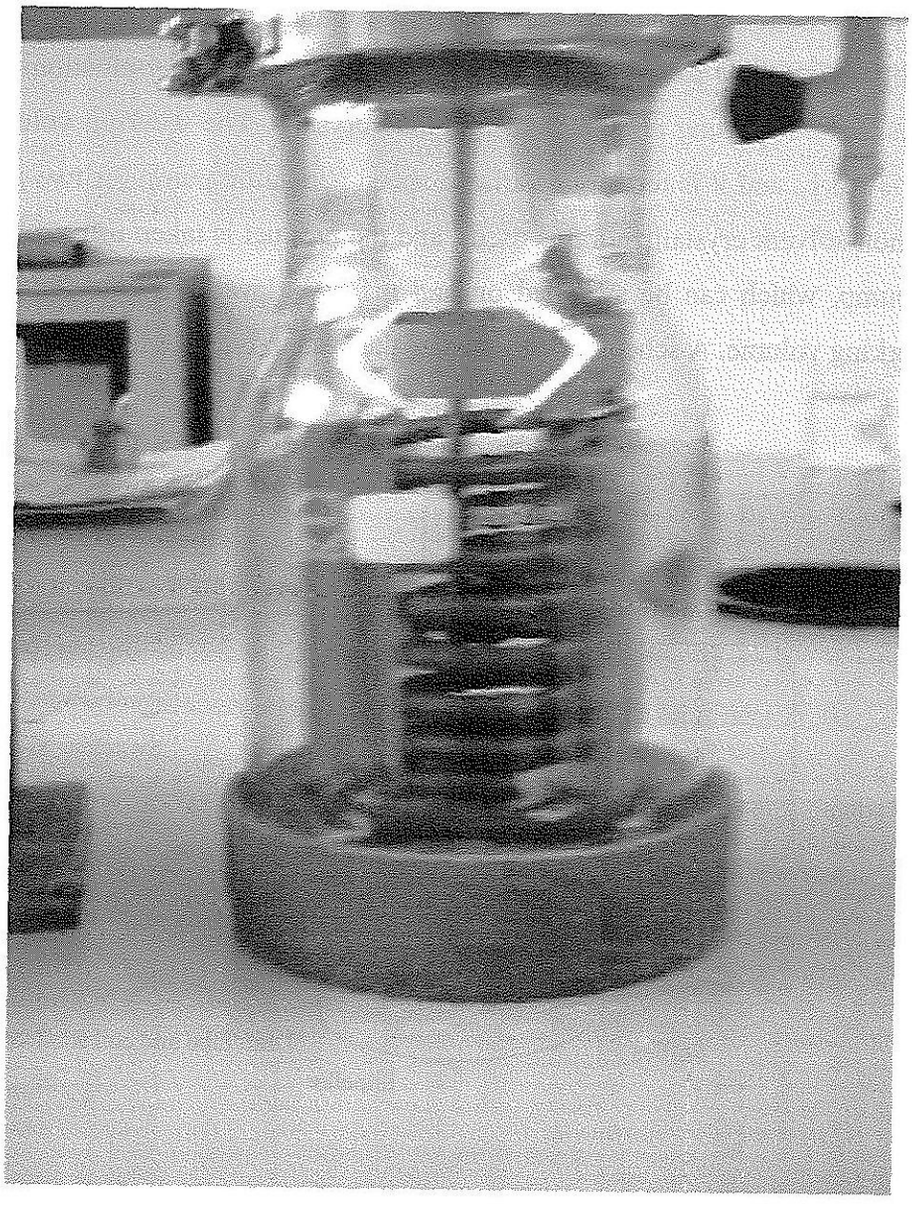

Fig. 4.2 The body of the experimental MSMPR crystallizer which was simulated.

The geometry of the crystallizer is a three dimensional object, and because of the feed and product tubes, and baffles, there is no possibility of reducing the geometry to a thin slice, which would allow the volume meshed to be greatly reduced, thereby reducing the computation time. The crystallization investigated in the study is the isothermal

crystallization of sucrose, which is neither a precipitation nor a non-solvent crystallization, which indicates that the second feed tube can be removed from the system. The product is taken from the body of the crystallizer halfway between two baffle plates, and the feed solution is feed into the draft tube (near the impeller location) along the same plane as the product.

It is possible to accurately complete the simulation using only half of the geometry since there is a symmetry plane at the plane through which the feed and product tubes are. The flow field will be symmetric across this plane. This reduces the volume contained in the geometry by half, and therefore also greatly reduces the computation time. It is not possible to further reduce the computational area. A schematic diagram of the crystallizer with the key features of the geometry highlighted is shown in Figure 4.3.

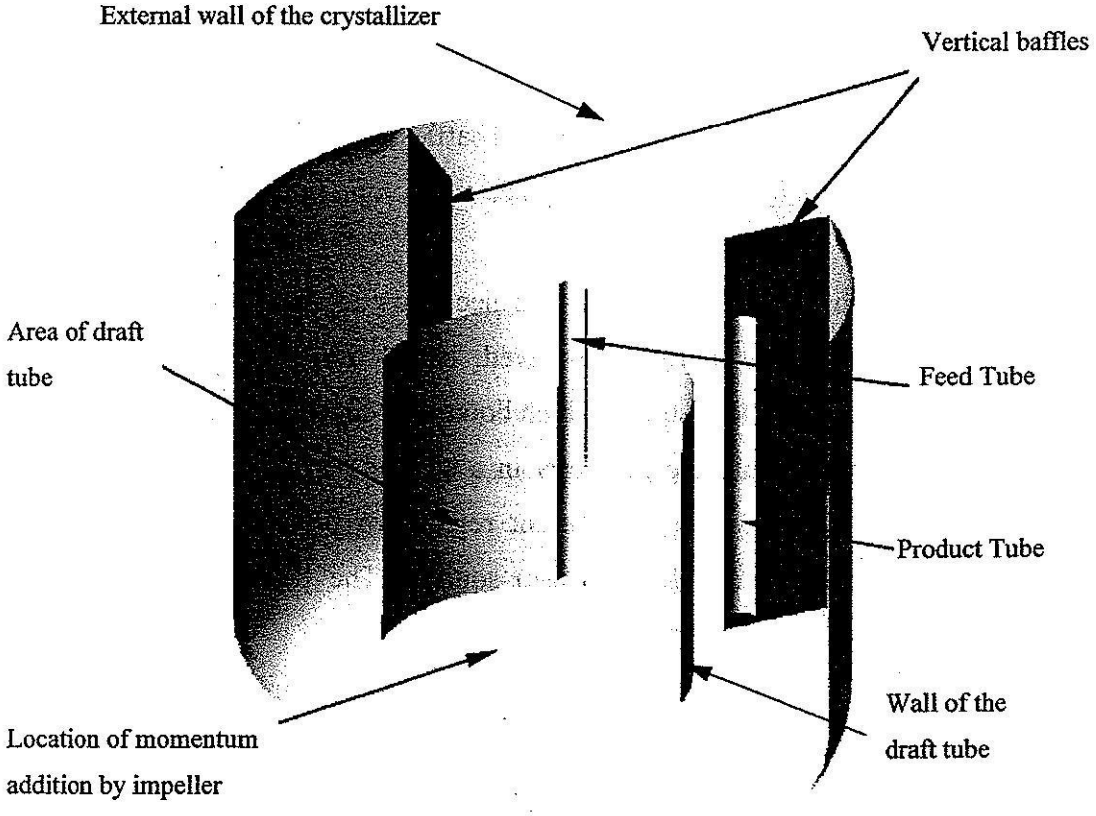

Fig. 4.3 Key feature of the geometry of the MSMPR crystallizer.

Careful measurements were taken of the laboratory crystallizer, including measurements of the curve describing the bases of the crystallizer body, and these

measurements were used to produce the crystallizer geometry in the program CFX-Build. Although it is possible to import geometries created in CAD-CAM programs into the CFX program, these programs were not available at SUT, and therefore the design was done with the basic geometry creation mechanisms in CFX. This is a relatively tedious job if the geometry is relative complex, as in the crystallizer being simulated. In addition, it was necessary to create several sub-volumes within the crystallizer to account for special features of the design, including the momentum source which models the impeller.

The crystallizer is a cylindrical vessel with a curved bottom to avoid stagnant areas around the outside of the base. The total height of the crystallization section is 133 mm, with 100 mm in a linear section above the base. The height of the draft tube is 70 mm, which allows the suspension sufficient area to flow over the draft tube into the central section. The height of the vertical baffles is 98 mm. The radius of the cylindrical section of the crystallizer is 68.5 mm, and the radius of the draft tube is 34.5 mm. Both feed and product tubes have diameters of 6 mm, and the feed and product tubes are submerged 75 mm below the top of the crystallizer. The complete geometry, included dimensions in mm, is shown in Figure 4.3. All internal surfaces (baffles, draft tube, and feed and product tubes) are considered as thin surfaces to reduce the complexity of the geometry and the further calculations.

Before creating fluid sub-regions it is necessary to create a 3D region of space containing the full domain which will be solved. This is done by choosing solid features (either bounding solids or cutout solids) which bound the entire 3D region of interest. Fluid sub-regions are created within the geometry in a similar way. These sub-regions can be used to specify different models in different regions of the simulation, or for special objects such as (momentum, heat, or mass) sources. The following sub-regions were created within the current geometry.

1. "Draft": The volume contained within the draft tube, but not the volume directly above or below the draft tube.
2. "Baffle": The volume in the baffled section of the crystallizer (outside the draft tube).
3. "Impeller": The region in which the impeller is located in the crystallizer. This region is a small disk located at the base of the draft tube. This allows a momentum source to be added in a small region as an analogue to an impeller. Trying to model a true impeller requires a moving grid approach, and with such

a complex geometry would require excessive computation time, without adding to the knowledge of the flow field at the outflow, which is what is most significant to this study. The momentum source used in the impeller region varied depending on the study. In some simulations momentum sources modeling a rotating input were added to the system, however the rotating momentum components were essentially fully damped by the baffles before it reach the outflow tube, and thus it was found not necessary to include these terms. In most cases simulated the impeller is modeled as a simple downflow momentum source (as the flow inside the draft tube is down, so that the flow in the baffled region is upflow to obtain a correct flow at the sampling point).

4. "Intube": The region inside the tube through which the inflow to the crystallizer flows. This region requires a smaller mesh than in the bulk to the crystallizer because of its narrow diameter.
5. "Outtube": The region inside the tube through which the outflow from the crystallizer flows. This region requires a smaller mesh than in the bulk to the crystallizer because of its narrow diameter.

The crystallizer geometry, 3D region, and sub-regions are defined within a file named "halfmodel.def". The name is used to indicate that it is modeling half of the crystallizer, with the center-line of the crystallizer being defined as a symmetry plane.

After defining the sub-regions it is necessary to define the properties of the system by defining the fluid domain. The reference pressure was defined as 101,325 Pa, and the simulation was set as a steady-state simulation with a stationary domain. The number of fluid is set as 1, and this fluid is defined as a sugar syrup. This fluid is defined as a pure fluid (it is not necessary to describe it as a mixture in this simulation), and the properties of the fluid are defined as: density = 1.3427×10^3 kg/m^3, and the dynamic viscosity = 0.23677 kg/m/s. These are typical values for the properties of the mother liquor in a crystallization of sugar in a continuous crystallizer. Because of the high viscosity of the sugar syrup, the flow fields are laminar in all locations in the crystallizer in the current simulations, and so a laminar fluid model is used. In addition the non-buoyant model is used, and no heat transfer model or radiation model is used.

Next it is necessary to describe the system boundaries. There are a large number of different types of boundary available in the CFX program: these include:

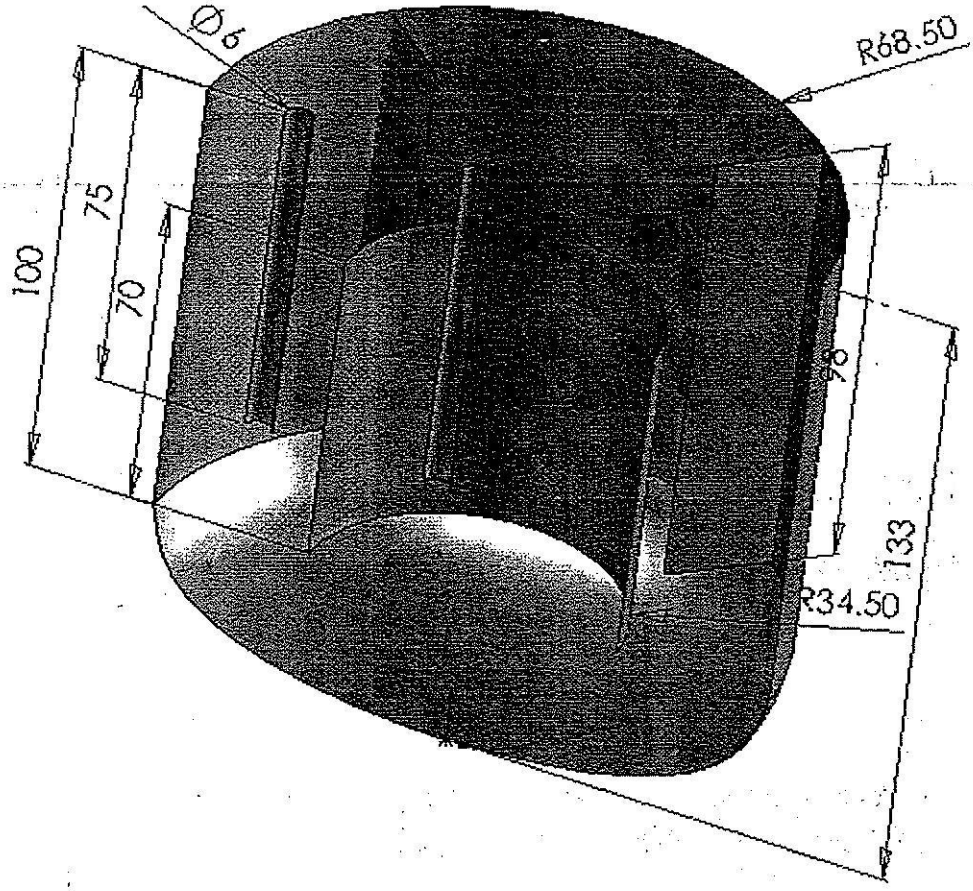

Fig. 4.4 Geometry of the crystallizer from CFX-Build.

1. Inlet: Across an inlet boundary it is only possible for fluid to flow into the system described by the solid formed in CFX-Build. (Flow out of the system across this boundary is stopped even if predicted by the CFD solution). An inlet may be classed as subsonic or supersonic. The flow involved in the current study was all well within the sub-sonic range. The flow can be defined via the cases: Normal Speed (the flow has a certain velocity normal to the plane of the inlet); Cartesian Velocity Components (the flow is in a direction away from the plane defining the inlet, with the velocity being described in vector notation: cylindrical velocity components are also possible); Total Pressure (the flow is calculated by the pressure gradient from the plane defining the inlet to the bulk fluid inside the volume simulated); Static Pressure (which is similar to the previous case, however the static pressure is used to define the boundary); and Mass Flow Rate

(a uniform mass flux of fluid through the inlet is assumed, or velocity components are used to describe the flow direction).

2. Outlet: Across an outlet boundary it is only possible for fluid to flow out of the system described by the solid formed in CFX-Build. (Flow into the system across this boundary is stopped even if predicted by the CFD solution). Outlets can be defined by: Static Pressure (similarly to the inflow); Normal Speed (similarly to the inflow); Cartesian Velocity Components (similarly to the inflow); Mass Flow Rate (similarly to the inflow); Velocity (for two-phase simulations); and Degassing (where one phase is a dispersed phase, and the dispersed phase only is allowed to exit through this outlet).
3. Opening: An opening is a boundary through which fluid can flow into or out of the system. Openings can be define by Cartesian velocity components, Pressure, or Static Pressure.
4. Wall: A wall is a solid feature through which flow is impossible. Walls may be No Slip (Stationary): Free Slip: No Slip (Moving): Counter-rotating Wall (available only with a rotating domain). A wall roughness can also be defined, either smooth, or rough with a given value of the surface roughness. Walls may be defined as exterior walls, or as thin surfaces, which are solid surfaces inside the geometry which are thin enough to be considered as a thin surface. The baffles, draft tube, and inlet and outlet tubes are considered as thin surfaces within the current simulation.
5. Symmetry: A symmetry plane occurs where the flow on one side of a plane is known to be a mirror image of the flow on the alternate side. In this case one half of the geometry can be modeled, and the alternate half predicted from the first, with suitable treatment of the interface between the two sides.
6. Periodic pair (rotational or translational). If the solution is known to have periodicity (such as where there is a finite number of fins or turbine blades) then a periodic boundary condition is suitable to reduce the size of the problem.

There are a large number of boundaries in the different sub-regions in the system. These are:

1. "Inflow": This is the top of the inflow tube, and is considered as a subsonic inflow normal to the plane of the inlet, with a specific mass flow rate of 4.6712×10^{-4} kg/s, which is a common condition for the crystallizer (giving a

particularly suitable value of the residence time). Giving the boundary condition at the top of the flow tube (rather than the bottom) allows for a fully developed flow to occur at the base of the tube, where the liquid feed flows into the crystallizer.

2. "Outflow": This is at the top of the outflow tube, and is a subsonic outflow boundary condition with a relative static pressure of 0 Pa.
3. "Draftwall011 and Draftwall012" are the inner walls of the drafttube. They are zero slip walls.
4. "Draftwall021 and Draftwall022" are the outer walls of the drafttube. They are zero slip walls.
5. "Inwall011", "Inwall012", "Inwall021" and "Inwall022" are the internal and external walls of the inflow tube. These are all no slip walls.
6. "Outwall1" and "Outwall2" are no slip walls defining the outlet tube.
7. "Baffle1" and "Baffle2" are no slip walls at the position of the baffles in the crystallizer.
8. "Sym" defines the symmetry plane in the crystallizer.
9. "Default" defines the other solid surfaces within the crystallizer, and these are no lip walls.

After the definition of the boundaries the initial values for the simulation variables are defined. The typical way of achieving this is to set the "Domain Initial Condition" to "Fully Automatic". In this case, if there is a previous solution for the domain, this solution will be used as an initial condition. If there is no previous solution in the domain then the CFX solver uses default initial values for all variables being solved. (The default values for pressure and velocities in the initial values for the system is zero: the average temperature of all boundary conditions is used as the default initial condition for temperatures if heat transfer is being studied).

Mesh creation is necessary to partition the geometry into finite regions for the computational technique. The first step of the mesh creation is to create a surface mesh on the surfaces of the volume using the Delauney Surface Mesher programmed into the CFX code. The parameter that controls creation of the surface mesh is the Maximum Edge Length. If this is set too large then the grid will not be sufficiently fine to produce an accurate solution, or to see small features in the flow field. If the value is set too low then the simulation will take an extremely long time to solve. The volume meshing (creating

mesh throughout the entire volume of the system) is done when the definition file is being written. The volume mesh is created by the Advancing Front and Inflation (AFI) algorithm.

The last details that the program requires before solution is the Solver Parameters. The first set of these parameters relate to the Convergence Control: the maximum number of timesteps was set at 100, and the physical timestep was set to Auto Timescale, where the solver will choose a suitable timescale based on the physics of the problem. The second set of parameters in the Solver Control is the Convergence Criteria: here, the Root Mean Square for Residuals criteria was selected, with a convergence target residual value of 1.0×10^{-10}. The advection scheme used was a first order upwind scheme.

After setting these parameters the definition file is written, ensuring to select the Write Mesh toggle selected so that the volume mesh is created when the definition file is written. The mesh for a typical run is shown In Figure 4.5.

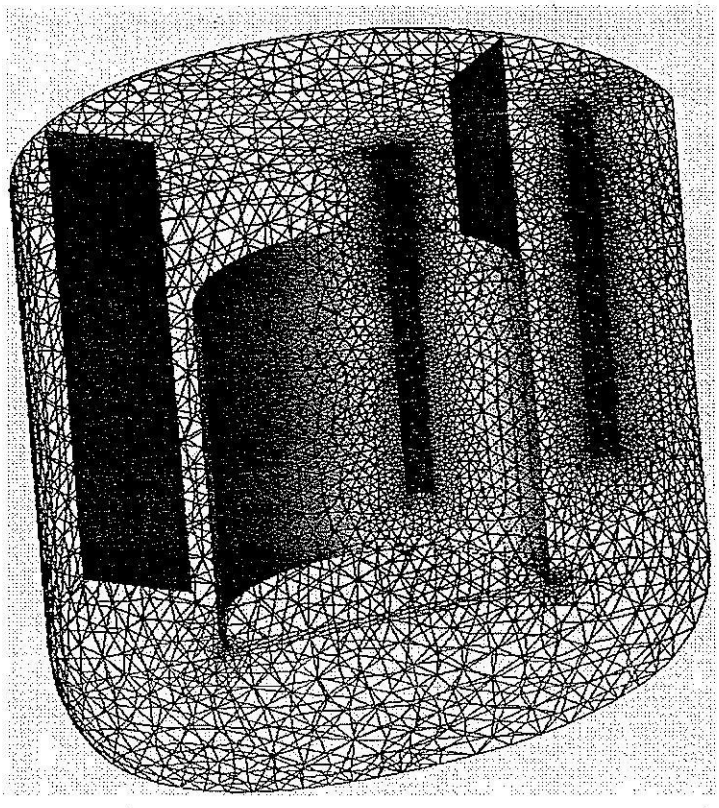

Fig. 4.5 Volume mesh used in a typical run.

It is very important to determine that a solution to a CFD problem is mesh size independent, indicating that the mesh is sufficient small as to accurately model the system. This is done by performing the same simulation using a range of different mesh sizes covering more than an order of magnitude in size. When the solutions converge into a single solution as the mesh size becomes smaller it is possible to determine at which mesh size the solution becomes mesh size independent. These calculations were performed in the current system to prove that the solutions obtained were accurate. A typical grid used (as shown previously) has 73735 nodes, 376481 elements and 40716 faces.

The solution was first obtained using a coarse grid. The calculation is performed iteratively until the residuals reduce to an acceptable level. To achieve grid independent results, the grids were refined step by step until changes in the numerical solution were unnoticeable.

After the system to be solved has been defined in the definition file, the system is solved using the program CFX-5 Solver. The finite volume methodology with an unstructured grid is built into the software and employed in this study. This program iterates the solution variables until a converged solution is reached. After a solution has been reached the solution can be visualized and plotted in the program CFX-Post. This allows for 2 and 3-dimensional plots of all variables solved, as well as plots of streamlines, regions of constant properties 9such as iso-velocity plots) and other significant features. CFX-Post also allows for visualization of the geometry and the mesh. Figures of the mesh and results shown in this report are plotted in CFX-Post.

Chapter V

Results and Discussion of the MSMPR Crystallizer Simulation

Simulations were performed using the geometry and physics described in Chapter IV. Simulations were performed to determine the maximum mesh size at which the results could be clearly known to be mesh size independent. This will allow for an accurate solution to be found using the minimum computational time. Seven test cases were performed varying the momentum source strength, which corresponds to the impeller speed used in the crystallizer. This will also depend on the type of impeller used in the crystallizer: for most downflow type impellers the total momentum added is approximately twice that used in producing the downflow effect: the remaining momentum is lost as swirl and other momentum components. This indicates that the total momentum added under these conditions in a real crystallizer would be very close to twice the momentum addition simulated. Momentum source values of 0, 1000, 10000, 15000, 18000, 30000 and 50000 $kg/m^2/s^2$ were used in the simulations. There are four main diagrams that can be used to demonstrate the results from the simulation, and these are: the velocity vector plot which shows the magnitude and direction of the stream flow at all points in the crystallizer (assuming the symmetry condition); the streamline plot, which shows examples of streamlines of the fluid between the inlet and outlet of the crystallizer; the velocity contour plot, which shows areas of particular velocity magnitude within the crystallizer; and the velocity vector plot around the outlet tube, specifically to show whether isokinetic sampling has been achieved for a particular momentum source. The results will be discussed with illustration by these four types of plot in order of the source of the volume rate of momentum addition.

Momentum Source Strength of 0 $kg/m^2/s^2$

If there is no momentum addition at the position of the impeller (equivalent to either having no impeller or having the impeller not rotating) then the only momentum addition to the system is due to the flow of the feed liquid into the tank. This does not indicate that the fluid is completely stagnant since there is still flow (and therefore momentum transfer) into and out of the vessel, causing flow between these two points. Since the flow area of the inlet tube is orders of magnitude lower than the area of either the draft tube or the annular space

outside the draft tube, the velocity of the fluid at all positions other than the volumes around the outlet and inlet is extremely small. The flow vectors in the volume of the crystallizer are shown in Fig. 5.1. The flow vectors in the inlet and product tubes correspond to flow rates of 2.5 l/hr through the tubes (which corresponds to 1.25 l/hr through the half inlet specified in this geometry).

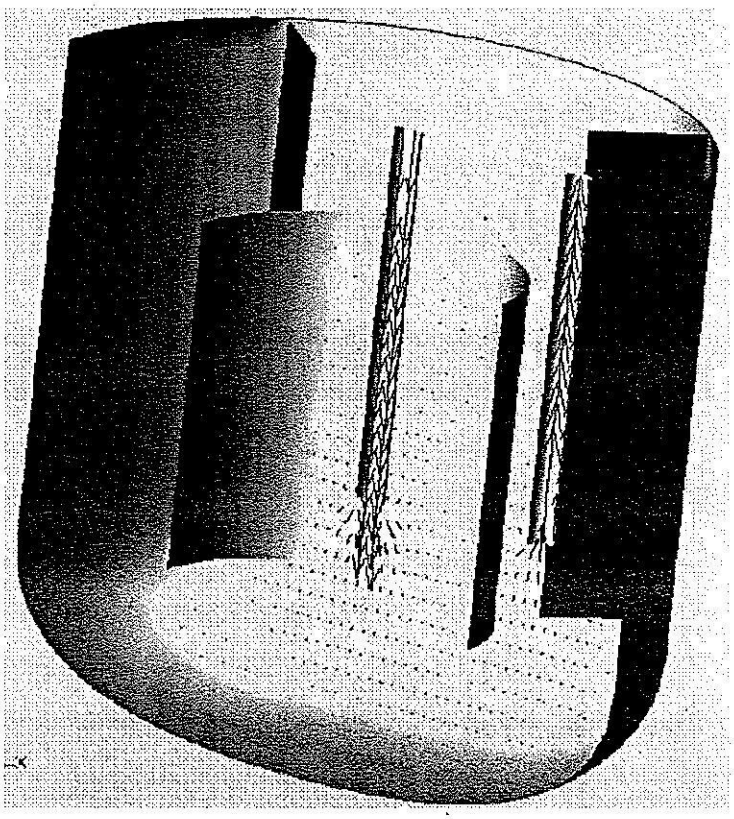

Fig. 5.1 Velocity vectors in the MSMPR crystallizer for a volume rate of momentum addition of 0 $kg/m^2/s^2$.

Fluid streamlines show that under conditions of no momentum input the fluid mostly bypasses the bulk of the volume of the crystallization vessel and moves directly between the inflow and the outflow tubes, with some expansion of the streamlines between the two points. A smaller number of the streamlines pass other directions in the crystallizer, so no area of the crystallizer is fully stagnant. The streamline plot is shown in Fig. 5.2.

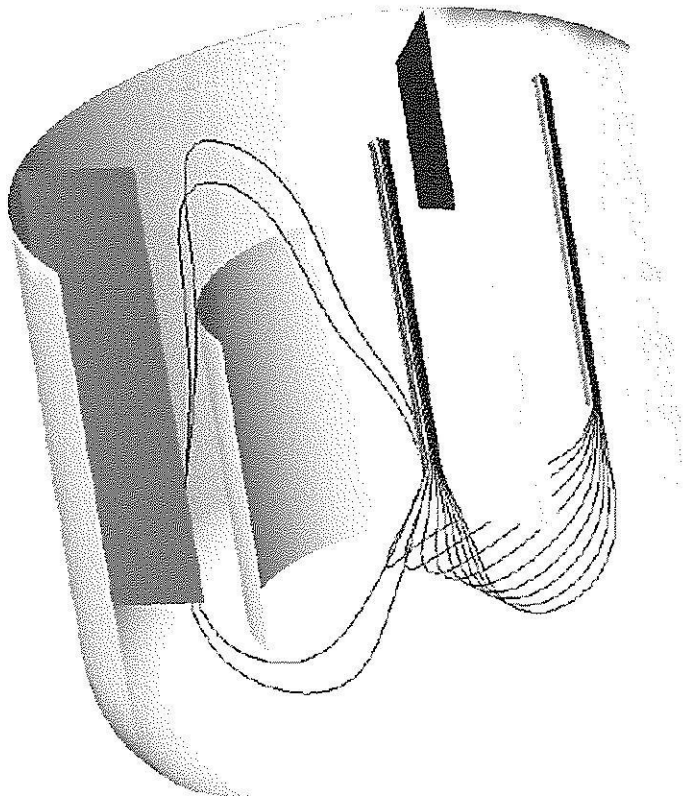

Fig. 5.2 Fluid streamlines in the MSMPR crystallizer for a volume rate of momentum addition of 0 $kg/m^2/s^2$.

The velocity contour plots for the vessel verify this result, with relatively high velocities inside the feed and product tubes, and adjacent to the mouths of these tubes, but very low velocities (much less than 0.01 m/s) in the remainder of the vessel. The condition of zero momentum input, equivalent to having no impeller, is clearly unsuitable for the crystallizer, even without seeing the solution for the CFD. However it is important to study this condition in order to obtain a baseline case to which the remaining CFD studies at higher momentum source additions can be compared.

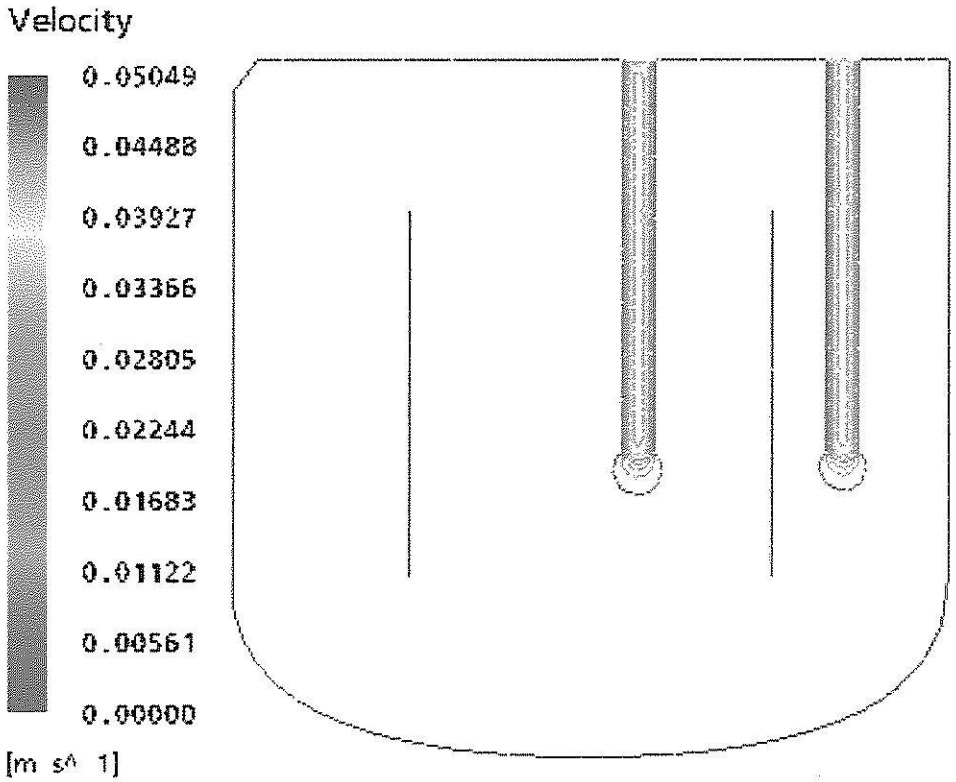

Fig. 5.3 Velocity contours in the MSMPR crystallizer for a volume rate of momentum addition of 0 $kg/m^2/s^2$.

Because the main focus of the project is to determine the point at which the flow through the product tube is isokinetic, thus optimizing the performance in terms of the MSMPR assumptions, it is useful to investigate carefully the flow in, and immediately around the mouth of the product tube. This is shown by the velocity vector plot in Fig. 5.4. The plot shows only the area around the mouth of the product tube, which is shown by the solid line. It is clear from this plot that the magnitude of the velocity in the product tube is an order of magnitude higher than the velocity in bulk of the vessel near the tube. This cause the streamlines to accelerate into the tube, pulling liquid toward the product tube from areas well away from the tube. The result of this is a suspension of small to medium sized particles is that the smaller particles will be drawn into the mouth of the product tube even if their original trajectory would have cause them to not be sampled in the tube. Large particles will not be withdrawn if their trajectory was not originally into the mouth of the tube, however: the momentum of the larger particles will be sufficient that they can continue more or less along their original path, and will therefore not enter the product tube

unless their original trajectory was into the tube. This will cause a larger than average particle density for the small particles, and violate the MSMPR assumption that the particle density function in the product is equal to that in the crystallizer vessel (the mixed product removal assumption). This would cause the calculate nucleation and growth kinetics from the crystallizer to be incorrect.

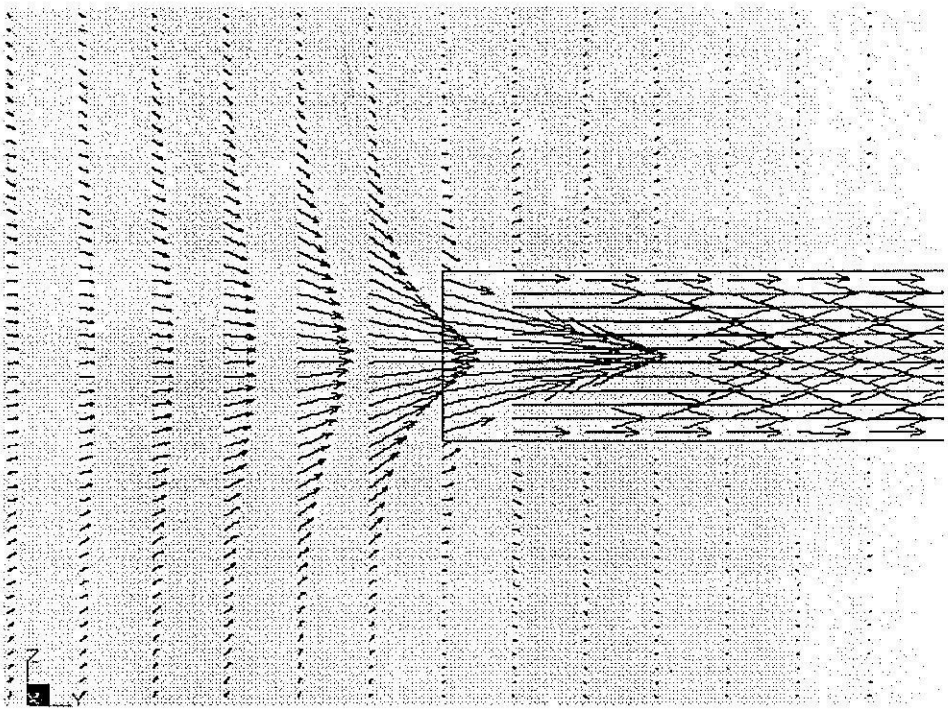

Fig. 5.4 Velocity vectors around the outlet tube of MSMPR crystallizer for a volume rate of momentum addition of 0 $kg/m^2/s^2$ (the figure is rotated 90° for convenience).

Momentum Source Strength of 1000 $kg/m^2/s^2$

It is difficult to be able to predict the necessary momentum input to obtain an isokinetic flow *apriori*. The first simulation after the base case was chosen to have a momentum input of 1000 $kg/m^2/s^2$, which the results show is still very much under the input required for the isokinetic condition. However this case does demonstrate a significant change in the flow structure of the vessel, and thus it is useful to discuss it in detail.

The first plot to discuss is the velocity vector plot for the entire crystallizer, shown in Fig. 5.5. Although the overall flow pattern is similar to that of Fig 5.1, a significant change

to the structure is evident. In this case there is a small but significant downward flow across the draft tube which is due to the pumping action of the impeller rather (as in the previous case) a small flow only due to the inlet flow. There is also a small flow upwards in the annular space outside the draft tube, also due to the pumping action of the impeller. This assists in forcing a vertical flow at the position of the outlet tube mouth: this is essential for isokinetic flow. Although the simulation shown has a momentum source term in the vertical direction only, experiments with 'swirl' (including tangential terms) in the momentum source did not appreciably affect the flow in the volume near the mouth of the outlet tube. The four vertical baffles straightened the flow in the space at the position of the outlet tube even when these momentum source terms were used in the simulation.

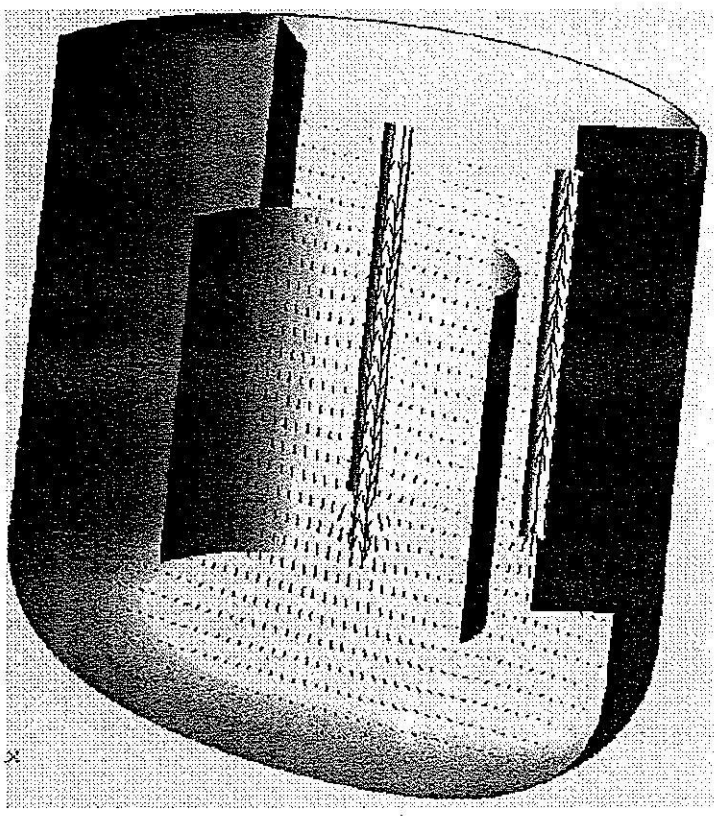

Fig. 5.5 Velocity vectors in the MSMPR crystallizer for a volume rate of momentum addition of 1,000 $kg/m^2/s^2$.

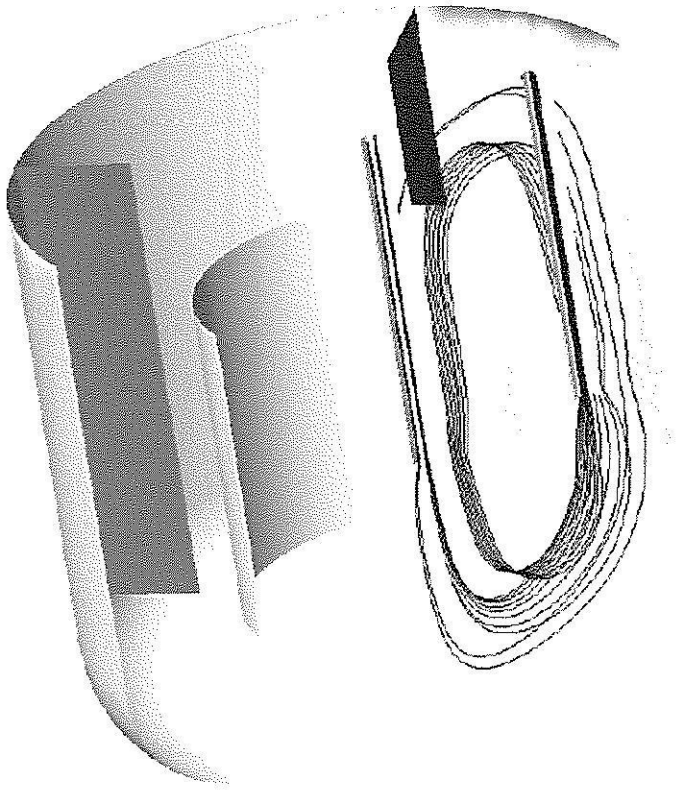

Fig. 5.6 Fluid streamlines in the MSMPR crystallizer for a volume rate of momentum addition of 1,000 $kg/m^2/s^2$.

The streamline plot (Fig. 5.6) shows similar features to the one for 1,000 $kg/m^2/s^2$, but in this case a much larger amount of recirculation, and a lower fraction of the streamlines bypassing the bulk of the vessel by flowing directly from the inlet to the outlet. A recirculation loop passing down through the draft tube and then up through the annular space is clearly evident in this plot.

The velocity contour plot (Fig. 5.7) is similar to the equivalent plot for 1,000 $kg/m^2/s^2$, but in this case there is a larger area of high velocity around the mouth of the inlet tube. The plot does not clearly show the slightly higher velocities in the draft tube and the annular space, but these are evident from Fig. 5.5.

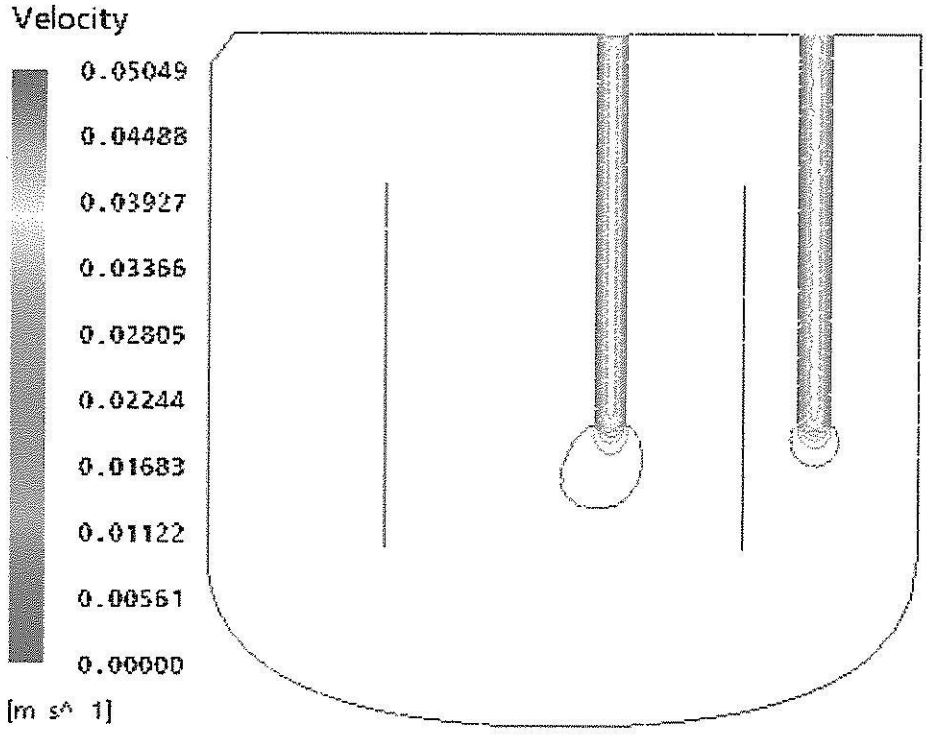

Fig. 5.7 Velocity contours in the MSMPR crystallizer for a volume rate of momentum addition of 1,000 $kg/m^2/s^2$.

The plot of the velocity vectors around the mouth of the product tube shows that the velocity in the annular space is still far too low for isokinetic sampling, and there is significant flow acceleration into the product tube. This again indicates that there will be a higher than acceptable amount of small particles in the product stream, violating the assumption of the MSMPR crystallizer.

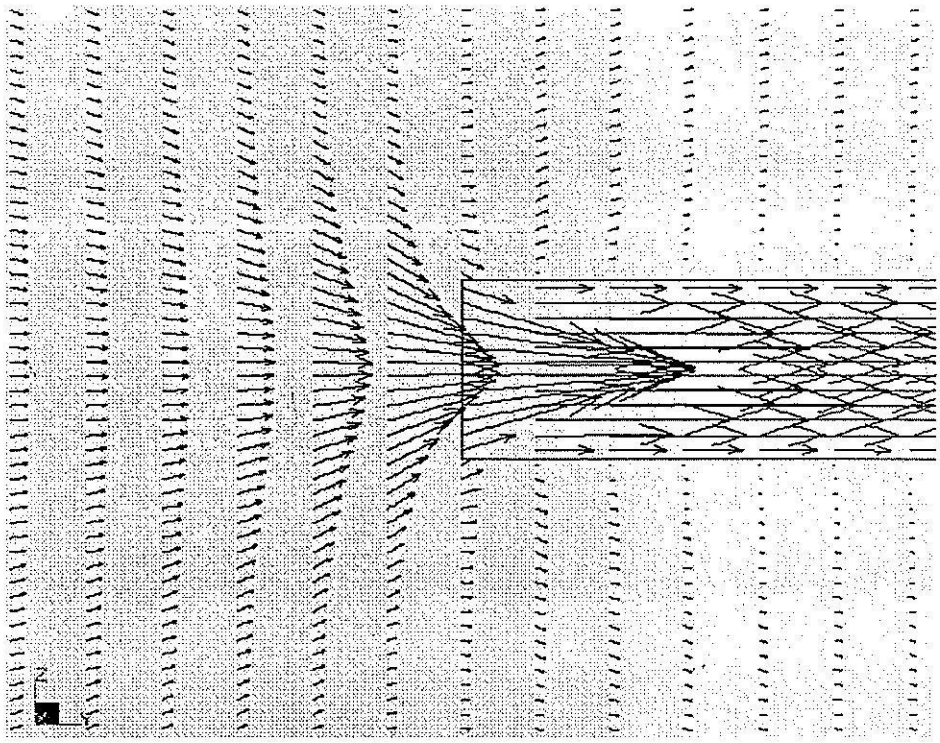

Fig. 5.8 Velocity vectors around the outlet tube of MSMPR crystallizer for a volume rate of momentum addition of 1,000 $kg/m^2/s^2$ (the figure is rotated 90° for convenience).

Momentum Source Strength of 10000 $kg/m^2/s^2$

For a momentum source of 1000 $kg/m^2/s^2$ the pumping action of the impeller is strong enough to create a strong circulation loop down through the draft tube and up through the annular space in the crystallizer, as evident in the velocity vector plot for the crystallizer (Fig. 5.9). It can be noted that the downward velocity in the draft tube is much higher than the upflow velocity in the annular space. This is due to the cross-sectional area in the annular space (1.47×10^{-2} m^2) being significantly larger than the cross-sectional area of the draft tube (3.74×10^{-3} m^2). The velocity in the left side of the annular space is higher than that in the right side of the annular space (near the product tube) because of the effect of a substantial amount of fluid from the right side being removed as a product. The flow around the product tube still does not appear isokinetic however.

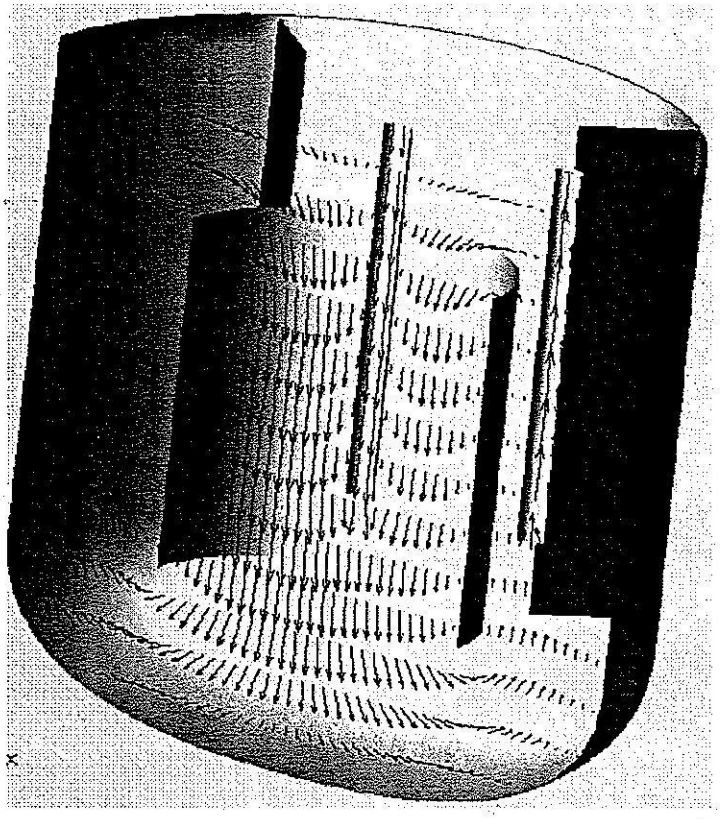

Fig. 5.9 Velocity vectors in the MSMPR crystallizer for a volume rate of momentum addition of 10,000 $kg/m^2/s^2$.

The fluid streamline plot (Fig. 5.10) shows that as the momentum addition through the impeller becomes larger the fluid circulates more in the crystallizer before leaving through the product tube.

The velocity contour plot for this momentum input describes a system that has a more complex flow pattern than for the lower momentum addition simulations. Firstly, the downflow velocity in the draft tube is quite high, comparable to that in the inflow tube. The exception to this is near the walls of the draft tube and near the walls of the inflow tube, which have a zero-slip boundary condition. Again, the upflow velocities in the annular space are less than the downflow velocities in the draft tube, due to the larger flow area in the annular space. There is also a small region between the product flow tube and the draft tube wall where the velocity is quite low due to the small distance between the two zero-slip boundary conditions. This occurs in only a very small region of the crystallizer because the product tube takes up only an extremely small fraction of the total

flow volume in the annular space. The region is emphasized in the figure shown because this is plotted through the plane of the product and feed tubes.

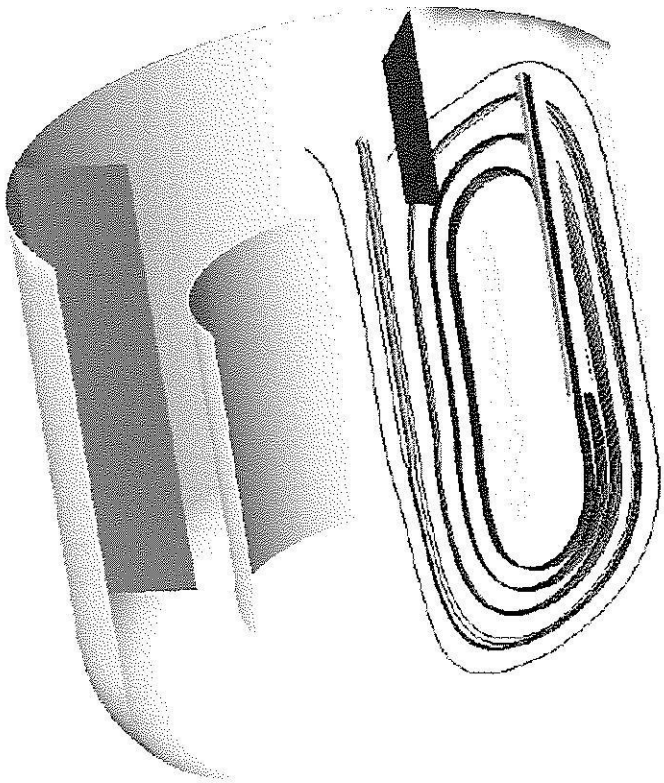

Fig. 5.10 Fluid streamlines in the MSMPR crystallizer for a volume rate of momentum addition of 10,000 $kg/m^2/s^2$.

A second interesting conclusion from the velocity contour plot is that a near stagnant zone is formed at the base of the vessel immediately below the impeller. This zone is problematic because it may allow large crystals to sediment in this zone, thus breaking the 'mixed suspension' assumption of the MSMPR crystallizer since the crystal size distribution in this area would significantly deviate from the bulk average of the crystallizer. This stagnant area would also affect the continuous operation of the crystallizer, as this zone would need to be purged of crystals periodically. This explains why modern crystallizers often have a raised area under the impeller.

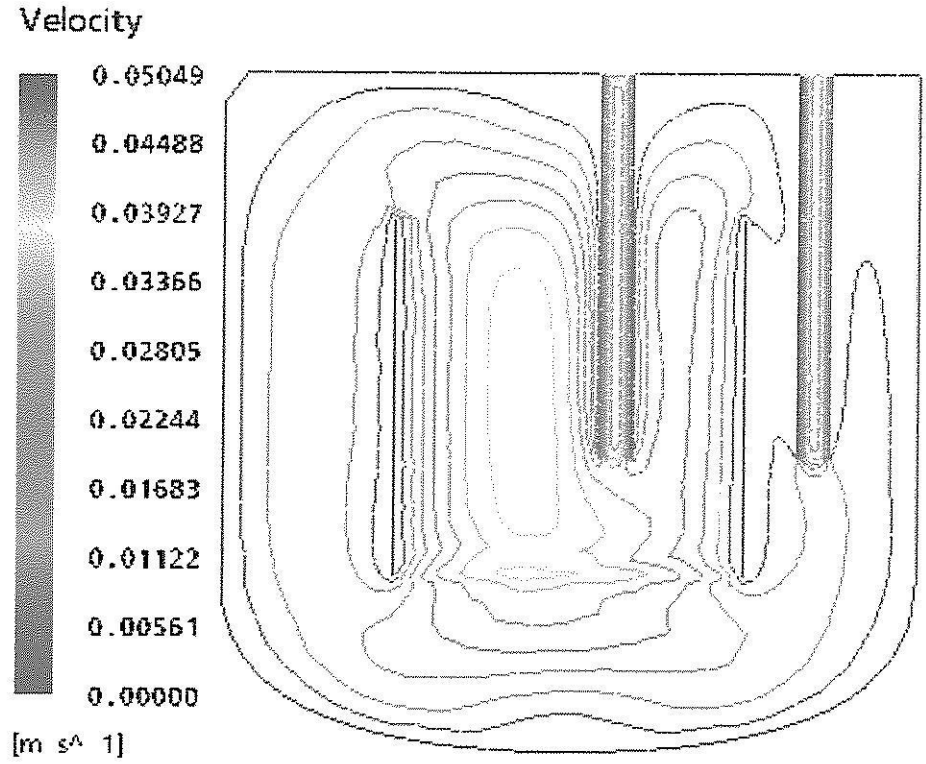

Fig. 5.11 Velocity contours in the MSMPR crystallizer for a volume rate of momentum addition of 10,000 $kg/m^2/s^2$.

The velocity vector plot for the fluid near the product tube shows that the product sampling is still not isokinetic. The flow acceleration before the fluid enters the product tube is evident, particularly in that the velocity vectors are equal at the plane on the left hand side of the plot, but have a significant (~25%) increase at the center for the vectors immediately before the mouth of the tube. There is flow divergence of the fluid outside the product tube in the region after the mouth of the tube, however this is due to divergence related to the zero-slip condition on the wall of the tube. Note that the fluid has essentially reached a steady profile for laminar flow of fluid through a cylindrical section (a parabolic velocity profile) by the time it reaches the end of the section plotted. This indicates that the average velocity in the tube can bet determined halving the maximum velocity present at the centre of the product tube. (The true average velocity in the tube can also be calculated from the product flow rate, the fluid density, and the cross-sectional area of the tube).

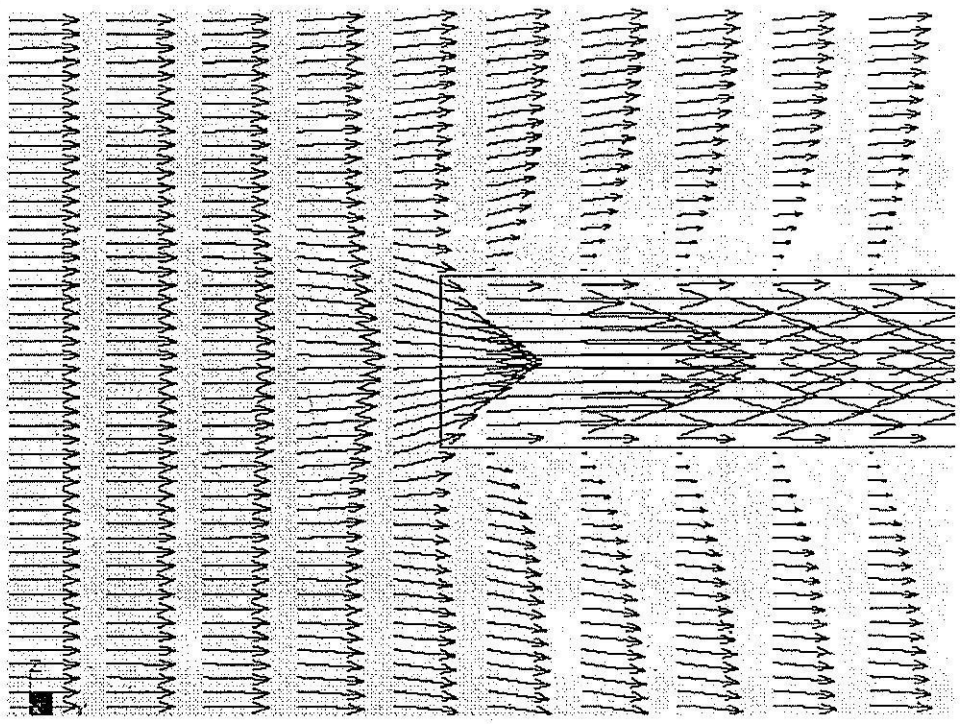

Fig. 5.12 Velocity vectors around the outlet tube of MSMPR crystallizer for a volume rate of momentum addition of 10,000 kg/m^2/s^2 (the figure is rotated 90° for convenience).

Momentum Source Strength of 15,000 kg/m^2/s^2

Increasing the momentum source strength from 10,000 to 15,000 kg/m^2/s^2 increases both the downward flow through the draft tube and the upflow velocity in the annular space. Now the downflow velocity in the draft tube is of a similar magnitude to the inflow velocity in the feed tube, and the pumping action of the impeller is quite sufficient to circulate the fluid throughout the crystallizer. The velocity vector plot is shown in Fig. 5.13.

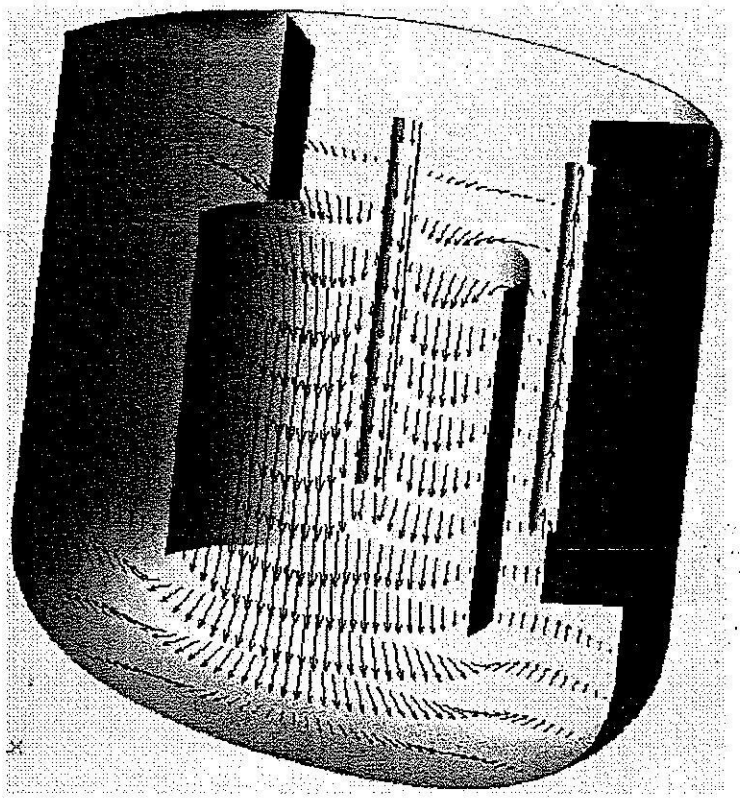

Fig. 5.13 Velocity vectors in the MSMPR crystallizer for a volume rate of momentum addition of 15,000 $kg/m^2/s^2$.

The streamline plot (Fig. 5.14) is similar to that displayed in the case of 10,000 $kg/m^2/s^2$: the fluid circulates reasonably well inside the body of the crystallizer. Although the streamlines chosen appear to be in almost a single plane of the crystallizer, the velocity vector plot does show fluid flow throughout the entire body of the crystallizer. When the swirl present below a true impeller is taken into account then the mixing in the crystallizer will be quite good, and the residence time distribution of the fluid will be similar to that of a true fully mixed vessel.

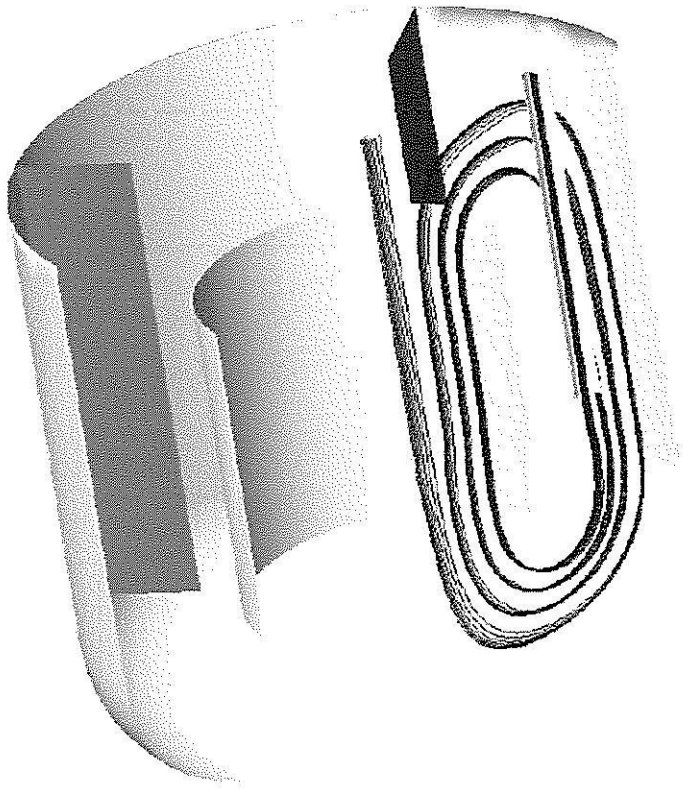

Fig. 5.14 Fluid streamlines in the MSMPR crystallizer for a volume rate of momentum addition of 15,000 $kg/m^2/s^2$.

The velocity contour plot for 15,000 $kg/m^2/s^2$ (Fig. 5.15) shows similar behavior to the similar plot at 10,000 $kg/m^2/s^2$, although there is a significantly (>30%) higher velocity in the draft tube, which has higher velocities than the feed tube at certain points. Again, the velocity in the region far from the inlet tube is much higher (approximately two times larger) than the velocity in the region of the draft tube close to the product tube. Also, the velocity in the region around the product tube is lower than the velocity in the bulk of the annular space. The velocity in the base of the crystallizer under the impeller has also improved slightly, but there still appears to be a small region of near stagnant fluid near the base of the crystallizer. It is important to note that although the streamlines for the inlet and product tubes look different to those in the previous cases this is only due to an increase in the maximum velocity in the crystallizer, which changes the coloring and scale on the plot. This is because the maximum velocity no longer occurs in the inlet and outlet tubes, but now occurs in the draft tube. In fact the velocity profiles in the inlet and outlet tubes are the

same for all conditions, with the exception of slight differences at the ends of the tubes due to end-effects.

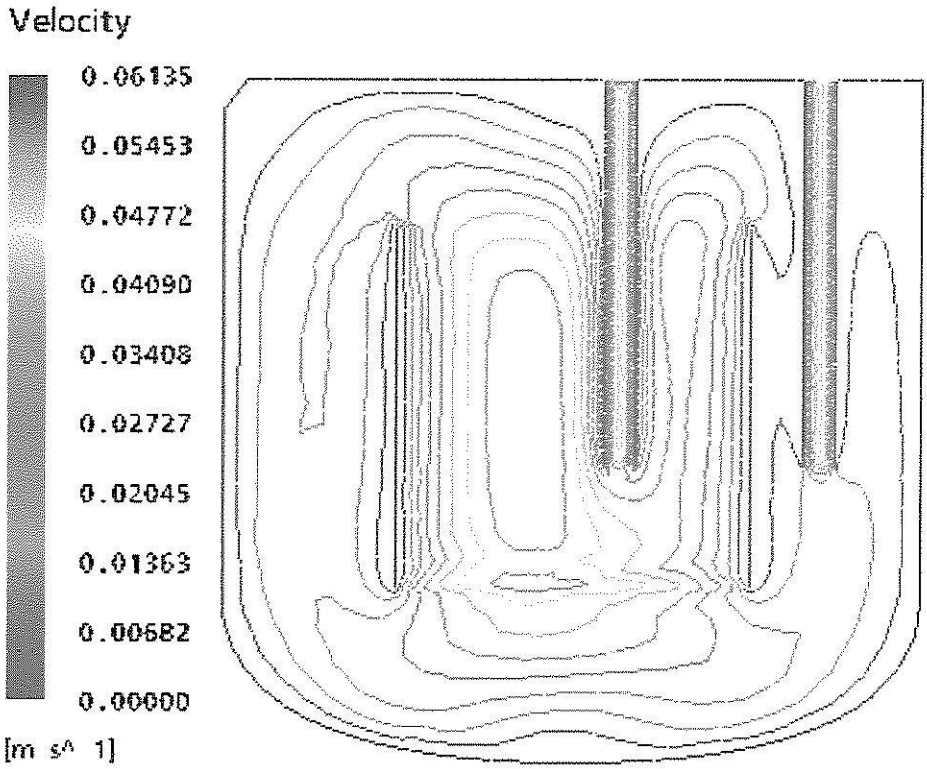

Fig. 5.15 Velocity contours in the MSMPR crystallizer for a volume rate of momentum addition of 15,000 $kg/m^2/s^2$.

The plot of the velocity vectors around the product tube show that the velocity of the streamlines near the entry to the product tube at the left hand side of Fig. 5.16 (far enough from the mouth of the tube to avoid the acceleration due to the laminar profile inside the tube) is almost half of the maximum velocity in the product tube, i.e. almost equal to the average velocity in the draft tube. This indicates that the product sampling is almost isokinetic, although still slightly deficient.

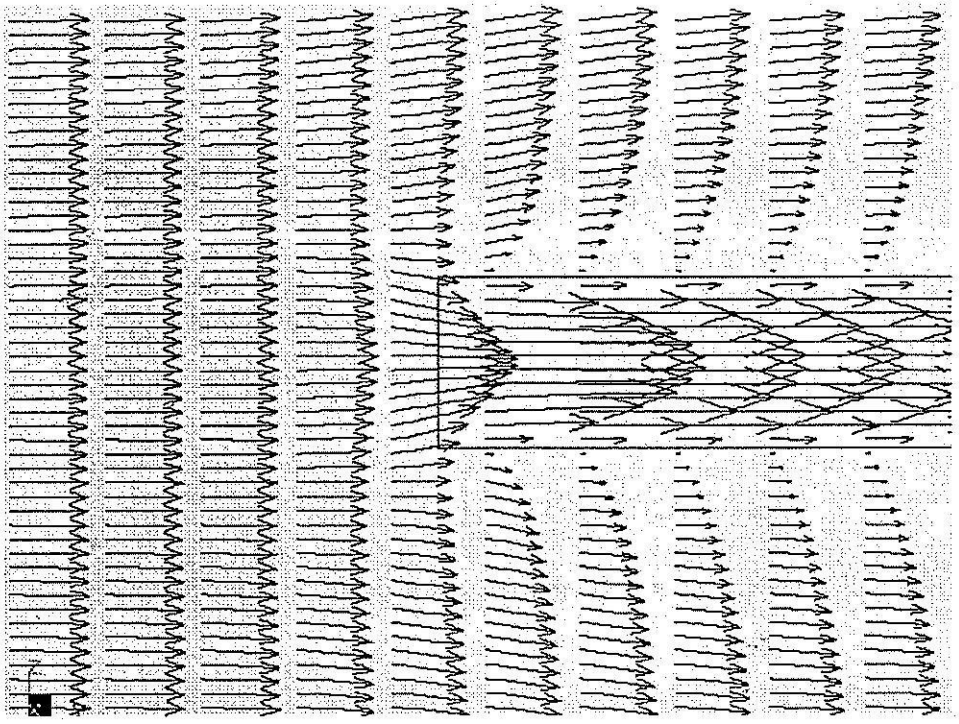

Fig. 5.16 Velocity vectors around the outlet tube of MSMPR crystallizer for a volume rate of momentum addition of 15,000 kg/m^2/s^2 (the figure is rotated 90° for convenience).

Momentum Source Strength of 18000 kg/m^2/s^2

The Momentum source strength of 18,000 was chosen since an extrapolation of previously performed data showed that this should be the point of isokinetic sampling in the crystallizer. It is evident that while there are strong similarities between the velocity vector plot for this (Fig. 5.17) case and for the 15,000 kg/m^2/s^2 case, in this case the velocity in the crystallizer has a higher magnitude particularly in the draft tube. The streamline plot (Fig. 5.18) appears identical to the plot for 15,000 kg/m^2/s^2, partly due to the fact that such plots only show directions of flow rather that the speed of the flow. The circulation of the fluid through the crystallizer is suitable for the system; although the streamlines chosen mainly appear to go through a plane, this is due to those streamlines plotted. In the real crystallizer, swirl below the impeller and the baffles will mixed fluid in this region, although the flow will straighten again due to the presence of the vertical baffles in the annular space.

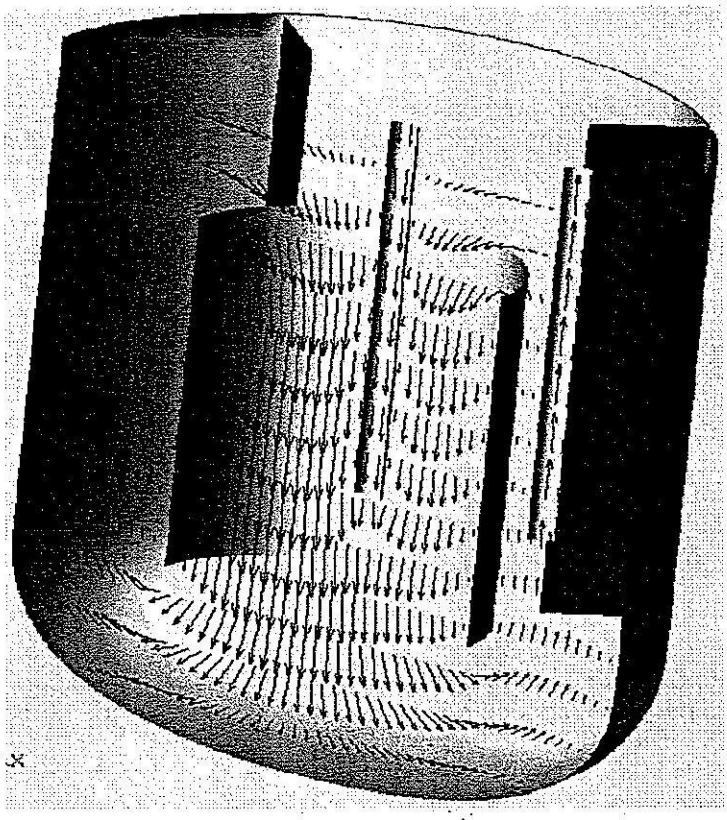

Fig. 5.17 Velocity vectors in the MSMPR crystallizer for a volume rate of momentum addition of 18,000 $kg/m^2/s^2$.

The velocity contour plot for the crystallizer with a source strength of 18,000 $kg/m^2/s^2$ is shown in Fig. 5.19. The velocity in the free are of the draft tube (in regions away from the feed tube) is higher than the velocity in the feed tube under this condition. The downflow velocity in the main area of the draft tube is now in excess of 7 cm/s, although this is not a particularly high velocity in industrial crystallizers, since in this situation the fluid has a very high viscosity relative to most aqueous phase crystallizations. (The high viscosity is due to the high sugar content required for a supersaturated solution if an aqueous crystallization is performed). The general flow features in this case are very similar to the case of 15,000 $kg/m^2/s^2$.

As in previous cases there is still a small region between the product tube and the wall of the draft tube that has a very low upflow velocity, less than 10% of the maximum velocity magnitude in the crystallizer. This area is undesirable, although it is difficult to avoid because of the need to have a product tube in the annular space, which is necessarily

a relatively thin area (to avoid very low upflow velocities in the entire space). The volume that this occurs in is a very small fraction of the total volume of the annular space.

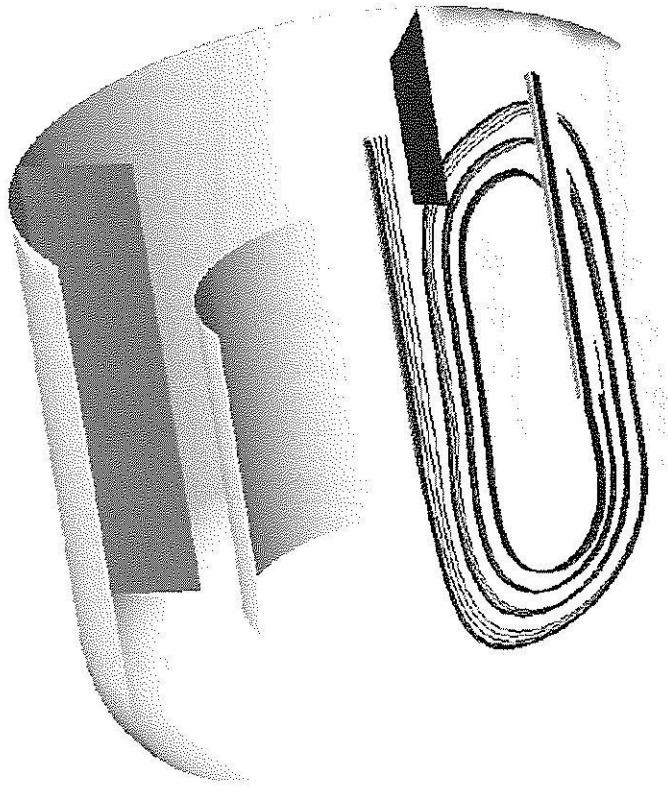

Fig. 5.18 Fluid streamlines in the MSMPR crystallizer for a volume rate of momentum addition of 18,000 $kg/m^2/s^2$.

The velocity vector plot around the product tube for a momentum source strength of 18,000 $kg/m^2/s^2$ is shown in Fig. 5.20. This figure indicates fully isokinetic sampling of the streams into the product tube. The velocity vectors are of constant magnitude across the region in front of the product tube until very close to the product tube. At this point the vectors very close to but just inside the plane of the tube wall turn inwards slightly in an end effect such that a parabolic velocity profile can begin to be formed in the tube. The vectors just outside the plane of the tube wall turn outwards slightly since there is a zero slip condition on the outside of the tube wall. Analysis of the flow (described later) confirms that the velocity in the section approaching the tube mouth is exactly the average velocity of the fluid inside the product tube, confirming isokinetic flow sampling.

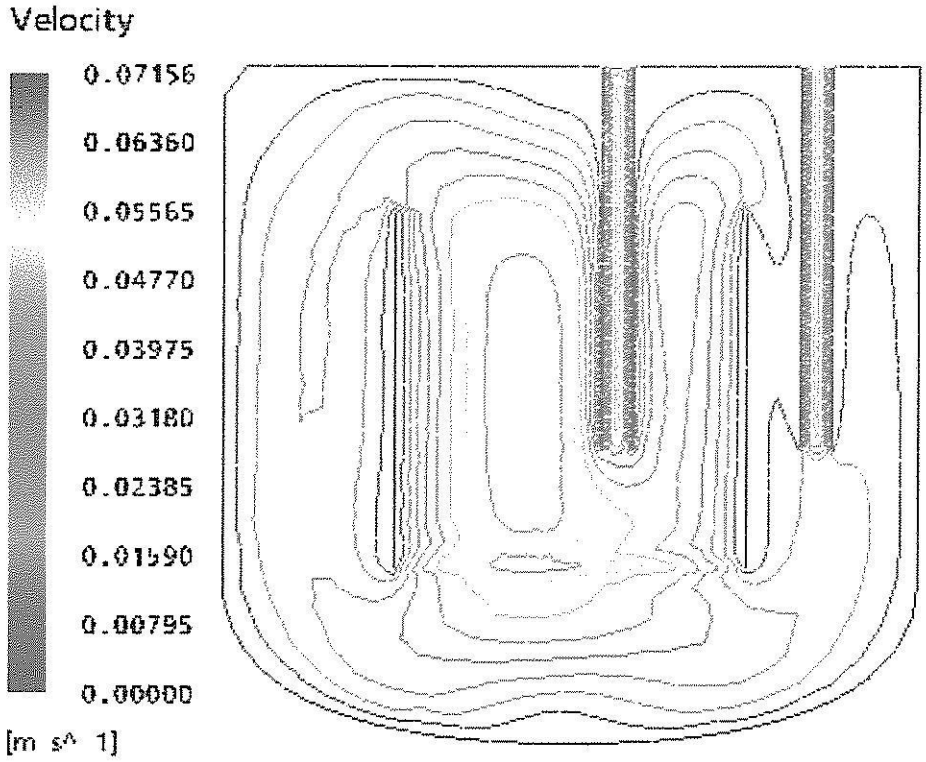

Fig. 5.19 Velocity contours in the MSMPR crystallizer for a volume rate of momentum addition of 18,000 $kg/m^2/s^2$.

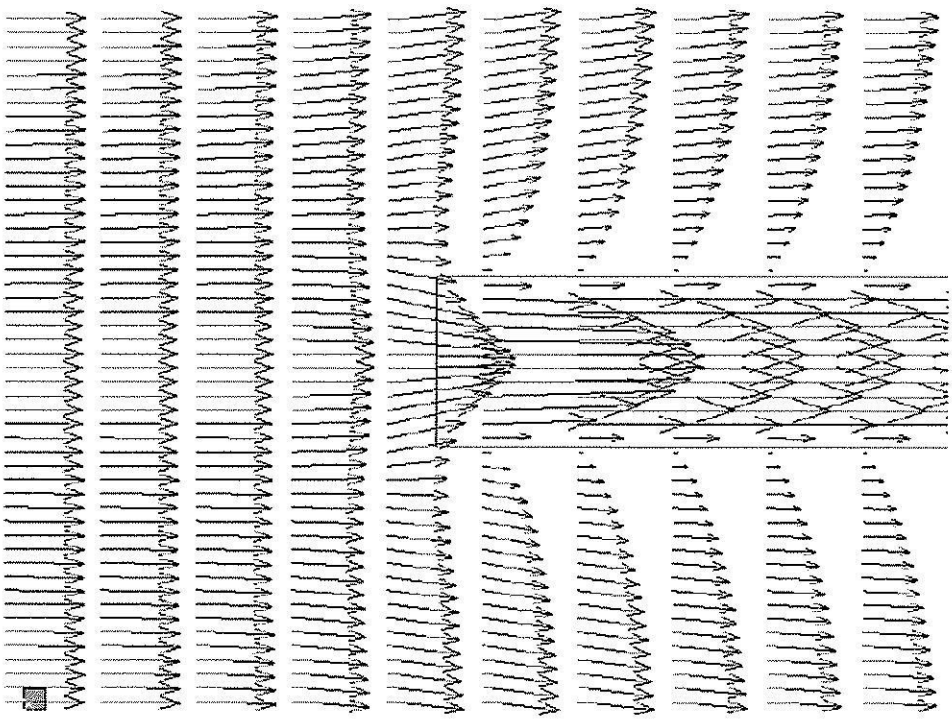

Fig. 5.20 Velocity vectors around the outlet tube of MSMPR crystallizer for a volume rate of momentum addition of 18,000 $kg/m^2/s^2$ (the figure is rotated 90° for convenience).

Momentum Source Strength of 30000 kg/m^2/s^2

Simulations at momentum source strengths larger than the isokinetic condition were also studied in order to visualize what occurs in the crystallizer if too high momentum source strengths (or equivalently excessive impeller power inputs) are used. This will cause the flow outside the product tube mouth to be too high, causing flow divergence away from the tube mouth. Under these conditions the small particles that should be sampled in the product tube are carried away from the mouth the tube, while the increased momentum of the larger particles allows them to enter the mouth of the tube rather than diverging away from the tube. This will result in an excess of large particles in the population density of the product, and therefore an incorrect measurement of the nucleation and growth rates in the crystallizer.

The velocity vector plot for the crystallizer using this momentum source strength is shown in Fig. 5.21.

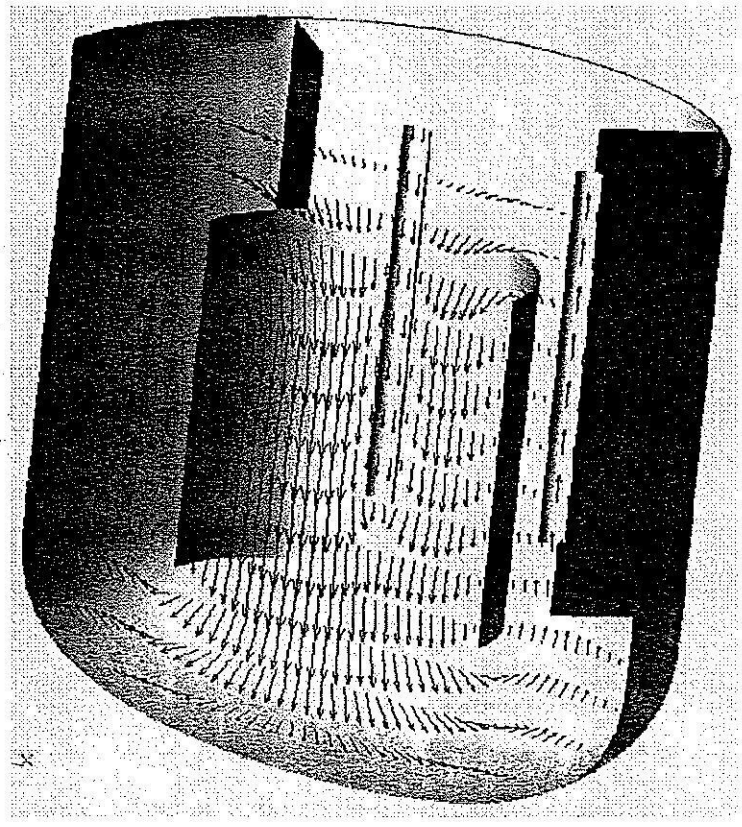

Fig. 5.21 Velocity vectors in the MSMPR crystallizer for a volume rate of momentum addition of 30,000 kg/m^2/s^2.

The velocity vector plot again shows similar behavior in the crystallizer to results of momentum source greater than 10,000 $kg/m^2/s^2$, however with higher downflow velocities in the draft tube, and slightly higher upflow velocities in the annular space. The streamline plot (Fig. 5.22) also shows similar behavior to the results for momentum source strengths greater than 10,000 $kg/m^2/s^2$.

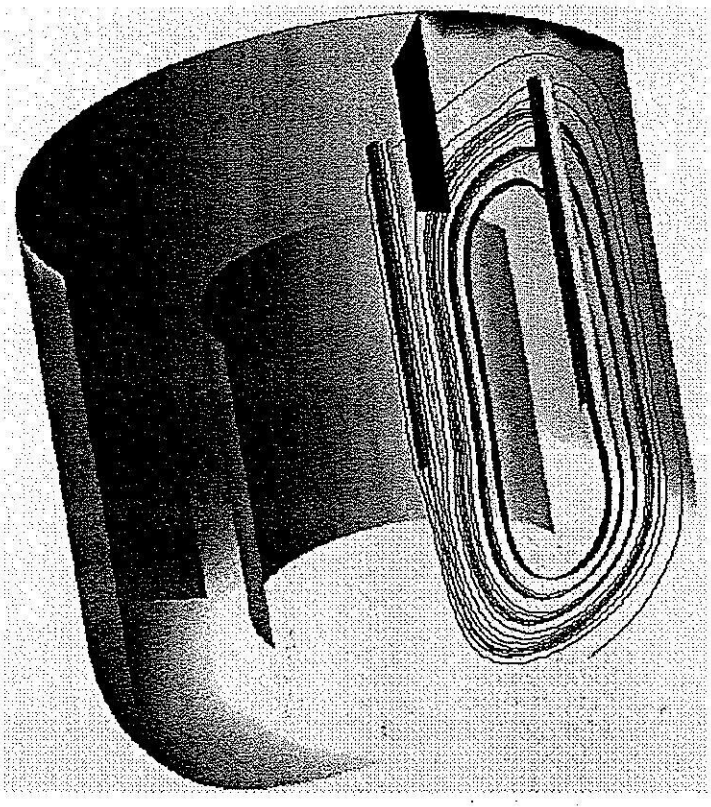

Fig. 5.22 Fluid streamlines in the MSMPR crystallizer for a volume rate of momentum addition of 30,000 $kg/m^2/s^2$.

The velocity contour plot for 30,000 $kg/m^2/s^2$ (Fig. 5.23) appears very similar to the equivalent diagrams for 15,000 $kg/m^2/s^2$ and 18,000 $kg/m^2/s^2$, however it is necessary to take into account the much higher maximum velocity evident in the contours (0.108 m/s) relative to the maximums in the previous plots (0.0716 and 0.0614 m/s respectively). It is also evident that the maximum velocity in the draft tube is now much larger than the average velocity (and indeed even the maximum velocity) in the feed tube. The low velocity area in the base of the crystallizer (under the impeller) still appears, however the

average velocity in this region is still higher than in previous simulations, which is apparent when the change in the scale of the velocity in the legend is taken into account.

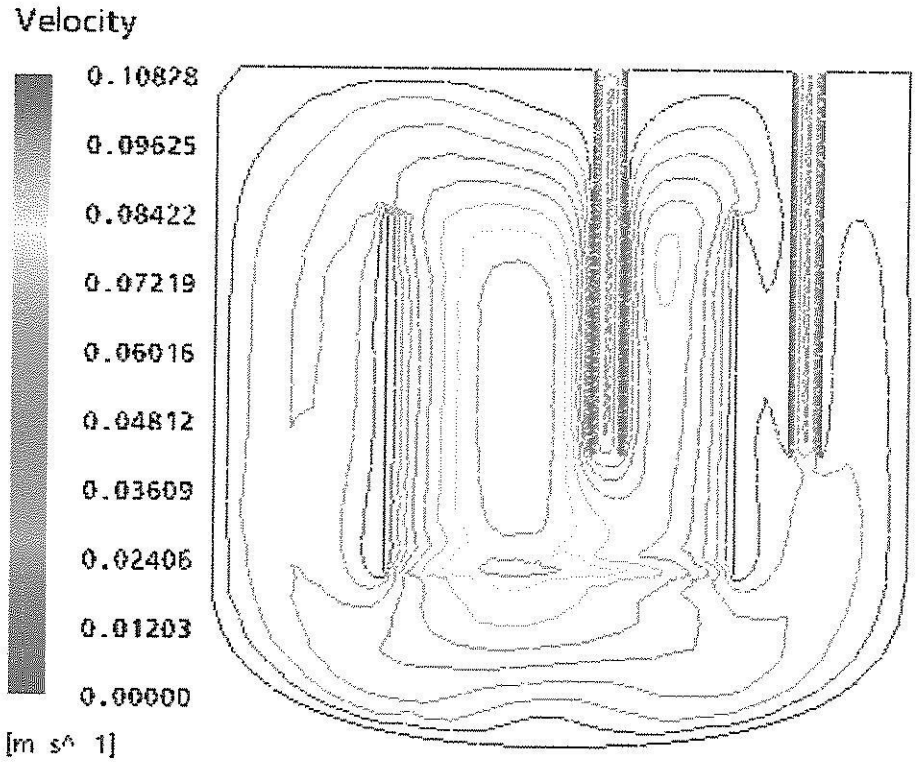

Fig. 5.23 Velocity contours in the MSMPR crystallizer for a volume rate of momentum addition of 30,000 $kg/m^2/s^2$.

The velocity vectors around the mouth of the outlet tube are shown in Fig. 5.24. The increased momentum source strength has a larger affect on the velocity in the downflow region of the draft tube than the upflow region near the product outlet tube, as can be seen when comparing Fig. 5.20 with Fig. 5.24. The velocity vectors in the tube in the two figures indicate the same velocity, since the flow out of the crystallizer is set as 2.5 L/hr in both cases, while the flow in the fluid around the tube has only a slightly increased velocity in Fig. 5.24. In spite of this it was found that the flow in the fluid around the mouth of the tube was in excess of the isokinetic velocity, indicating that the flow is not isokinetic at 30,000 $kg/m^2/s^2$.

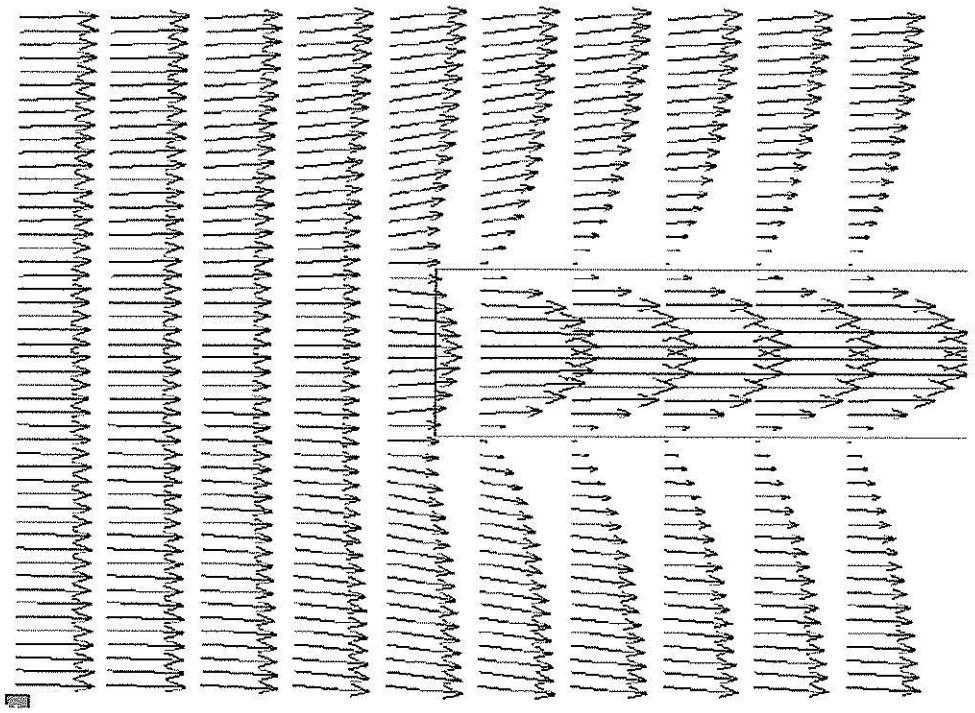

Fig. 5.24 Velocity vectors around the outlet tube of MSMPR crystallizer for a volume rate of momentum addition of 30,000 kg/m^2/s^2 (the figure is rotated 90° for convenience).

Momentum Source Strength of 50000 kg/m^2/s^2

The velocity vector plot for the crystallizer with a momentum source strength of 50,000 kg/m^2/s^2 is shown in Fig. 5.25. The flow in the crystallizer is similar to the study at 30,000 kg/m^2/s^2, however the flow in the draft tube is now relatively high in all regions, even those very close to the zero slip condition on the wall of the inlet tube. The velocity of the flow close to the outlet tube is still much lower than that in the rest of the annular space, as is evident from a comparison of the vectors on the left hand side of Fig. 5.25 to those on the right hand side near the outlet tube. The strong downward velocity in the draft tube is likely to almost entirely remove the stagnant zone in the base of the crystallizer. It is also possible to see that since the downflow velocity in the draft tube due to the momentum addition is far higher than the velocity of the fluid at the mouth of the inlet tube. This creates a strong flow from the high velocity region of the draft tube into the space below the mouth of the inlet tube, as evident in the velocity vectors directed into this space. This is a similar affect to that which creates the non-isokinetic sampling, however on a larger scale here since the differences in velocity are higher. This is not as significant

however: typically there are no particles in the inflow, and if there were particles in the inflow, the assumption of complete mixing would be helped by this phenomenon.

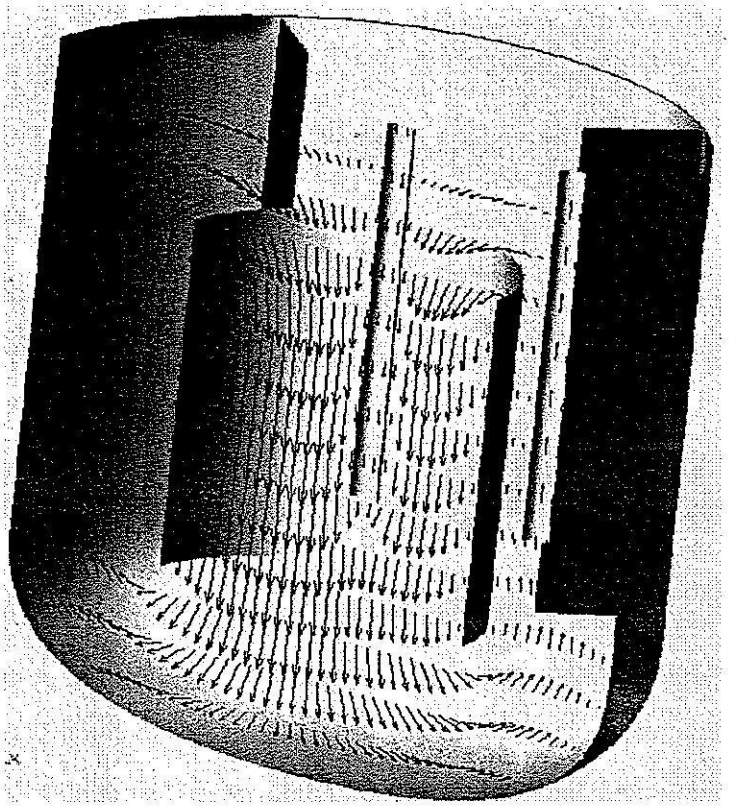

Fig. 5.25 Velocity vectors in the MSMPR crystallizer for a volume rate of momentum addition of 50,000 $kg/m^2/s^2$.

The streamline plot for a momentum source strength of 50,000 $kg/m^2/s^2$ is shown in Fig. 5.26. The streamline plot in this case does not add much detail to the analysis, as we see complete circulation in the crystallization, as before, but have little idea of velocity magnitudes from the streamlines. There is a small amount of flow diversion at the mouths of the inlet and outlet tubes.

The velocity contour plot for 50,000 $kg/m^2/s^2$ (Fig. 5.27) again appears similar to that for 30,000 $kg/m^2/s^2$: however in this case the maximum contours are in the range of 0.16 m/s which is a relatively large velocity for a highly viscous liquid in a crystallizer, but not sufficient to make the flow turbulent. The velocities in the region of the draft tube far from the inlet tube (particularly in the left hand side of Fig. 5.27) are much higher than those in the region of the inlet tube.

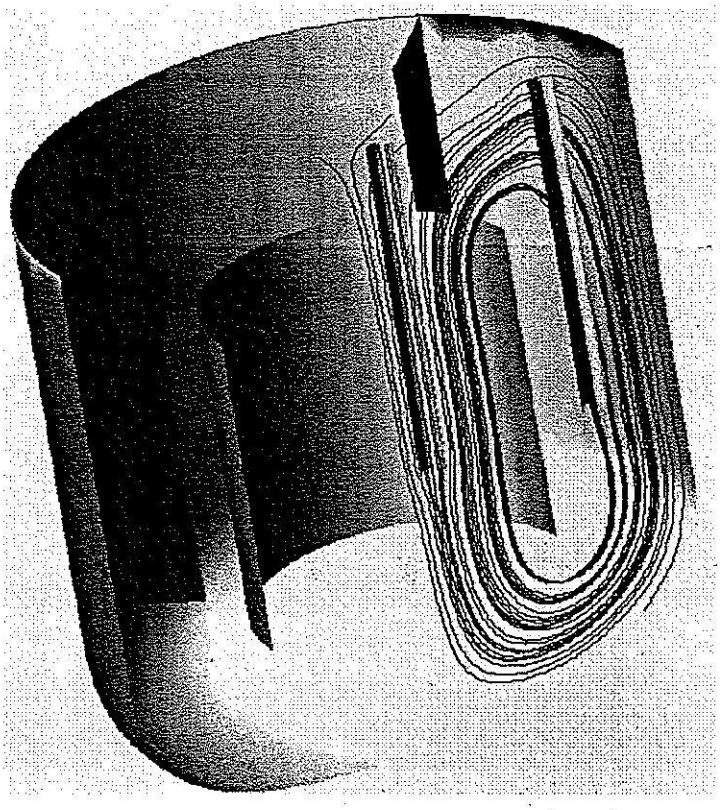

Fig. 5.26 Fluid streamlines in the MSMPR crystallizer for a volume rate of momentum addition of 50,000 $kg/m^2/s^2$.

Fig. 5.28 shows the velocity vectors in the region of the outlet tube for a momentum source strength of 50,000 $kg/m^2/s^2$. It is evident that the maximum velocity in the outlet tube is only slightly higher than the velocity in the tank at a point close to the mouth of the tube. This indicates that the average velocity in the tube (half of the maximum velocity for laminar flow in a tube far enough from the end that end-effects can be neglected) is substantially lower than the average velocity in the tank at that point. It is also clearly seen that the flow lines diverge from the tube at the point of entry into the tube. Both these indicate that the sampling is strongly sub-isokinetic at this value of the momentum source strength. Under these conditions large particles will be sampled at much higher efficiencies than smaller particles, and hence the particle population density in the product will be significantly different to the particle population density within the crystallizer. This will lead to incorrect estimates for the crystal growth rate and nucleation rates from this crystallizer.

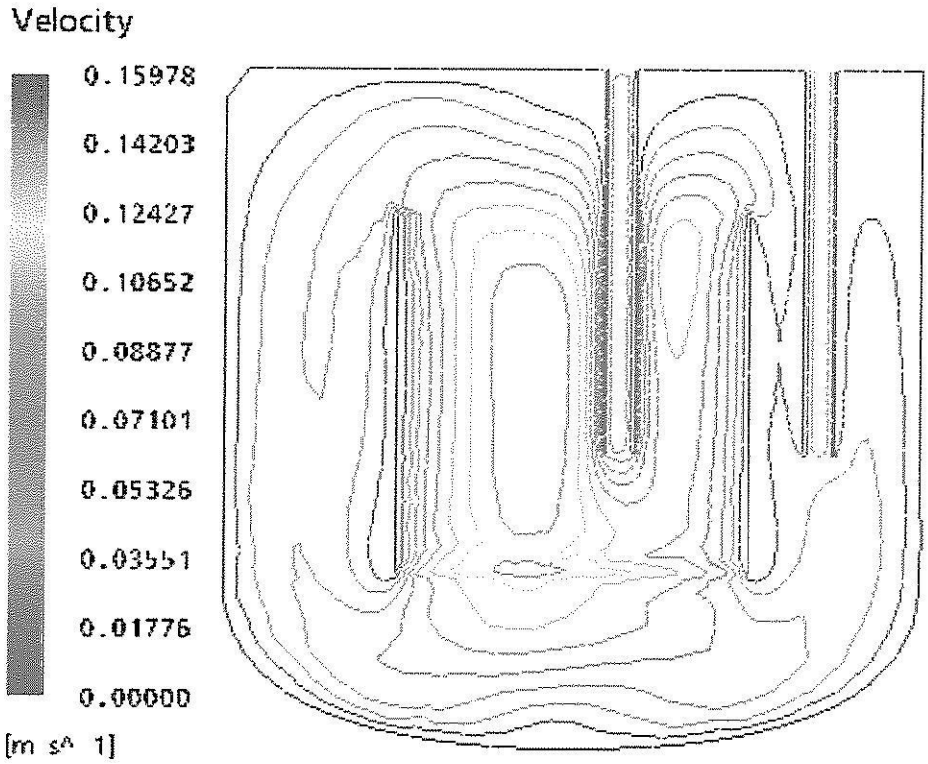

Fig. 5.27 Velocity contours in the MSMPR crystallizer for a volume rate of momentum addition of 50,000 kg/m^2/s^2.

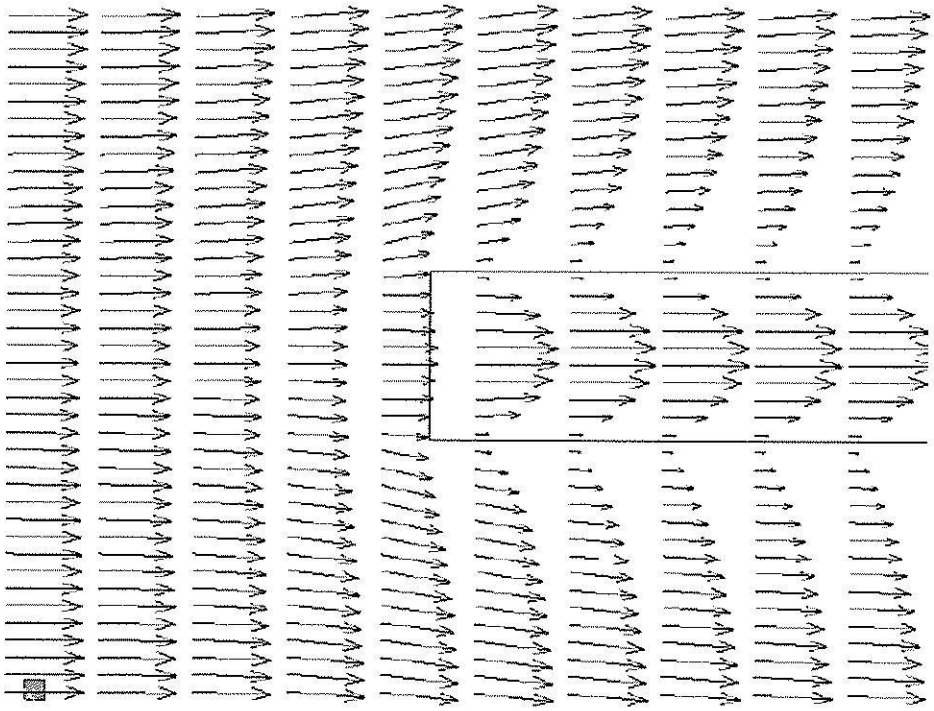

Fig. 5.28 Velocity vectors around the outlet tube of MSMPR crystallizer for a volume rate of momentum addition of 50,000 kg/m^2/s^2 (the figure is rotated 90° for convenience).

Figures 5.29, 5.30, and 5.31 show the overall velocity vectors, the enlarged velocity vectors near the mouth of the outlet tube, and the streamlines near the mouth of the outlet tube, respectively, for 0, 1000, 18000 and 50000 $kg/m^2/s^2$ together for easier comparison. These figures indicate that for the baseline case (no momentum addition at the impeller location) the overall magnitude of the velocity of the flow field is rather low (Figure 5.29a), except for those portions near and within the inlet and outlet tubes. As such, the overall flow feature is non-uniform. Flow acceleration and a convergent flow pattern near the mouth of the outlet tube (Figures 5.30a and 5.31a) are quite obvious. This, as mentioned earlier, is undesirable because it will lead to a poor size distribution of the crystals in the product tube, with a greatly exaggerated amount of fine particles in the product.

As the momentum added through the impeller increases the velocity vectors become larger, both in the downflow section in the draft tube, and in the upflow area in the annular space. This results in a stronger flow at the bottom of the draft tube, and also a higher velocity flow up in the annular space, which will assist in suspension of particles. Since the flow in the circular product tube is laminar, it is possible to determine the average flow velocity in the tube as half of the maximum flow, which occurs at the central point of the tube (assuming this is performed far enough from the tube end so that entrance effects are not significant). Thus it is evident from Figures 5.30 and 5.31 that the flow velocity in the annular space approaches, but is slightly less than, the average flow velocity in the product tube when the momentum added is 18,000 $kg/m^2/s^2$, while at 50,000 $kg/m^2/s^2$ the flow velocity outside the product tube is significantly higher than the isokinetic condition.

Overall velocity magnitude contours are depicted in Figure 5.32 wherein it is observed that they are basically of the same general feature without any drastic change in structure, such as the formation of the recirculation zones inside the draft tube sometimes observed within a flow with an impeller.

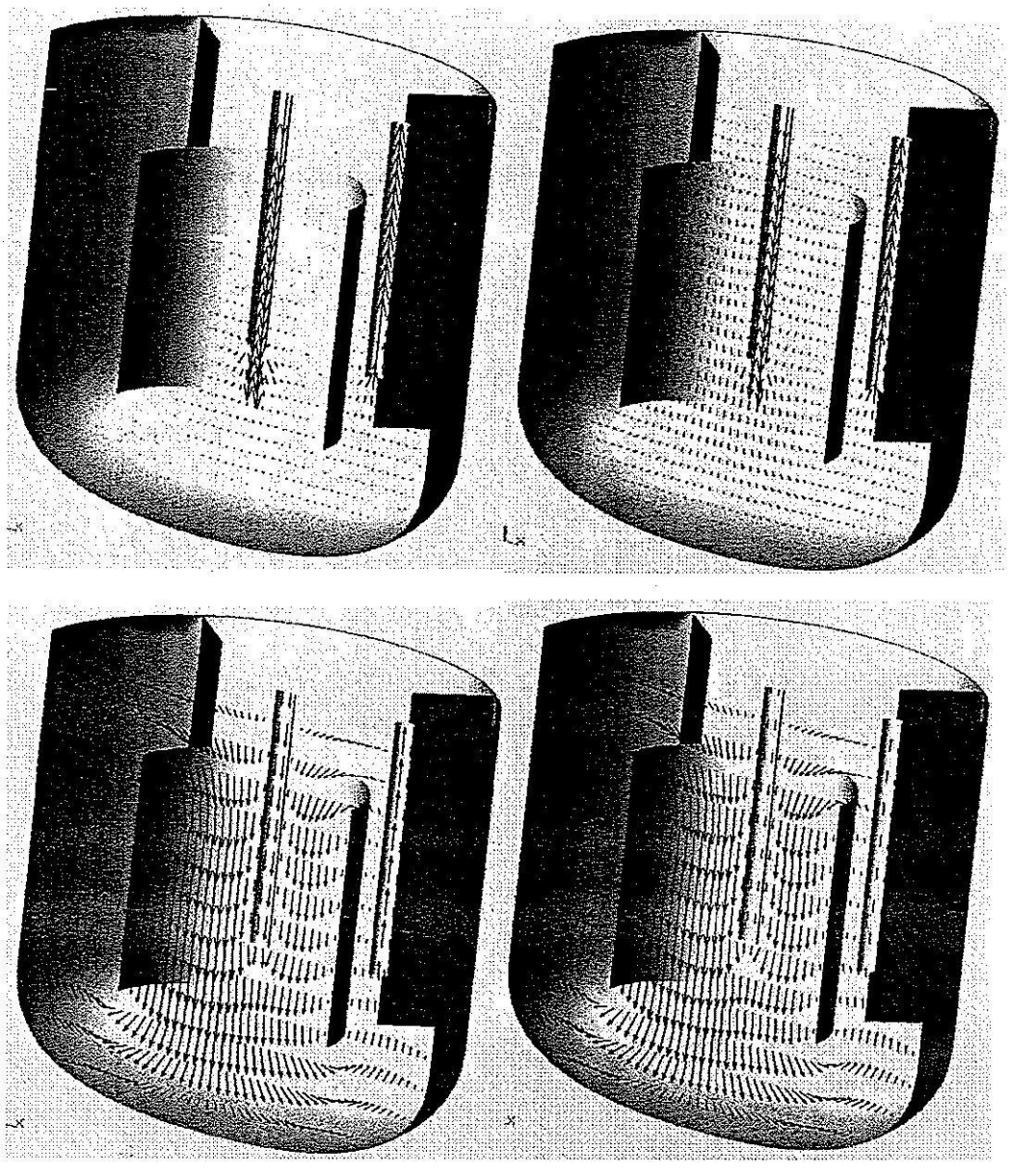

Fig. 5.29 Flow vectors in the MSMPR crystallizer for momentum source terms of 0, 1000, 18000, and 50000 $kg/m^2/s^2$.

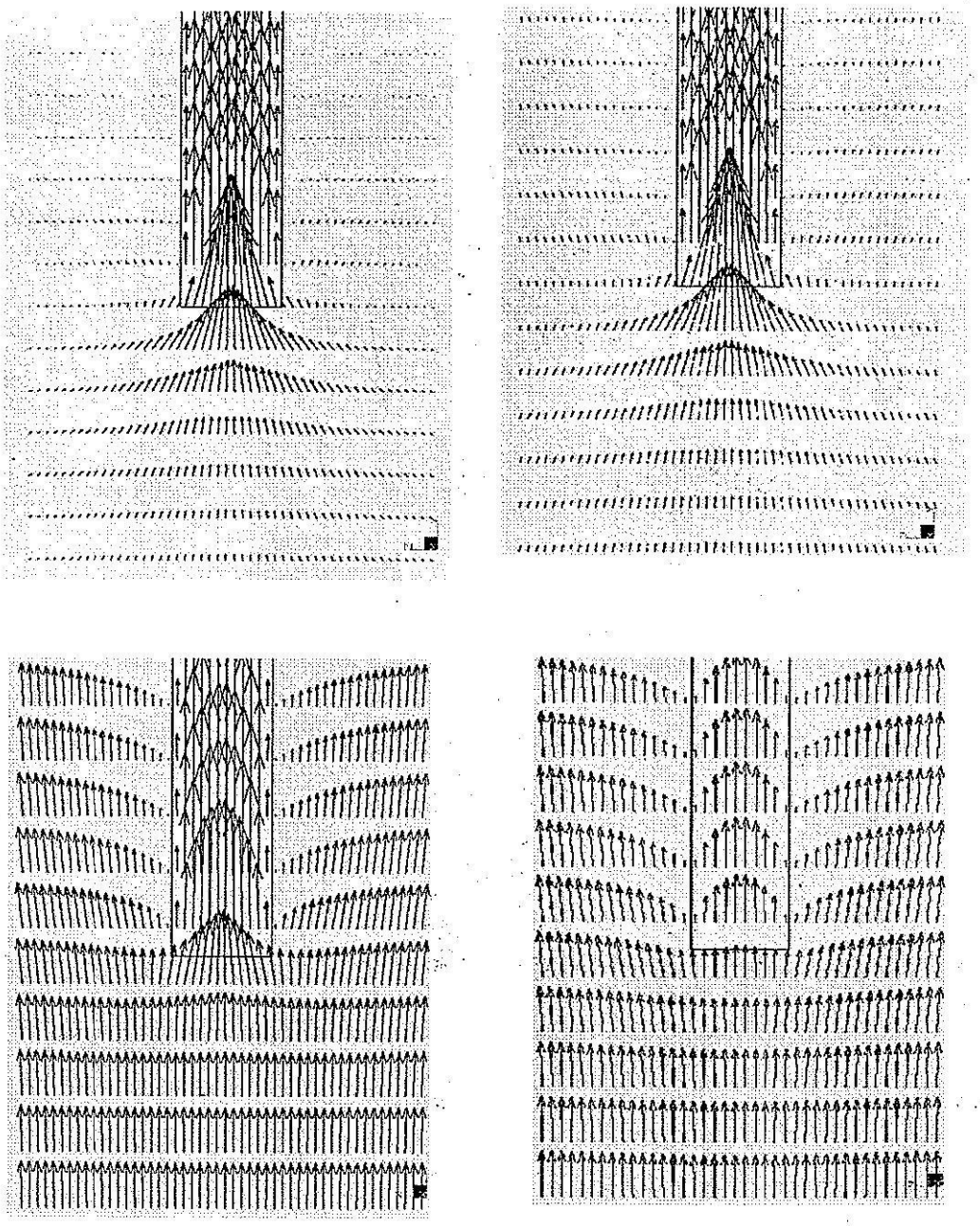

Fig. 5.30 Flow vectors near the product removal tube for momentum source terms of 1000, 18000, and 50000 $kg/m^2/s^2$.

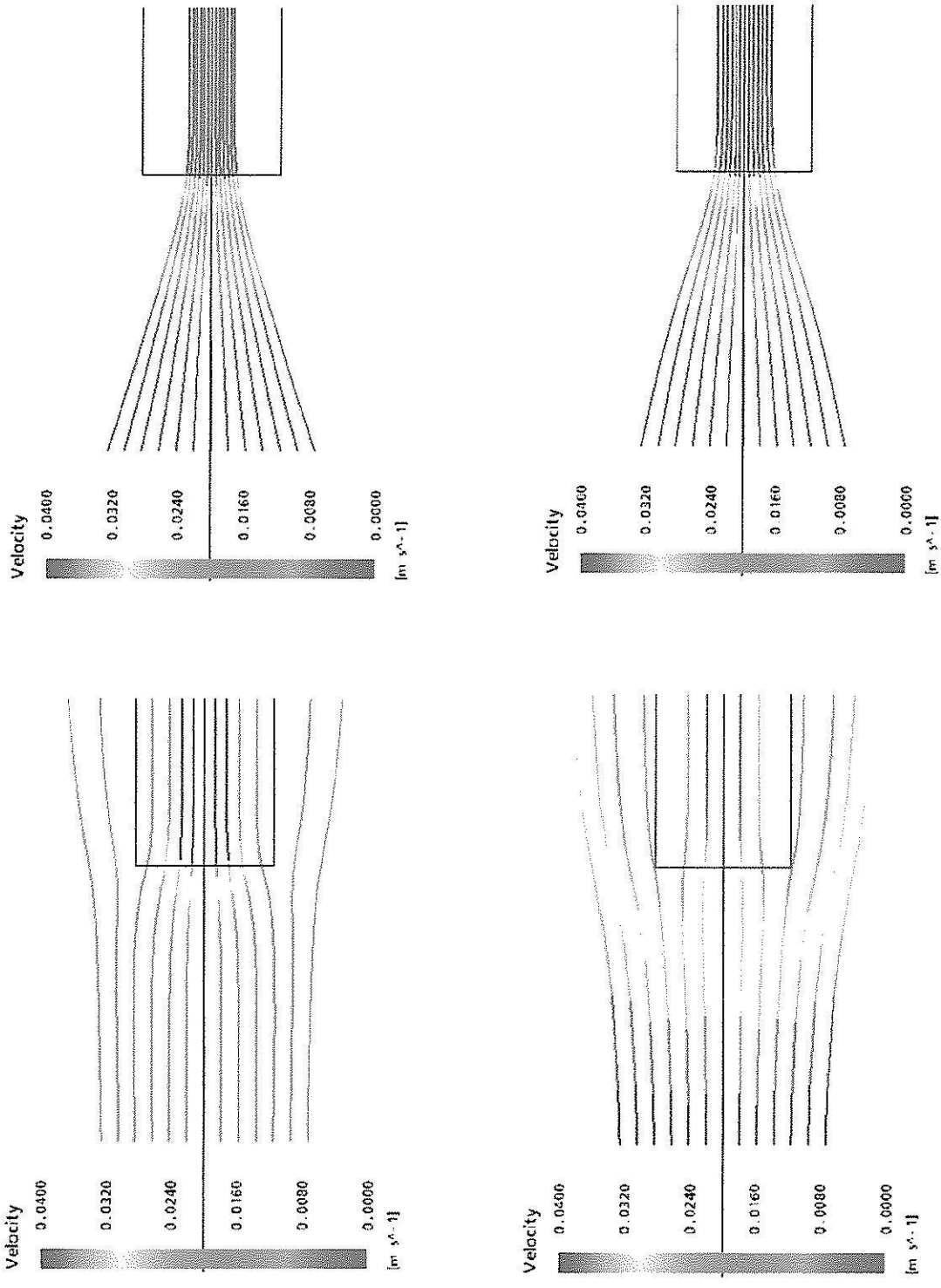

Fig. 5.31 Streamlines near the product removal tube with color indicating flow velocity, for momentum source terms of 0, 1000, 18000, and 50000 $kg/m^2/s^2$.

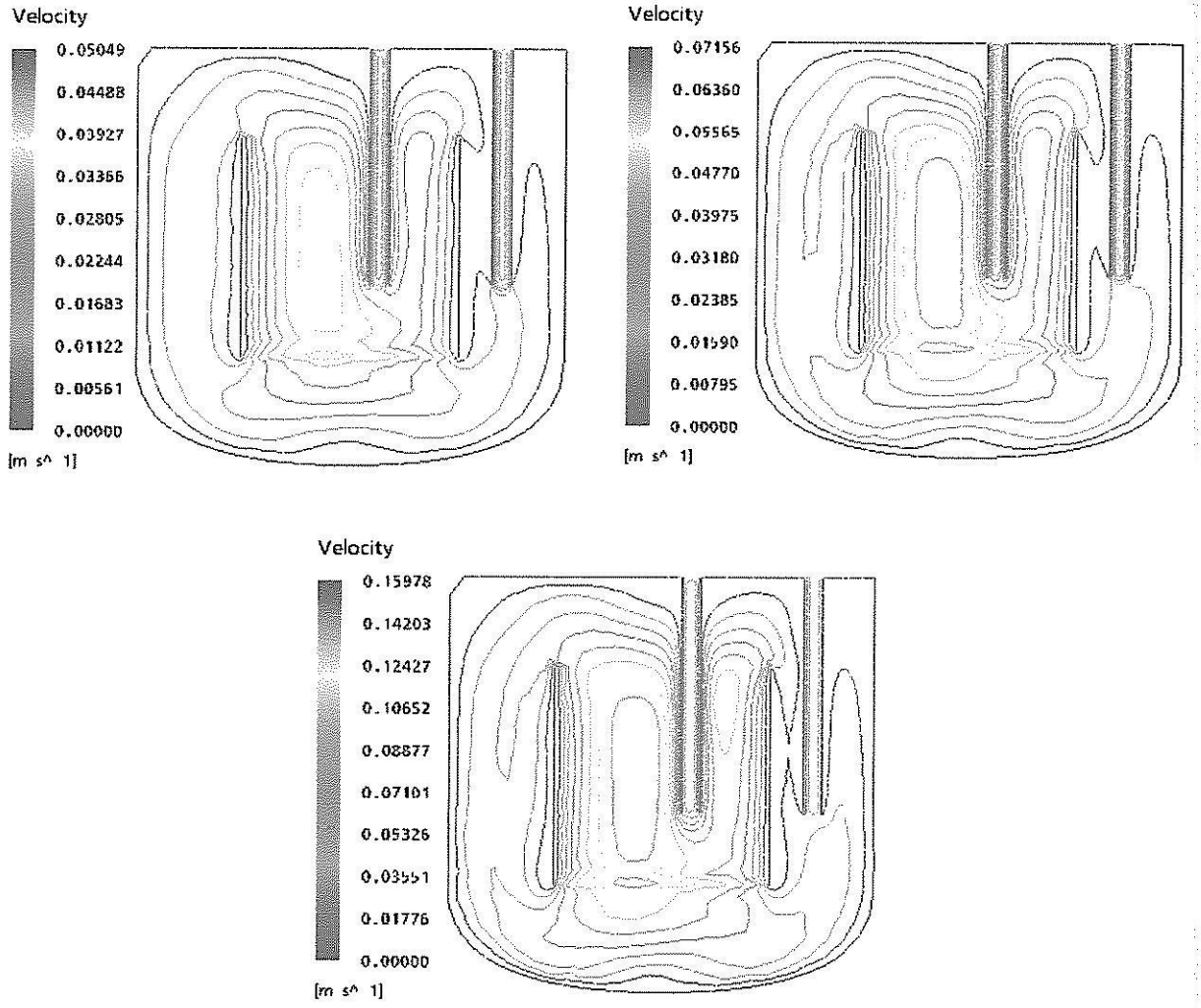

Fig. 5.32 Velocity contours in the MSMPR crystallizer for momentum source terms of 0, 1000, 18000, and 50000 $kg/m^2/s^2$.

As described previously, isokinetic withdrawal leads to the desirable crystal size distribution. It is useful to estimate the appropriate value of the momentum source that gives the isokinetic condition. Plane A in Figure 5.33 is used to obtain the average velocity. It will be compared with the average velocity inside the outlet tube. With the results obtained from the seven test cases, the fitted curve for the velocity ratio (the current velocity divided by the velocity at no source condition) versus the percent of momentum source added is shown in Figure 9 (the percent increase is calculated based on the momentum flux of the baseline value.) The appropriate value of the momentum added that gives the isokinetic withdrawal is estimated as 6.43 % of the baseline condition; this corresponds to the absolute momentum value of approximately 25400 $kg/m^2/s^2$. Then the power transmitted by impeller shaft is 0.58 Watt. The impeller rotational speed could be determined iteratively from the impeller

power correlation curve of Bates et al. [6]. In the laboratory crystallizer, which is normally used with an impeller of diameter : height ratio 8:1, with a 45° pitched blade turbine, it requires approximate 2.2 rev/s to obtain the isokinetic condition.

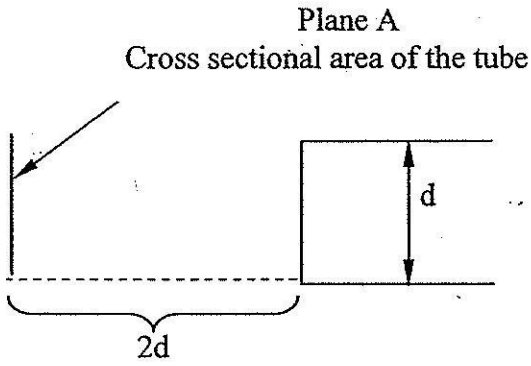

Fig 5.33 Location of the plane used to check for the isokinetic flow condition.

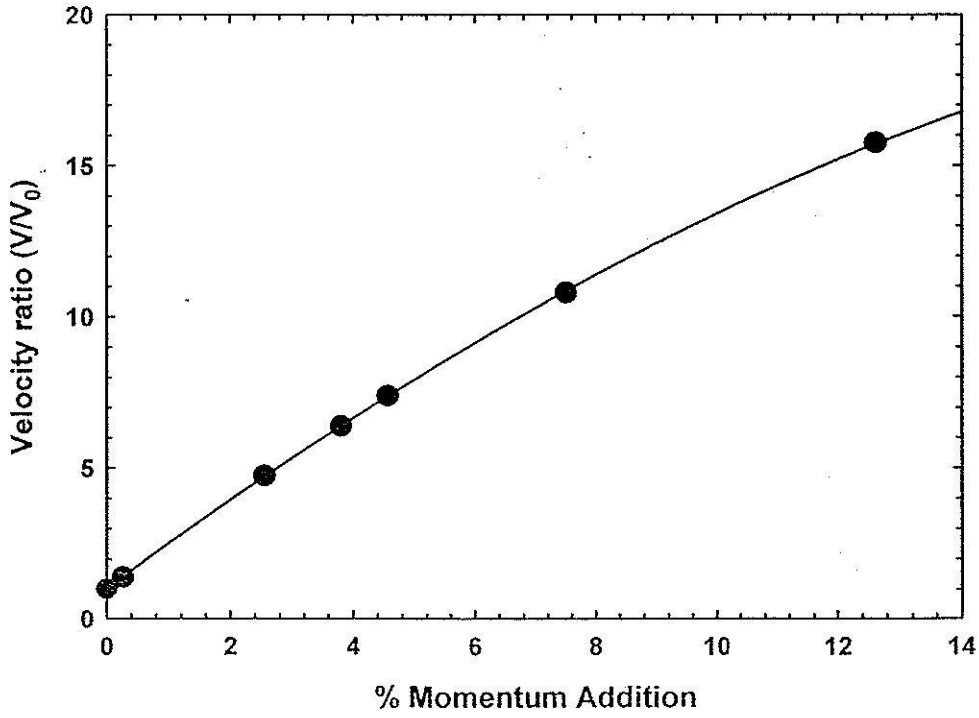

Fig. 5.34 Velocity at a plane near the outlet of the crystallizer as a function of the amount of momentum added by the impeller.

The difficulty in design of mixed-suspension crystallizers is that isokinetic flow at the product point is not a sufficient criterion to ensure the product size distribution, it is also essential that the crystals in the vessel are sufficiently well suspended in the mother liquor. Suspension of crystals only occurs if the upflow velocity of the fluid produces sufficient drag to overcome the effect of the weight of the individual particles. The suspension quality in a vessel is an extremely difficult parameter to determine experimentally, as suspensions are typically opaque, meaning that the common light sensing methods cannot detect suspension quality. Because of this, a typical parameter used to describe impeller speeds suitable for sufficient suspension is the "just suspended" criterion: this criterion states that no particle should spend more than 1-2 s on the base of the vessel at any time if the solids in the vessel is are be considered well suspended.

The most well known correlation to determine the impeller speed required in a stirred vessel to achieve a suspension at the just suspended condition is then Zwietering equation [7]

$$N_{js} = S\frac{\nu^{0.1} D_p^{0.2} \left(g\Delta\rho/\rho_l\right)^{0.45} X^{0.13}}{D^{0.85}} \tag{5.1}$$

where S is some function of the ratio of the tank diameter to the impeller diameter (T/D) and the ratio of the tank diameter to the impeller clearance (T/C_B). The impeller clearance is the distance from the base of the impeller to the bottom of the vessel. The most commonly used equation for the parameter S was developed by Nienow [8]

$$S = 2\left(\frac{T}{D}\right)^{1.33} \tag{5.2}$$

A more recent correlation [9] also accounts for variations in the impeller clearance. For a pitched blade impeller similar to the type used in the laboratory scale crystallizer, the correlation is

$$N_{js} = 2.32\left(\frac{T}{D}\right)^{0.84}\left(0.72\frac{C_B}{T}+1\right)D^{-0.82}X^{0.11}D_p^{0.23}\nu^{0.09}\left(\frac{g\Delta\rho}{\rho_l}\right)^{0.51} \tag{5.3}$$

Unfortunately, these correlations (and other similar correlations) are based on results in flat bottomed vessels without draft tubes, whereas the crystallizer being modeled has a round bottom and a draft tube, for which no correlation for suspension conditions is available in the literature. Draft tubes, in particular, greatly increase the ability of an agitator to suspend particles in a vessel because they create a condition where the upward flow and downward flow parts of the flow loop are clearly segregated, allowing a high upflow velocity in the annular space of the vessel. This means that results of these correlations will predict impeller speeds that are higher than necessary to suspend a particle in a vessel such as we are using, but it is still instructive to use them to obtain an idea of the general magnitude of the particles suspended at the isokinetic condition.

The Zwietering correlation (equations 5.1 and 5.2) and the Armenante correlation (equation 5.3) were used to estimate a value for the size of particles that would be suspended if the stirrer was operated at 2.2 rev/s in the experimental crystallizer. Geometrical parameters for the crystallizer were the same as used in the CFD model (see Figure 1), as were the fluid and particle properties. Using the calculated impeller speed to achieve isokinetic flow at the product point (2.2 rev/s), it is possible to estimate the maximum size of particle that would be fully suspended in the crystallizer. At a solid suspension of one percent (a typical value for the laboratory crystallizer studied here) the Zwietering correlation predicts that only particles smaller than 10 micrometer will be suspended adequately, while the Armenante correlation predicts particles small than 20 micrometer will be suspended adequately. These correlations may be inadequate for the crystallizer being investigated because they are for flat bottomed vessels not containing a draft tube. As mentioned above, the draft tube increases the agitator's ability to suspend particles by more completely segregating the upflow and downflow parts of the flow loop in the vessel. In addition, the kinematic viscosity of the fluid in the crystallizer (176×10^{-6} m^2/s) is higher than that of the most viscous liquid used to predict the correlation (148×10^{-6} m^2/s). This suggests that the crystallizer may suspend particles larger than those suggested by the correlations (and introductory two-phase simulations suggest that this is true). However the correlations do indicate that the larger particles in the crystallizer (which may be in the order of 100 μm) will not be well suspended, particularly if they approach the dead zone at the base of the crystallizer, where the fluid velocity is very low.

This leads to one of the apparent contradictions in the design of crystallizers: the agitator speed required for complete suspension may be quite different to the speed

required for isokinetic flow at the product outlet. These two conditions (suspension of particles and isokinetic flow) may appear to be related, but in fact they are quite different. Isokinetic flow can be achieved at any product flow rate either by varying the agitator speed, or by adjusting the diameter of the product tube. Smaller diameter tubes create higher velocities at the sampling point for a particular product flowrate. The typical method used to correct this in laboratory crystallizers is to have a periodic outflow in the product tube, which allows for a significantly higher flow velocity over a shorter period (typically 10 – 20 percent of the total operating time). This allows for much higher agitation speeds to be used, allowing for larger particles to be completely suspended, while maintaining an approximately isokinetic flow condition at the outlet so that the sampling of particles is ideal. This approach is very difficult to model with CFD because the simulation becomes transient (over a significant period of time to see the entire flow period), and requires a free surface as the crystallizer empties slightly during the sampling period, and refills during the period the outflow is stopped.

Chapter VI

Summary

The proposed computational study to obtain flow fields within the model sugar crystallizer appears to be a successful endeavour and the results obtained appear to be reasonable. The overall magnitude of the velocity within the crystallizer can be increased by increasing the axial momentum source. Isokinetic withdrawal condition can be achieved at approximately 25,400 $kg/m^2/s^2$ of the momentum source value, in accordance with the 2.2 rev/s for an 8:1 diameter : height, 45° pitched blade turbine. In all the seven test cases studied, the overall flow patterns remain generally the same, which is desirable because it would not complicate the design optimization process. Even with higher values of the momentum source, the velocity at the center of the tank's bottom is still low; this is undesirable because sugar crystals may settle, causing a lump of settled crystals there. The velocity magnitude inside and outside the draft tube is rather different due to the effect of the flow area; this problem could be eliminated by designing the two regions to have equal areas.

References

1. Randolph, A., Larson, M.A. Theory of Particulate Processes: Analysis and techniques of Continuous Crystallization, 2nd Ed. (1988) Academic Press, San Diego.
2. Tangtonsakulwong, J. (2003) Numerical Simulation and Analysis of Flow in a Crystallizer for Sugar production. M.E. Thesis, Suranaree University of Technology, Nakhon Ratchasima, Thailand.
3. Mersmann, A. (Ed.) Crystallization Technology Handbook (2001) Marcel Dekker, New York.
4. Flood, C., Flood, A.E. (2006). Removal of Color from the raw Sugar Manufacturing Process by Membrane Treatment. Suranaree J. Sci. Technol. 13(4): 331-342.
5. ANSYS Canada Ltd. ANSYS CFX-4.5 Manual (2002).
6. Bates RL, Fondy PL and Corpstein RR (1963). An examination of some geometric parameters of impeller power. *I&EC Process Design and Development* **2**, 310-314.
7. Zweitering TN (1958). Suspending solid particles in liquid by agitators. *Chem. Eng. Sci.* 8, 244-253.
8. Nienow AW and Miles D (1968). Suspension of solid particles in turbine-agitated, baffled vessels. *Chem. Engng Sci.* **23**, 1453-1459.
9. Armenante PM and Nagamine EU (1998). Effect of low off-bottom impeller clearance on the minimum agitation speed for complete suspension of solids in stirred tanks. *Chem. Engng Sci.* **53**, 1757-1775.

International Journal Publications

1. Jaruwan Tangtonsakoolwong, Adrian E. Flood, and Tawit Chitsomboon, "Flow Fields in an experimental mixed-suspension mixed-product-removal crystallizer: A numerical Analysis" *ScienceAsia* 32(3), 231-239 (2006).

Other Publications

1. Jaruwan Tangtonsakulwong, Adrian E. Flood, and Tawit Chitsomboon, "Flow fields in a sugar crystallizer: A numerical study" Proceedings of the 10th Tri-University International Joint Seminar and Symposium 2003, Mie, Japan.

2. จารุวรรณ ตั้งต้นสกุลวงศ์ เอเดรียน ฟลัด และ ทวิช จิตรสมบูรณ์ (2546).การจำลองเชิงตัวเลขและการวิเคราะห์การไหลในถังตกผลึกเพื่อผลิตน้ำตาล. ใน เอกสารการประชุมวิชาการเครือข่ายวิศวกรรมเครื่องกลแห่งประเทศไทย ครั้งที่ 17 (หน้า 26) กรุงเทพ : สถาบันเทคโนโลยีพระจอมเกล้าพระนครเหนือ
3. จารุวรรณ ตั้งต้นสกุลวงศ์ เอเดรียน ฟลัด และ ทวิช จิตรสมบูรณ์ (2547). การไหลในถังตกผลึกเพื่อผลิตน้ำตาล : การวิเคราะห์เชิงตัวเลข ใน เอกสารการประชุมเสนอผลงานวิจัยระดับบัณฑิตศึกษาแห่งชาติ ครั้งที่ 4 (หน้า 145) เชียงใหม่ : มหาวิทยาลัยเชียงใหม่

Appendix A

Example of a Definition File (.def) and Output File (.out) from CFX-Solver

```
This run of the CFX-5.5.1 Solver started at 17:36:38 on 7 Jul 2003 by user
Jackie1 on JACKIE (intel_athlon_winnt5.1) using the command:
C:\CFX\CFX-5.5.1\bin\5.5.1\perllib\cfx5solve.pl -stdout-comms -batch -ccl
-Using the CFX-5 Solver optimised for the winnt architecture from
C:\CFX\CFX-5.5.1\bin\5.5.1\winnt\solver-pvm.exe.
Setting up CFX-5 Solver run ...
+--------------------------------------------------------------+
| |
| CFX Command Language for Run |
| |
+--------------------------------------------------------------+
LIBRARY :
MATERIAL : sugar
Option = Pure Substance
PROPERTIES :
Option = General Fluid
Density = 1.3427E3 [kg m^-3]
Dynamic Viscosity = 2.3677E-1 [kg m^-1 s^-1]
END
        END
                END
EXECUTION CONTROL :
PARTITIONER STEP CONTROL :
Runtime Priority = Standard
PARTITIONING TYPE :
MeTiS Type = k-way
Option = MeTiS
        END
                END
RUN DEFINITION :
Definition File = d:/cfxwork/crystallyzer/halfmodel/halfmodel.def
Initial Values File = d:/cfxwork/crystallyzer/halfmodel/halfmodel_025.r\
es
Run Mode = Full
        END
SOLVER STEP CONTROL :
Runtime Priority = Standard
EXECUTABLE SELECTION :
Double Precision = Off
Use 64 Bit = Off
        END
PARALLEL ENVIRONMENT :
Option = Serial
Parallel Mode = PVM
        END
                END
                        END
```

```
FLOW :
SOLUTION UNITS :
Mass Units = [kg]
Length Units = [m]
Time Units = [s]
Temperature Units = [K]
Angle Units = [rad]
Solid Angle Units = [sr]
        END
SIMULATION TYPE :
Option = Steady State
        END
DOMAIN : halfmodel
Location = halfmodel
Coord Frame = Coord 0
Fluids List = sugar
DOMAIN MODELS :
DOMAIN MOTION :
Option = Stationary
        END
BUOYANCY MODEL :
Option = Non Buoyant
        END
REFERENCE PRESSURE :
Reference Pressure = 1.0133E5 [Pa]
        END
                END
FLUID MODELS :
TURBULENCE MODEL :
Option = Laminar
        END
HEAT TRANSFER MODEL :
Option = None
        END
THERMAL RADIATION MODEL :
Option = None
        END
                END
SUBDOMAIN : draft
Location = draft
Coord Frame = Coord 0
        END
SUBDOMAIN : baffle
Location = baffle
Coord Frame = Coord 0
        END
SUBDOMAIN : outtube
Location = outtube
Coord Frame = Coord 0
        END
SUBDOMAIN : impeller
Location = impeller
```

```
Coord Frame = Coord 0
SOURCES :
MOMENTUM SOURCE :
Momentum Source X Component = 0.00 [kg m^-2 s^-2]
Momentum Source Y Component = -50000 [kg m^-2 s^-2]
Momentum Source Z Component = 0.00 [kg m^-2 s^-2]
        END
                END
                        END
SUBDOMAIN : intube
Location = intube
Coord Frame = Coord 0
        END
BOUNDARY : inflow
Boundary Type = INLET
Location = inflow
Coord Frame = Coord 0
BOUNDARY CONDITIONS :
FLOW REGIME :
Option = Subsonic
        END
MASS AND MOMENTUM :
Option = Mass Flow Rate
Mass Flow Rate = 4.6712E-4 [kg s^-1]
        END
FLOW DIRECTION :
Option = Normal to Boundary Condition
        END
                END
                        END
BOUNDARY : outflow
Boundary Type = OUTLET
Location = outflow
Coord Frame = Coord 0
BOUNDARY CONDITIONS :
FLOW REGIME :
Option = Subsonic
        END
MASS AND MOMENTUM :
Option = Static Pressure
Relative Pressure = 0.00 [Pa]
        END
                END
                        END
BOUNDARY : draftwall011
Boundary Type = WALL
Location = draftwall011
Coord Frame = Coord 0
BOUNDARY CONDITIONS :
WALL INFLUENCE ON FLOW :
Option = No Slip
END
```

```
END
END
BOUNDARY : draftwall012
Boundary Type = WALL
Location = draftwall012
Coord Frame = Coord 0
BOUNDARY CONDITIONS :
WALL INFLUENCE ON FLOW :
Option = No Slip
END
END
END
BOUNDARY : draftwall021
Boundary Type = WALL
Location = draftwall021
Coord Frame = Coord 0
BOUNDARY CONDITIONS :
WALL INFLUENCE ON FLOW :
Option = No Slip
END
END
END
BOUNDARY : draftwall022
Boundary Type = WALL
Location = draftwall022
Coord Frame = Coord 0
BOUNDARY CONDITIONS :
WALL INFLUENCE ON FLOW :
Option = No Slip
END
END
END
BOUNDARY : inwall011
Boundary Type = WALL
Location = inwall011
Coord Frame = Coord 0
BOUNDARY CONDITIONS :
WALL INFLUENCE ON FLOW :
Option = No Slip
END
END
END
BOUNDARY : inwall012
Boundary Type = WALL
Location = inwall012
Coord Frame = Coord 0
BOUNDARY CONDITIONS :
WALL INFLUENCE ON FLOW :
Option = No Slip
END
END
END
```

```
BOUNDARY : inwall021
Boundary Type = WALL
Location = inwall021
Coord Frame = Coord 0
BOUNDARY CONDITIONS :
WALL INFLUENCE ON FLOW :
Option = No Slip
END
END
END
BOUNDARY : inwall022
Boundary Type = WALL
Location = inwall022
Coord Frame = Coord 0
BOUNDARY CONDITIONS :
WALL INFLUENCE ON FLOW :
Option = No Slip
END
END
END
BOUNDARY : outwall1
Boundary Type = WALL
Location = outwall1
Coord Frame = Coord 0
BOUNDARY CONDITIONS :
WALL INFLUENCE ON FLOW :
Option = No Slip
END
END
END
BOUNDARY : outwall2
Boundary Type = WALL
Location = outwall2
Coord Frame = Coord 0
BOUNDARY CONDITIONS :
WALL INFLUENCE ON FLOW :
Option = No Slip
END
END
END
BOUNDARY : baffle1
Boundary Type = WALL
Location = baffle1
Coord Frame = Coord 0
BOUNDARY CONDITIONS :
WALL INFLUENCE ON FLOW :
Option = No Slip
END
END
END
BOUNDARY : baffle2
Boundary Type = WALL
```

```
Location = baffle2
Coord Frame = Coord 0
BOUNDARY CONDITIONS :
WALL INFLUENCE ON FLOW :
Option = No Slip
END
END
END
BOUNDARY : sym
Boundary Type = SYMMETRY
Location = sym
Coord Frame = Coord 0
END
BOUNDARY : Default
Boundary Type = WALL
Location = Default
Coord Frame = Coord 0
BOUNDARY CONDITIONS :
WALL INFLUENCE ON FLOW :
Option = No Slip
END
END
END
INITIALISATION :
Option = Automatic
END
END
SOLVER CONTROL :
CONVERGENCE CONTROL :
Maximum Number of Iterations = 100
Timescale Control = Auto Timescale
END
CONVERGENCE CRITERIA :
Residual Type = RMS
Residual Target = 1.E-10
END
ADVECTION SCHEME :
Option = Upwind
END
DYNAMIC MODEL CONTROL :
Global Dynamic Model Control = Yes
END
END
END
COMMAND FILE :
Version = 5.5.1
END
+--------------------------------------------------------------+
| |
| Solver |
| |
+--------------------------------------------------------------+
```

```
+--------------------------------------------------------------+
| |
| CFX-5 Solver 5.5.1 |
| |
| Version 2002.05.29-23.00 Wed May 29 23:00:33 2002 |
| |
| |
| |
| |
| |
| Copyright 1996-2002 AEA Technology plc. |
+--------------------------------------------------------------+
+--------------------------------------------------------------+
| Job Information |
+--------------------------------------------------------------+
Run mode: serial run
Host computer: JACKIE
Job started: Mon Jul 7 17:37:21 2003
+--------------------------------------------------------------+
| Memory Usage Information |
+--------------------------------------------------------------+
Data Type Kwords Words/Node Kbytes Bytes/Node
Real 25760.8 349.37 100628.1 1397.48
Integer 11914.4 161.58 46540.6 646.34
Character 890.3 12.07 869.4 12.07
Logical 10.0 0.14 39.1 0.54
Double 16.0 0.22 125.0 1.74
+--------------------------------------------------------------+
| Total Number of Nodes, Elements, and Faces |
+--------------------------------------------------------------+
Domain Name : halfmodel
Total Number of Nodes = 73735
Total Number of Elements = 376481
Total Number of Tetrahedrons = 376481
Total Number of Faces = 40716
+--------------------------------------------------------------+
| Initial Conditions Supplied by Fields in the Input Files |
+--------------------------------------------------------------+
Domain Name : halfmodel
Pressure
Pressure.Gradient
Shear Strain Rate
Total Pressure
Velocity
+--------------------------------------------------------------+
| Average Scale Information |
+--------------------------------------------------------------+
Domain Name : halfmodel
Global Length = 9.7038E-02
Density = 1.3427E+03
Dynamic Viscosity = 2.3677E-01
Velocity = 2.8414E-02
```

```
Advection Time = 3.4152E+00
Reynolds Number = 1.5636E+01
+-----------------------------------------------------------------+
| The Equations Solved in This Calculation |
+-----------------------------------------------------------------+
Subsystem Name : Momentum and Mass
U-Mom
V-Mom
W-Mom
P-Mass
CFD Solver started: Mon Jul 7 17:37:29 2003
CFD Solver finished: Mon Jul 7 19:13:25 2003
Execution terminating: maximum number of time-step iterations,
or maximum time has been reached.
================================================================
==================
Boundary Flow and Total Source Term Summary
================================================================
==================
+-----------------------------------------------------------------+
| U-Mom |
+-----------------------------------------------------------------+
Boundary : baffle1 1.2295E-03
Boundary : draftwall011 2.2233E-03
Boundary : draftwall021 5.4820E-05
Boundary : inflow 3.0889E-06
Boundary : inwall011 5.4429E-05
Boundary : inwall021 4.1167E-04
Boundary : outflow -2.0465E-07
Boundary : outwall1 1.0160E-03
Boundary : sym -2.9413E-07
Boundary : Default -3.9056E-03
Boundary : draftwall012 -9.9255E-04
Boundary : draftwall022 -1.4029E-05
Boundary : inwall012 3.4362E-06
Boundary : inwall022 -3.0552E-06
Boundary : outwall2 6.8126E-06
Boundary : baffle2 -8.7440E-05
----------
Global Balance : -8.7100E-08
Global Imbalance, in %: 0.0000 %
+-----------------------------------------------------------------+
| V-Mom |
+-----------------------------------------------------------------+
Boundary : baffle1 -4.6596E-03
Boundary : draftwall011 -6.9397E-03
Boundary : draftwall021 6.5068E-05
Boundary : inflow -1.0329E-02
Boundary : inwall011 4.8499E-03
Boundary : inwall021 1.0193E-03
Boundary : outflow -2.5701E-05
Boundary : outwall1 -1.4851E-03
```

```
Boundary : sym 1.7902E-08
Boundary : Default 9.2094E-02
Boundary : draftwall012 2.2858E-02
Boundary : draftwall022 4.9161E-04
Boundary : inwall012 3.4096E-03
Boundary : inwall022 2.1762E-03
Boundary : outwall2 -5.4912E-03
Boundary : baffle2 -4.6841E-03
Sub-Domain : impeller -9.3349E-02
-----------
Global Balance : 5.2154E-07
Global Imbalance, in %: 0.0000 %
+---------------------------------------------------------------+
| W-Mom |
+---------------------------------------------------------------+
Boundary : baffle1 1.2863E+00
Boundary : draftwall011 -1.8441E+00
Boundary : draftwall021 -2.6562E-02
Boundary : inflow -4.9548E-05
Boundary : inwall011 -9.9345E-02
Boundary : inwall021 -6.6061E-02
Boundary : outflow 4.2976E-05
Boundary : outwall1 -1.7364E-01
Boundary : sym -6.6244E+00
Boundary : Default 6.7921E+00
Boundary : draftwall012 1.6887E+00
Boundary : draftwall022 2.5776E-02
Boundary : inwall012 1.2680E-01
Boundary : inwall022 1.1387E-01
Boundary : outwall2 8.7846E-02
Boundary : baffle2 -1.2873E+00
-----------
Global Balance : 2.0266E-06
Global Imbalance, in %: 0.0000 %
+---------------------------------------------------------------+
| P-Mass |
+---------------------------------------------------------------+
Boundary : inflow 4.6712E-04
Boundary : outflow -4.6707E-04
-----------
Global Balance : 5.4832E-08
Global Imbalance, in %: 0.0117 %
================================================================
====================
Wall Force and Moment Summary
================================================================
====================
Note: Pressure integrals exclude the reference pressure. To include
it, set the expert parameter 'include pref in forces = t'.
+---------------------------------------------------------------+
| Pressure Force On Walls |
+---------------------------------------------------------------+
```

X-Comp. Y-Comp. Z-Comp.
baffle1 -1.1272E-03 1.5370E-08 -1.2867E+00
draftwall011 -1.9686E-03 -2.6586E-03 1.8414E+00
draftwall021 -4.8741E-05 2.7003E-05 2.6530E-02
inwall011 -3.0126E-06 -4.6799E-07 9.9302E-02
inwall021 -1.9404E-04 -1.7073E-06 6.6031E-02
outwall1 -5.0330E-04 1.8375E-07 1.7356E-01
Default 3.8898E-03 -1.2390E-01 -6.7867E+00
draftwall012 1.8296E-03 2.5251E-03 -1.6912E+00
draftwall022 4.0935E-05 -2.6518E-05 -2.5747E-02
inwall012 3.4431E-06 6.8453E-07 -1.2678E-01
inwall022 4.0594E-06 9.3028E-06 -1.1392E-01
outwall2 -2.9104E-07 -6.1646E-06 -8.7868E-02
baffle2 1.7869E-04 -1.5348E-08 1.2863E+00

+----------+
| Viscous Force On Walls |
+----------+

X-Comp. Y-Comp. Z-Comp.
baffle1 -1.0220E-04 4.6596E-03 4.9541E-04
draftwall011 -2.5473E-04 9.5983E-03 2.6204E-03
draftwall021 -6.0796E-06 -9.2071E-05 3.1933E-05
inwall011 -5.1420E-05 -4.8494E-03 4.3677E-05
inwall021 -2.1763E-04 -1.0176E-03 3.0634E-05
outwall1 -5.1265E-04 1.4849E-03 7.3270E-05
Default 1.5756E-05 3.1803E-02 -5.3383E-03
draftwall012 -8.3720E-04 -2.5383E-02 2.4885E-03
draftwall022 -2.6906E-05 -4.6509E-04 -2.9712E-05
inwall012 -6.8925E-06 -3.4103E-03 -2.6764E-05
inwall022 -9.9353E-07 -2.1856E-03 5.1280E-05
outwall2 -6.5248E-06 5.4974E-03 2.1524E-05
baffle2 -9.1713E-05 4.6841E-03 1.0290E-03

+----------+
| Pressure Moment On Walls |
+----------+

X-Comp. Y-Comp. Z-Comp.
baffle1 -6.4085E-02 9.0986E-05 4.6562E-05
draftwall011 6.6945E-02 -1.8159E-07 9.8299E-05
draftwall021 4.0040E-05 -9.4588E-09 9.7630E-07
inwall011 4.7900E-03 -8.9372E-04 -4.7366E-09
inwall021 5.6482E-03 -5.9428E-04 1.6388E-05
outwall1 1.0828E-02 -8.4179E-03 3.8833E-05
Default -2.4536E-01 -5.9571E-05 -4.2906E-04
draftwall012 -6.2037E-02 2.2176E-07 -1.1982E-04
draftwall022 -3.8686E-05 -5.1381E-08 -9.4452E-07
inwall012 -6.3393E-03 1.1410E-03 -7.4244E-08
inwall022 -9.8050E-03 1.0253E-03 -3.1776E-07
outwall2 -4.3957E-03 4.2616E-03 -3.1934E-07
baffle2 6.4074E-02 -1.2983E-05 -8.3409E-06

+----------+
| Viscous Moment On Walls |
+----------+

X-Comp. Y-Comp. Z-Comp.

baffle1 2.0293E-04 8.5835E-06 2.1671E-06
draftwall011 3.3557E-04 1.8561E-05 4.0177E-06
draftwall021 -1.3605E-06 5.0121E-07 3.9422E-07
inwall011 -8.3225E-06 -2.0227E-07 -4.0134E-05
inwall021 6.0071E-07 4.4871E-07 9.0005E-06
outwall1 1.1409E-05 -1.8492E-06 1.1128E-04
Default 1.9925E-03 1.6190E-05 -6.4487E-05
draftwall012 -4.0270E-04 2.1654E-05 3.8903E-05
draftwall022 -8.7107E-06 1.6337E-07 1.5511E-06
inwall012 -7.1644E-06 2.5158E-07 -3.0511E-05
inwall022 9.3747E-07 -4.5888E-07 -1.9577E-05
outwall2 1.0940E-05 -1.0350E-06 2.6683E-04
baffle2 2.6448E-04 8.2787E-06 2.3294E-06

Locations of Maximum Residuals				
Equation	Node #	X	Y	Z
U-Mom	70262	5.112E-02	2.466E-02	-3.141E-02
V-Mom	7991	5.017E-02	1.000E-01	-2.494E-03
W-Mom	17147	2.872E-02	-2.518E-02	2.963E-10
P-Mass	42583	4.923E-02	9.634E-02	-1.926E-03

Peak Values of Residuals			
Equation	Loop #	Peak Residual	Final Residual
U-Mom	2	2.55650E-04	7.73714E-08
V-Mom	1	2.31765E-03	2.09388E-07
W-Mom	2	2.45396E-04	8.80229E-08
P-Mass	2	1.20873E-04	2.37551E-08

False Transient Information		
Equation	Type	Elapsed Pseudo-Time
U-Mom	Auto	1.05761E+02
V-Mom	Auto	1.05761E+02
W-Mom	Auto	1.05761E+02
P-Mass	Auto	1.05761E+02

Average Scale Information

Domain Name : halfmodel
Global Length = 9.7038E-02
Density = 1.3427E+03
Dynamic Viscosity = 2.3677E-01
Velocity = 4.1368E-02
Advection Time = 2.3457E+00

```
Reynolds Number = 2.2764E+01
+--------------------------------------------------------------+
| Variable Range Information |
+--------------------------------------------------------------+
Domain Name : halfmodel
+--------------------------------------------------------------+
| Variable Name | min | max |
+--------------------------------------------------------------+
| Velocity u | -7.21E-02 | 7.00E-02 |
| Velocity v | -1.60E-01 | 5.52E-02 |
| Velocity w | -6.85E-02 | 7.10E-02 |
| Pressure | 3.55E-01 | 7.54E+02 |
| Density | 1.34E+03 | 1.34E+03 |
| Dynamic Viscosity | 2.37E-01 | 2.37E-01 |
+--------------------------------------------------------------+
+--------------------------------------------------------------+
| CPU Requirements of Numerical Solution |
+--------------------------------------------------------------+
Subsystem Name Discretization Linear Solution
(secs. %total) (secs. %total)
----------------------------------------------------------------
Momentum and Mass 4.45E+03 80.9 % 1.05E+03 19.1 %
-------- ------- -------- ------
Summary 4.45E+03 80.9 % 1.05E+03 19.1 %
+--------------------------------------------------------------+
| Job Information |
+--------------------------------------------------------------+
Host computer: JACKIE
Job finished: Mon Jul 7 19:13:39 2003
Total CPU time: 5.679E+03 seconds
or: ( 0: 1: 34: 38.515 )
( Days: Hours: Minutes: Seconds )
End of solution stage.
This run of the CFX-5 Solver has finished.
```

CURRICULUM VITAE

Name: Dr. Adrian Evan Flood

Present Position: Associate Professor, School of Chemical Engineering, Institute of Engineering, Suranaree University of Technology, Nakhon Ratchasima 30000 Thailand.

Education: B.E. (Hons) (Chem. Eng.), The University of Sydney, Australia, 1990.

Ph.D. (Chem. Eng.), The University of Queensland, Australia, 1996.

Ph.D. Thesis : Crystallization of D-Fructose from Aqueous Ethanolic Solutions.

Research Fields: Crystallization Processes.

Teaching Experience : Chemical Engineering Thermodynamics (at undergraduate and graduate levels), Mass Transfer Operations (Process Equipment Design and Operation III), Chemical Process Dynamics and Control, Crystallization & Population Balance Modeling (graduate level), Experimental Design and Statistical Analysis (graduate level), State Variable Control (graduate level), Linear System Theory (graduate level), and others.

Experience :

1991-1992: Air Water Noise (AWN) Consultants (Environmental Engineering)

1993-1995: Consulting projects on inorganic crystallization, ammonium nitrate evaporation and fertilizer surface structure.

1996-2000: Lecturer in Chemical Engineering, Suranaree University of Technology.

2000-2006: Assistant Professor in Chemical Engineering, Suranaree University of Technology.

2006-current: Associate Professor in Chemical Engineering, Suranaree University of Technology.

International Publications:

1. Adrian E. Flood, Michael R. Johns, Edward T. White, "Mutarotation of D-Fructose in Aqueous-Ethanolic Solutions and its Influence on Crystallization", *Carbohydrate Res.* 288 (1996) 45-56.
2. A. E. Flood, J. Addai-Mensah, M. R. Johns, and E. T. White, "Refractive Index Viscosity, Density and

Solubility in the System Fructose + Ethanol + Water at 30, 40 and 50°C", *J. Chem. Eng. Data* 41(3) (1996) 418-421.

3. Adrian E. Flood, Michael R. Johns, and Edward T. White, "Crystal Growth Rates and Dispersion for D-Fructose from Aqueous Ethanol", AIChE Journal 46(2) (2000) 239-246.
4. A. E. Flood and S. Puagsa, "Refractive Index, Viscosity, and Solubility at 30°C, and Density at 25°C for the System Fructose + Glucose + Ethanol + Water", *J. Chem. Eng. Data 45*(5) (2000) 902-907.
5. Adrian E. Flood, "Thoughts on Recovering Particle Size Distributions from the Moment Form of the Population Balance", *Dev. Chem. Eng. Min. Proc.* 10(5/6) (2002) 501-519.
6. Pareena Pantaraks and Adrian E. Flood, "Correlation between Single Crystal Growth Rates and Dissolution Rates of Sucrose", *Chem. Eng. Trans.* (1) (2002) 347-352.
7. Pareena Pantaraks and Adrian E. Flood, "Effect of Growth Rate History on Current Crystal Growth: A Second Look at Surface Effects on Crystal Growth Rates", *Cryst. Growth Des.*5(1) (2005) 365-371.
8. Sukanya Srisa-nga, Adrian E. Flood, and Edward T. White," The Secondary Nucleation Threshold and Crystal Growth of α-Glucose Monohydrate in Aqueous Solution", *Cryst. Growth Des.* 6(3) (2006) 795-801.
9. Jaruwan Tangtonsakoolwong, Adrian E. Flood, and Tawit Chitsomboon, "Flow Fields in an experimental mixed-suspension mixed-product-removal crystallizer: A numerical Analysis" *ScienceAsia* 32(3), 231-239 (2006).
10. Pareena Pantaraks, Masakuni Matsuoka, and Adrian E. Flood, "Effect of Growth Rate History on Current Crystal Growth 2: Crystal Growth of Sucrose, $KAl(SO_4)_2 \cdot 12H_2O$, KH_2PO_4, and K_2SO_4" *Cryst. Growth Des.* 7(12), 2635-2642 (2007).
11. Lek Wantha and Adrian E. Flood, "Numerical Simulation and Analysis of Flow in a DTB Crystallizer" *Chem. Eng. Comm.* 195, 1345-1370 (2008).
12. Adrian E. Flood, "Recent Patents on the Optical Resolution of Amino Acid Enantiomers by Crystallization from solution" *Rec. Patents Mat. Sci.* 1, 98-115 (2008).
13. Arwut Promraksa, Adrian E. Flood and Philip A. Schneider, "Measurement and Analysis of the Dextran partition Coefficient in Sucrose Crystallization" *J. Cryst. Growth* 311, 3667-3673 (2009).
14. Feedback between Crystal Growth Rates and Surface Roughness. *CrystEngComm.* 2009 [Accepted].

Positions and Honours

1. Editorial Advisory Board, "Recent Patents on Materials Science", Bentham Science, 2008 – present.
2. Scientific Committee, "15th International Workshop on Industrial Crystallization (BIWIC 2008)", September 10 – 12 2008, Max Planck Institute for Dynamics of Complex technical Systems, Magdeburg, Germany.
3. Invited Speaker, "The 2009 International Meeting on Crystal Engineering & Drug delivery System" Tianjin, China, 5 – 8 September 2009.
4. Reviewer for International Journals, including Crystal Growth and Design (ACS), CrystEngComm (RSC)", Journal of Pharmaceutical Sciences (Elsevier), Chemical Engineering Research and Design (IChemE), Chemical Physics Letters (Elsevier), Journal of Chemical and Engineering Data (ACS), among others.

Awards and Research Grants:

1. Alcoholic Crystallization of High Fructose Syrup (Adrian Flood). TRF Young Researcher Award. (Complete).
2. A Study into the Mechanism of Crystal Growth Rate Dispersion. RGJ PhD Program, The Thailand Research Fund (Complete).
3. The Effect of the Mutarotation Reaction on the Crystallization of Glucose Monohydrate. RGJ PhD Program, The Thailand Research Fund (Complete).
4. Removal of Dextran from the Raw Sugar Manufacturing Process. RGJ PhD Program, The Thailand Research Fund.
5. Modeling of Breakage in Industrial Crystallizers. RGJ PhD Program, The Thailand Research Fund.
6. Crystallization from Mixed Surfactant Solutions. RGJ PhD Program, The Thailand Research Fund.
7. Separation of Proteins using Crystallization. RGJ PhD Program, The Thailand Research Fund.
8. Crystallization of Amino Acids. MOE (Ministry of Education) Ph.D. Scholarship.
9. CFD Modeling of an MSMPR Crystallizer. SUT Research Fund.
10. An Investigation into the Effect of Mutarotation on the Crystallization of Simple Carbohydrates. SUT Research Fund.
11. Improvements to Industrial Crystallizers through CFD Modeling. SUT Research Fund.
12. Synthesis and Structure Determination of Dihexulose Dianhydrides and Related Materials. SUT Research Fund.
13. A Study into the Effectiveness of Crystallization in Purification of Amino Acids. SUT Research Fund.